AN ACARS CLIMATOLOGY OF THE BOUNDARY LAYER NEAR THE COAST OF SOUTHERN CALIFORNIA

BY

Chris Mitchell

Submitted to the graduate degree program in Geography and the Graduate Faculty of the University of Kansas in partial fulfillment of the requirements for the degree of
Master of Science

_____

David Rahn
Chairperson

_____

David Mechem

_____

David Braaten

Date Defended: 7/24/2015

The Thesis Committee for Chris Mitchell
Certifies that this is the approved version of the following thesis:

AN ACARS CLIMATOLOGY OF THE BOUNDARY LAYER NEAR THE COAST OF SOUTHERN CALIFORNIA

_____

David Rahn
Chairperson

Date approved: 7/29/2015

ABSTRACT

Typical late spring and early summertime conditions over California's southern bight consist of a well-mixed coastal boundary layer (CBL) capped by warm and dry air associated with the subsiding branch of the subtropical Hadley circulation. The CBL in this region is often conceptualized as two overlapping layers that are laterally constrained on one side. The CBL significantly dominates daily weather throughout the southern California coastal region and is often responsible for frequent air traffic delays and impacts pollution events. An increasing number of commercial aircraft carry meteorological instruments that collect temperature and wind data at resolution scales. Fortunately since 2001 an abundance of sounding data has been achieved providing an opportunity to produce a climatological record of the diurnal cycle of the lower atmosphere. Meteorological variables such as wind patterns, boundary layer height, and inversion strength can be closely examined with high resolution over a record length of more than a decade. This study explores both the difficulties associated with using ACARS to produce a robust climatology and the benefits of using ACARS to characterize the lower atmosphere. Emphasis for this climatology is placed at Los Angeles International Airport (LAX). Considering distinct differences exist between the CBL just offshore and inland, data from nearshore flight paths must be analyzed when constructing CBL climatologies. Results from this study suggest the depth of the CBL depends greatly on downward mixing of radiatively cooled air from a cloud-topped CBL, and that the CBL does not deepen significantly on clear nights. The wind climatologies suggest downsloping northerly winds from the coastal mountain ranges directly to the north is unlikely the main control over the mean depth of the boundary layer because the CBL deepens at the peak time for northerly flow. In addition, southerly flow dominates the tops of the CBLs for both LAX and SAN throughout the morning and early afternoon, which is especially prominent for the CBL over LAX and suggestive of a low level coastal jet. Furthermore, persistent height difference exists between San Diego and Los Angeles with higher heights toward the south, forcing an acceleration of alongshore southerly flow overnight with a minimum in height difference and thus a minimum in the alongshore acceleration in the afternoon.

Table of Contents

1. Introduction

Off the coast of California during the spring and summer the wind within the coastal boundary layer (CBL) is persistently from the north. Wind speed is greatest at the top of the CBL, which is marked by a sharp temperature inversion typically found around 200-600 m. Mountainous terrain along the coast acts as a lateral boundary to the low-level wind and CBL. Several coastal phenomena can occur including hydraulic features when the flow is supercritical (e.g., expansion fans and hydraulic jumps), coastally trapped wind reversals, and Catalina eddies. Observational studies offshore are typically limited to either buoy data or obtained from case studies using research aircraft, radiosondes launched from ships or small islands. As a result, scarce measurements are available to diagnose and understand the climatology and forcing of coastal phenomena. Meteorological data from the Aircraft Communications Addressing and Reporting System (ACARS) is a promising dataset that may be well-suited for understanding several key questions. These include fundamental climatological characteristics of the lower atmosphere such as the CBL height, mean wind profile and inversion strength.

Focus of the analysis will be on southern California due to the high volume of air traffic at Los Angeles (LAX) and surrounding airports. An ACARS-derived climatology of CBL properties is constructed. Of particular interest in understanding coastal processes are the seasonal and *diurnal* cycle of CBL height. *The climatology will be the basis of this work since this will be the first time that such a complete, long-term study of the diurnal changes in CBL height have been documented.* Several issues will have to be addressed at the outset including how to most efficiently create a database, how to objectively determine variables such as the CBL height, and how to account for any potential biases that could result from the flight path.

After creating the climatology, average conditions can be constructed for California's southern bight for May and June. For instance, two proposed forcing mechanisms for a Catalina eddy are an ageostrophic response to blocked onshore flow and an offshore flow aloft that creates a mesoscale leeside trough that induces cyclonic motion, which can be investigated using ACARS. Further investigations into southerly surges, land-falling mid-latitude cyclones, and anomalies to the general circulation such as the Madden Julian Oscillation could also be explored with this data set. In this work, the crucial steps of constructing the climatology and understanding the strengths

and limitations of the data are the central focus, but the application of the data to Catalina eddies will highlight its usefulness.

2. Background Discussion

Sinking air from the subsiding branch of the Hadley and Walker cells occurs over a turbulent well-mixed marine boundary layer off the coast of California (Burk and Thompson 1996; Pomeroy and Parish 2001). A temperature inversion caps the cool, moist marine air and separates it from the warm, dry troposphere aloft. The contrast between the Pacific high and the thermal low over the desert southwest is associated with a large scale pressure gradient that forces surface winds to orient roughly parallel to the coast from north to south. Generally, the overall speed of the equatorward wind within the CBL is governed by the strength of the large scale pressure gradient, although smaller scale processes such as topography can have an effect on local wind speed maxima at specific locations along the coast (Dorman and Koračin 2008).

Depth of the CBL varies diurnally, seasonally, and with distance from the shoreline. Changes to CBL depth depends on a range of processes from the microscale (e.g., turbulence) to the synoptic scale (e.g., strength of the subsidence). There have been many studies over the years aimed at finding the characteristics of the CBL. Observations by Pomeroy and Parish (2001) found the average CBL depth increases from 300 m near shore to over 500 m further offshore. The sloping CBL indicates a horizontal temperature gradient and therefore, a thermal wind. The thermal wind is associated with a change from northerly winds at the surface to more southerly winds aloft (Zemba and Friehe 1987; Gerber et al. 1989). However, this is the mean condition, which is modified by many processes such as cross-shore sea breezes and hydraulic effects associated with the coastal topography.

Diurnally, the depth of a cloudy CBL deepens overnight due to longwave radiative cooling of cloud tops which drives turbulent mixing which increases entrainment of free-atmosphere into the lower boundary layer. As the column cools overnight the stratus layer thickens until morning when daytime heating can offset the convectively unstable entrainment mixing. The rest of the shortwave radiation that travels through the stratus layer is often negligible and is not responsible for significant differences of the CBL due to the ocean's large heat capacity; however does have an impact on the ocean mix-layer energy budget.

The dominant mechanisms controlling the depth of the CBL differ from a land based boundary layer in which the depth is largely influenced by daytime shortwave heating. This of course adds complication to this study because Los Angeles is located in the transitional zone between the marine boundary layer and the inland boundary layer. A general illustration of a typical summertime stratus capped CBL along and off the coast of California can be found in Figure 9 of Oliver et al. (1978), which depicts an enhanced depth during the overnight and early morning hours. Since their model describes an ideal system for a marine environment away from the influence of land, how descriptive is this for a particular coastal city that is influenced by both marine and inland features? Does this change from Los Angeles to San Diego?

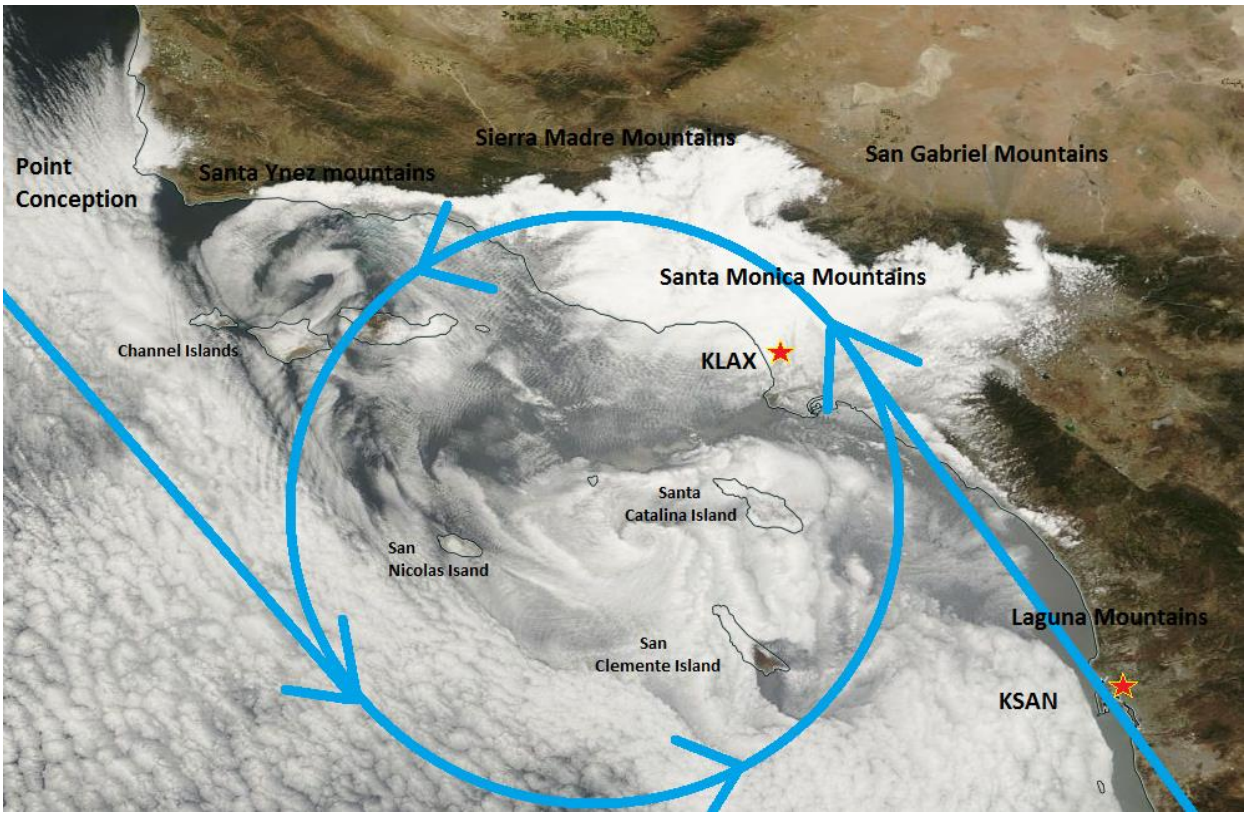

Figure 2. Topographical map of the area of interest including relevant mountains and airports. The straight blue arrow shows the average path of the low level jet and the blue circle outlines the general circulation in the bight region.

Variation in the depth of the boundary layer also occurs in relation to convergence by the sea breeze. Neiburger (1944) described the general relationship with the sea breeze and the depth of the marine layer as a diurnal cycle that begins with the onset of shortwave heating over land.

As the land surface is heated the air over the land becomes less dense than the surrounding air and lifts. As the thermal gradient increases and pressure lowers, cooler moist marine air replaces the lifted air and thus a circulation develops called a sea breeze. At night, the land surface cools weakening the sea breeze and if the surface cooling is sufficient, land breeze develops.

To describe the fluid dynamics, the CBL can be approximated by a shallow water system acting as a single layer incompressible flow (Rahn et al. 2013). The top of the cool CBL is often below the height of the surrounding coastal range and therefore, the topography acts as a lateral barrier redirecting the flow along the coast. When the speed of the flow is sufficiently fast and the CBL depth relatively shallow, hydraulic features may manifest in the flow (e.g., Dorman and Koračin 2008). These features depend on the topography of the coastline. For example, Point Conception's influence on the marine layer is tied to a local wind maximum that extends southward and is associated with a 90° bend in the coastline near the Santa Ynez mountain range that directly influences the lower atmosphere and surrounding coastal communities.

Theoretically, a Froude number greater than 1 is supercritical, which means that the propagation of gravity waves in the flow is slower than the flow itself and therefore, cannot propagate upstream. This has implications for geostrophic adjustment because the mass cannot be distributed evenly and can result in a marked deepening or thinning of the CBL. Slowing and deepening of the CBL may occur if the supercritical CBL layer is impinging on topography that blocks the inbound stream. This interaction forms a hydraulic jump upstream that extends offshore to form an oblique angle with the coast (Rogers et al. 1998; Dorman et al. 1999). A local high pressure perturbation results from the deepening of the CBL. In subcritical conditions with a Froude number less than 1, gravity waves are able to travel upstream and distribute mass evenly throughout the layer, so there will be a smoother compression bulge upwind of the impinging topography. If the Froude number of the inbound flow is between 0.5 and 1, then a transcritical situation develops in which the flow is supercritical within an expansion fan due to the hydraulically induced increase in wind speed (Rogerson 1999; Dorman and Koračin 2008).

A thinning of the flow can occur on the lee side of a corner that bends away in which an expansion fan can form with an associated low pressure perturbation and high wind speeds (Dorman and Koračin 2008). This hydraulic feature is limited to the immediate downstream of the bend and is supported by different numerical models (Skyllingstad et al. 2001; Burk et al. 1998; Pickett and Paduan 2003; Koračin et al. 2004) buoy and land measurements (Halliwell and Allen

1987; Dorman and Winant 2000; Dorman et al. 2000), aircraft measurements (Rogers et al. 1998), and satellite measurements (Koračin et al. 2004).

The top of the CBL forms a slope from the compression bulge, to an inflection point downstream of the leeside flow. The wind speed maximum is found at the top of the CBL where wind speeds that can reach 30 m s^{-1} (Neiburger et al. 1961; Bridger et al. 1993; Pomeroy and Parish 2001). This is due to dual influences of friction near the surface and a rapid decrease in the PGF associated with the thermal wind (Zemba and Friehe 1987). Each cape and point along the coast may modify the mean flow and result in localized extrema of CBL heights and wind speeds due to hydraulic effects.

Sloping of the CBL, directional changes and a low level jet all support an expansion fan, but the synoptic environment is still the primary forcing mechanism of the low level jet and hydraulic interactions occur in this general flow. Local wind maxima embedded in the low level jet are closely associated with the lee of major coastal points protruding into the Pacific Ocean (Winant et al. 1988; Samelson 1992; Burk and Thompson 1996; Cui et al. 1998; Rogerson 1999; Burk et al. 1999).

Another class of coastal flow is the so-called coastally trapped wind reversals (CTWRs) or southerly surges that occur along the coast of California (Nuss et al. 2007). A buoy derived climatology of these events from 1981 to 1991 reveals that CTWRs occur 1.5 times a month for about 36 hours and most frequent from April to September (Bond et al. 1996). CTWRs are characterized by a reversal from the dominant northerly winds to southerly winds with wind speeds averaging 7-8 m s^{-1} (Mass and Bond 1996), accompanied with fog and low marine stratus that moves northward. These events can significantly influence the temperature and visibility and can impact coastal communities, especially aviation.

Difficulties remain in determining the dynamic mechanisms governing the development of CTWRs. One explanation for CTWRs is that they are topographically trapped density currents (Dorman 1987; Mass and Albright 1987; Reason and Dunkley 1993). Dorman (1985, 1988) suggests that these events are coastally trapped Kelvin waves. A study of a single event by Ralph et al. (1998) has shown the CTWR to be consistent with the structure of an internal bore or Kelvin wave within the inversion; however the kinematic field was not consistent.

Mass and Albright (1987) suggest that these wind reversals are produced by synoptic-scale forcing in which the coastal southerlies are the trapped ageostrophic response to a synoptic-scale

reversal in the pressure gradient where lower pressure develops to the north and a geostrophic flow is not possible due to topography. Mass and Bond (1996) constructed a climatology that showed a consistent pressure gradient reversal along the coast due to lee side troughing to the north along the coast. While this explains the initial development of these CTWRs, it does not explain the northward propagation very well (Nuss et al. 2007). An idealized model of CTWRs with synoptic-scale forcing by Skamarock et al. (1999) describe the reversal in winds as the result of the evacuation of the CBL to the north which causes an alongshore pressure gradient. A northerly propagating coastally trapped Kelvin wave then develops due to this alongshore pressure gradient reversal. The largest forces concerning the reaction to the pressure gradient are the direct interactions by synoptic-scale flow and indirectly by topography (Mass et al. 1986; Mass and Albright 1987, 1988).

The third major phenomenon in the marine boundary layer off the coast of California and a focus for this study after the climatology of the coastal boundary layer is the Catalina eddy. In spring and summer the northerly low-level wind roughly parallels the coast until Point Conception. The average low level wind field during June indicates that the flow beyond this point turns toward the east within the bight region and commonly results in a cyclonic circulation which is often centered near Catalina Island giving the Catalina eddy its name, although there are other circulations with the bight. The so-called midchannel eddy located in the Santa Barbara Channel and the Gaviota eddy located near the coast of Gaviota, California are other smaller closed circulations that have been identified (Smith et al. 1983).

Often associated with a Catalina eddy is a persistent low level stratocumulus deck that develops and deepens along with the genesis of the eddy, but this is not always the case. Catalina eddies have been observed in satellite imagery containing a limited amount of cloud coverage. During a Catalina eddy, the stratus deck often extends inland and up the coastal mountain range as low level clouds and fog, the extent of which depends on the depth of the CBL. Along with deepening the low level stratocumulus, Catalina eddies have the potential to deepen the CBL by 1400 meters within 24 hours Eichelberger (1971). Catalina eddies have even been documented to advect pollutants from the industrial parts of Los Angeles to the Santa Barbara and Ventura regions (Wakimoto 1986; Wilczak et al. 1991) demonstrating the human impacts beyond limiting visibility and lowering temperatures.

There is still some debate regarding the exact forcing behind the development of Catalina eddies and this is one of the main driving forces behind applying this climatology to these eddies. An analysis of an event on 21 July 1992 with numerical models (Burk and Thompson 1996) and case studies (e.g., Mass and Albright 1989) all suggest synoptic scale forcing results in an intensification of the horizontal east-west pressure gradient near the coast with higher pressure to the south. The enhanced pressure gradient initiates southerly flow which is trapped by topography along the shore. The ageostrophic southerly wind in conjunction with the strong northerly flow near Point Conception associated with the coastal jet described above enhances the cyclonic vorticity (Davis 2000). Given a favorable synoptic setup, some Catalina eddies can also "break out" of the bight region and evolve into a southerly surge that propagates north of Point Conception. These cyclonic circulations were prevalent throughout field studies (BASIN, Wakimoto et al. 1986 and PreAMBLE, Parish et al. 2013) and in satellite imagery (e.g. Rosenthal 1968; Brandli et al. 1977; Dorman 1985). Wakimoto (1987) contrasts Dorman (1985) by stating that there appears to be a strong topographical influence on the genesis of the Catalina eddy. In addition, Wakimoto (1987) suggests that it is similar to vortices produced by plates accelerating in a fluid at rest with the strengthening of the horizontal pressure gradient by the thermal low producing an acceleration of the northwesterly flow as an atmospheric equivalent. The study done by Mass and Albright (1989) proposes that as long as the pressure gradient exists, Catalina eddy events will continue until the alongshore pressure gradient weakens and reverses. A numerical modeling study by Ulrickson (1995) shows the low in the bight forms because of leeside subsidence warming and insignificant daytime diabatic heating of the flow is insignificant. Furthermore, Bosart (1983) proposes the appearance of cyclonic shear vorticity offshore is in response to lee troughing downstream of the coastal mountains between Vandenberg and Pt. Mugu and the dissipation of the eddy occurs with the onset of a broad onshore flow with the eastward progression of the synoptic ridge.

3. Motivation

One of the largest limitations for studying the CBL along the coast of California is a lack of observations. There are two stations that launch daily radiosondes in southern California. Vandenberg Air Force Base launches radiosondes only at 1200 UTC. The Marine Corps Air Station, Miramar launches radiosondes at 0000 UTC and 1200 UTC. In northern California,

radiosondes are launched at Oakland International Airport at 0000 UTC and 1200 UTC. It is apparent that the radiosonde data from these locations lack the temporal and spatial resolution required to sufficiently capture the diurnal cycle, adequately represent rapid changes forced by synoptic systems, and reliably detect other features of the lower atmosphere. Past work has analyzed nearshore buoy data to relate the behavior of several meteorological surface variables as a response to potential low level forcing mechanisms involved, additional sources are imperative to accurately assess the characteristics of the layer aloft and to discern the appropriate forcing mechanisms at play. Observational studies that specifically investigate the CBL include radiosondes (e.g. Blaskovic et al. 1991) and aircraft measurements (Rahn et al. 2013). However, radiosondes are infrequent, expensive, and tied to one location and while aircraft data does have high temporal and spatial resolution, the observational campaigns typically only capture single events over a few months. To put together a diurnal climatology of the CBL, high frequency (at least hourly) measurements are needed over a much longer period of time.

ACARS data offers an opportunity to obtain frequent measurements of the lower atmosphere over more than a decade at times other than 0000 UTC and 1200 UTC. Aircraft from 38 different airlines (as of November 2014) including the United Postal Service (UPS), Delta Air Lines, United Air Lines, Lufthansa and Northwest Air Lines provide a platform for meteorological instruments that are able to take and record measurements. At a cruising altitude typically about ~13 km recordings of wind, pressure, temperature and altitude at 5 minute intervals are sufficient for an adequate observation of the upper atmosphere. Due to the importance of capturing data in the lower atmosphere and the limited amount of time spent at low levels, the ACARS system records at much higher intervals during take offs and landings. This results in measurements as high as every 6 seconds with an altitude gap of less than 60 m (Stanley and Schwartz 1999).

Figure 1 illustrates several issues between the measurements from ACARS and from operational soundings. The example is a single sounding obtained from a radiosonde launched at Miramar compared to a sounding extracted from ACARS at San Diego International Airport (SAN) roughly 16 km away at the same time. Both measurements are in close agreement in the free atmosphere, but there is little agreement in the lower atmosphere where mesoscale processes such as sea breezes can have a major impact on the temperature within the boundary layer.

There is a ~200 meter difference in the height of the inversion base and a 4ºC difference in the maximum temperature within the inversion layer, which cannot be explained by differences in instrumentation alone, e.g. the accuracy of ACARS is 0.5K (Benjamin and Schwartz 1999) and the accuracy of radiosondes are less than 1K (Kitchen 1988). The marine base Miramar is 146 meters in elevation whereas; San Diego International is around 5 meters explaining ~140 meters of the base inversion height difference. The temperature in the CBL is about 8ºC cooler in the ACARS observations illustrating how dynamic the lower boundary layer can be 16 km away.

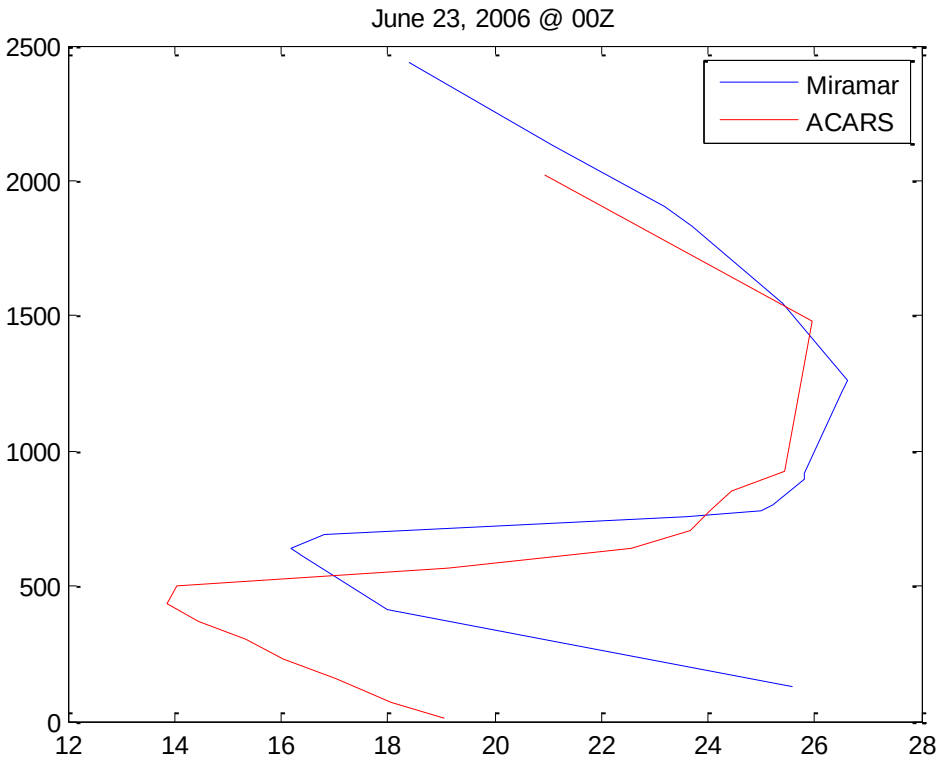

Figure 1. Comparison between the vertical temperature profiles extracted from ACARS (red) and the 00Z operational sounding out of the Marine Corps Air Station Miramar on June 23, 2006.

Although numerical models are another way to investigate the characteristics of the lower atmosphere, features such as the CBL have proven to be difficult to simulate correctly and much work is being done to improve the models (e.g., PreVOCA, Wyant et al. 2010). Offshore of southern California, Rahn et al. (2014) demonstrate the discrepancies between observations and

numerical simulations of the lower atmosphere near Point Conception. There were 14 different Weather Research and Forecasting (WRF) model configurations that were ran in an effort to recreate the aircraft observations and it was clear that the model was sensitive to the choice of parameterizations and no set of choices adequately captured the structure of the observed sounding in that case. The base of the temperature inversion was consistently lower altitude in the WRF simulations than in the observations. The winds were also poor when compared to the observations below 1 km.

4. Methods and pre-processing

Brief history of ACARS

Meteorological observations from aircraft have been obtained since World War I. Before the National Oceanic and Atmospheric Administration (NOAA) and the National Weather Service (NWS), the Weather Bureau would pay pilots to fly with aerometeorographs attached to their aircraft to record observations of pressure, temperature and relative humidity (Hughes and Gedzelman 1995). Pilots were paid to fly to at least 13,500 feet with a 10% pay bonus for every 1,000 feet after that; however, pilots trying to increase their pay would sometimes blackout due to the limited oxygen at high altitudes which made this line of work dangerous. These types of dangerous flights eventually gave way to radiosondes in 1940's and automated aircraft reports from commercial aviation in 1979 (Sparkman et al. 1981; Lord et al. 1984). Automated aircraft reports increased substantially in the 1990s. In 2002 more than 170,000 point data were available daily (Moninger et al. 2003) and currently there are over 400,000 point observations per day (World Meteorological Organization 2014). Observations are expected to keep growing partly because the National Weather Service plans to use part of the Disaster Relief Appropriations Act of 2013 to expand coverage (NOAA 2014, SCN14-36). Generally these reports include temperature, horizontal wind components and turbulence, but some reports also include dew point-temperature. Use of ACARS reports has been primarily for assimilation into numerical weather prediction models and short-term forecasting. Because there are now over ten years of data, the research community could use this data for a range of applications. One of the obstacles that may be holding back more widespread use of the data for long term studies is the large amount of data

processing involved. There is great real-time information provided to approved users by NOAA (e.g. http://amdar.noaa.gov), but creating a climatology from the archived data takes additional steps. If the code is provided and the issues of the dataset such as a directional bias at coastal airports are clearly stated, then this becomes an incredibly valuable dataset is more likely to be used in other research applications.

Because of the variety of international programs that were involved with the re-emergence of aircraft data, several different systems and labels are used to refer to the aircraft data (Moninger et al. 2003). The meteorological reports are referred to as Aircraft Meteorological Data Relay (AMDAR) reports. Because of the importance of this aircraft data, a low-cost airborne instrument was installed on short-haul and commuter aircraft that serve small and medium size airports to improve coverage. This came from the Tropospheric AMDAR program (TAMDAR, Moninger et al. 2010). In the United States, it is common to call the entire dataset of aircraft observations as the ACARS data. This system is actually a service provided by Aeronautical Radio, Inc. that also includes other information related to the operation of the aircraft in addition to weather information. Another term used is the Meteorological Data Collection and Reporting System (MDCRS, Petersen 1992). For this study, the data as a whole will be referred to as ACARS.

Processing ACARS

To get a climatology of the CBL, aircraft soundings have been extracted from the ACARS point data available from the Meteorological Assimilation Data Ingest System (MADIS). Several processing steps were taken to isolate data points and define a sounding starting first with location. The orographic features of interest within the study area (Figure 2) include the Sierra Madre Mountains north of Santa Barbara, the Santa Monica Mountains north and west of Los Angeles, the San Gabriel Mountains north of Los Angeles, the Channel Islands and Santa Catalina Island within the bight region, and Point Conception.

Although the time for each aircraft reading is recorded in the file, due to the size of the dataset and the time it would take to process, the file name was used to select specific times instead of opening each file and sorting through the several million timestamps. However, the time follows through along with each data point extracted for future uses and verification purposes. In an effort to reduce processing time further and minimize the size of the processed data since the CBL is the

focus of this study, a maximum height of 3,000 m was implemented for each processed sounding. This was also done with the assumption that the majority of CBL heights will be below this limit.

After the data is sorted by latitude, longitude and time, a sounding is extracted by grouping data points together and given an index number with at most 300 seconds separating each sounding. Once the data points are grouped together by number, each group is then broken up further by tail number to isolate each plane's ACARS report. This approach insures that all data points around the same time are from the same plane so that measurements from multiple planes are not plotted as one sounding. After isolating each tail number, these subsets are defined to be soundings.

Filtering and quality control

The ACARS dataset is not perfect and requires some amount of monitoring and quality control. A limited quality control is performed for incoming raw ACARS data at NOAA's Forecasting Systems Laboratory (FSL) in which problematic tail numbers of planes that are known to give erroneous reports are flagged and isolated from the main dataset before ingestion into a numerical model. Errors are most frequent as mere formatting problems by certain digital flight data acquisition units (DFDAQs) rather than errors associated with the data sensor itself Benjamin and Schwartz (1999). The Moninger-Miller checks (Moninger and Miller 1994) that are relevant for this study include a temporal consistency and a reasonable range check.

Just one erroneous ACARS report can play havoc with a numerical model if it ends up being assimilated and not discarded. This is a high quality dataset, such that 1.3% of the data found to be in error from 937,000 observations analyzed since 1 December 1993 reported by Moninger and Miller (1994), would produce an error on the order of meters when used to analyze CBL heights. Comparing this to the errors gained when applying the algorithm used to create the climatology indicates that the errors by the ACARS reports are insignificant for the purposes of a climatology.

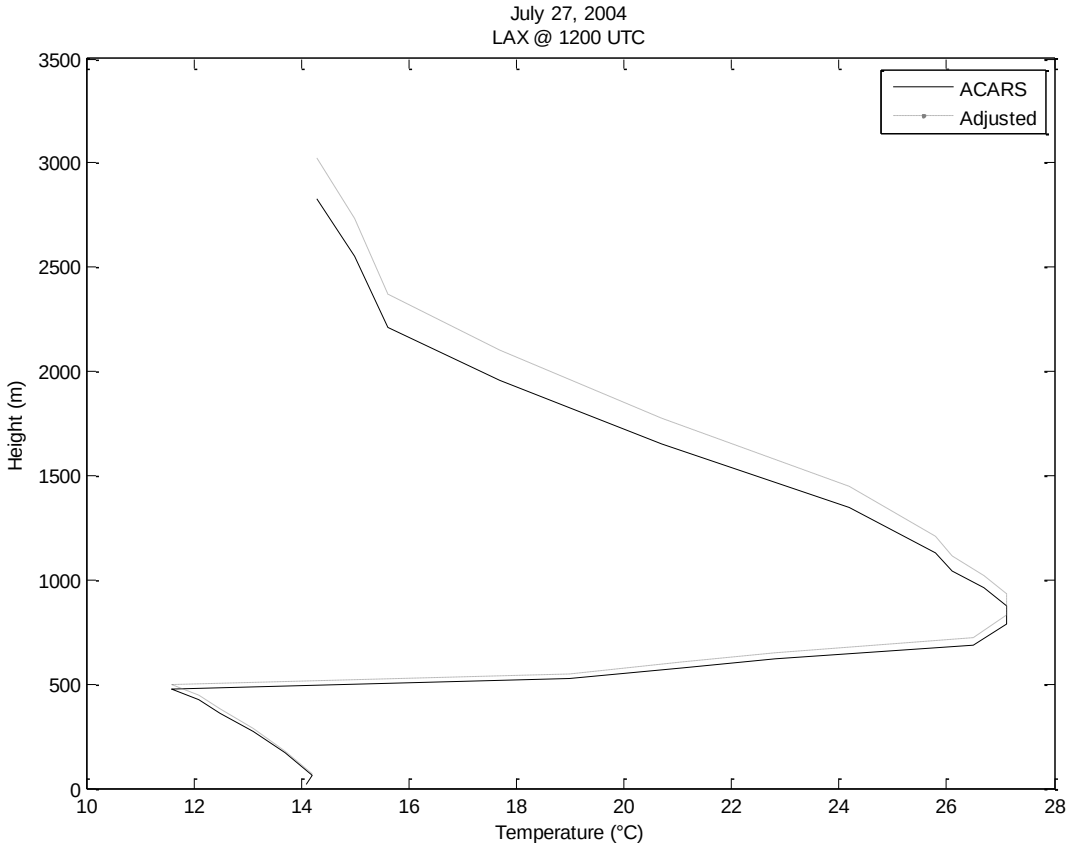

Figure 3. An ACARS sounding using standard atmosphere (solid black line) with the same sounding adjusted using hypsometric equation (black dashed line) illustrating the difference between the two.

The altitude reported in the ACARS dataset is determined by the physical variable pressure, which is converted to altitude using a standard atmosphere. This procedure is used for all altitudes and pressures for consistency. The use of the standard atmosphere instead of integrating the full hypsometric equation for height assumes that the lapse rate of temperature with height doesn't change for the first 11 km (applicable for this study). To see whether adjusting these heights using the hypsometric equation instead of using the standard atmosphere is significant for this study, the standard atmospheric height from ACARS is converted to pressure using,

$$P = 101.325\ kPa\ * \left(\frac{288.15K}{288.15K - 6.5\frac{K}{km} * H}\right)^{-5.255877} \quad (1)$$

as given in Equation 1.20 Stull (2000), which is then used with temperature from ACARS and the hypsometric equation to obtain an adjusted height. The result in figure 3 is typical of all adjusted soundings from ACARS. Results show that the difference in height in measurements are accumulative and are insignificant at lower levels (0 to ~2000 meters). The difference between the two methods is ~20 meters at the base inversion height level. The difference in height is less than the average vertical gap of ~130 meters between each ACARS measurement. The difference between the two methods starts to become important around 2,000 meters, which is well above the maximum height in the diurnal cycle found in this study and therefore, the adjustment, is not used.

Validating and CBL height

After quality control, soundings were compared to NOAA's Aircraft Meteorological Data Relay (AMDAR) data display which outputs individual ACARS soundings that were processed using slightly different criteria. The two methods were consistent. Identifying and validating CBL heights are more difficult. Under an ideal situation there would be a well-mixed layer extending from the surface until the base of a temperature inversion that would mark the top of the CBL. The atmosphere is not always ideal. The inversion may be weak or non-existent, there may be a layer above the nocturnal boundary layer with some residual turbulence left over from the previous day, or other complicating features may exist. Using an algorithm to find the bottom point of an inversion layer is a first step but, there may be several small temperature fluctuations that the algorithm may interpret as inversions which that would give false CBL heights. To complicate matters further, the boundary layer over land often decouples during the overnight hours with a stable layer developing from the surface which shows up in soundings as two distinct inversions. Depending on which inversion is chosen, a discontinuity can appear in the climatology due to a sudden shift in CBL heights to the lower or upper inversion height. These and other complications are why it is crucial to accurately and objectively locate CBL heights.

Figure 4 is an example of some of the complications that may arise when processing these ACARS soundings. The example consists of a vertical temperature profile extracted from ACARS at 1204 UTC (0504 LST) July 2001 from a flight taking off from LAX and heading to the southwest over the bight region. It is clear from the sounding that there are two distinct temperature inversions, one inversion at roughly 900 meters and another lower inversion at roughly 400 meters. The algorithm developed for this study may pick up either one of these inversions. Which one should the algorithm report? The technique to address this issue is explained below and is by no means the only approach.

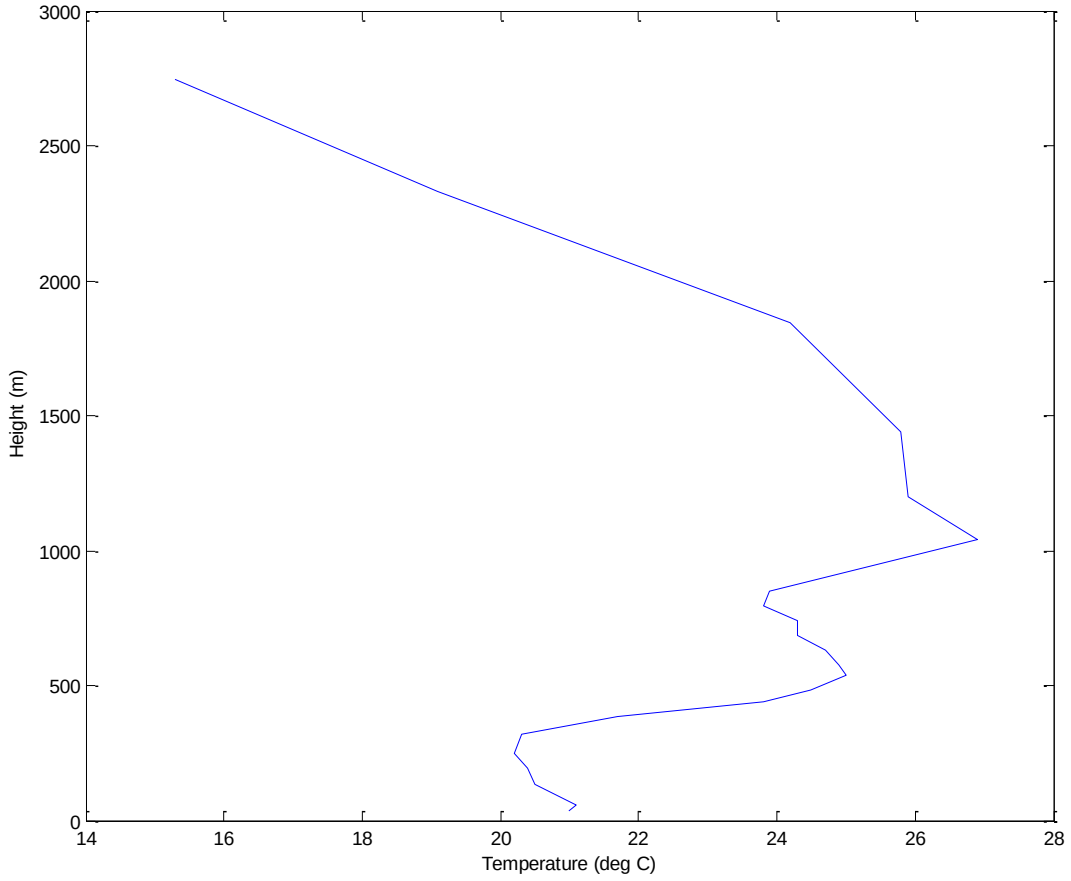

Figure 4. An ACARS temperature profile from on July 4, 2001 @ 1204 UTC from aircraft # 735 illustrating two inversion layers.

For this study, the height of the CBL is defined as the base of the inversion layer and this is determined in the temperature profile as any increase of temperature with height. For the

algorithm, this specific point will need to have the lowest value within the search criteria. For some ACARS soundings, the lowest temperature may be the bottom or top point and therefore, cannot be confidently determined to be the base of the inversion. To address this issue, the algorithm will only mark it if the temperature above and below the potential height is higher. Taking into account that the profile often has minute kinks along with potentially multiple inversions, several steps were needed. Typical CBL heights are around 400 meters and below and therefore, each temperature profile is first looked at within this range. If there are no candidates, meaning points which satisfy the criteria, then the range is shifted to 300 meters through 800 meters. 300 meters purposefully overlaps the 400 meter and below range to account for a point at 400 meters, but without a point above to satisfy the inversion definition even though it may well be the inversion. The upper bound 800 meters was determined as an upper limit of a typical CBL height as roughly 72% of all heights found fall below this height. If a point still isn't found to satisfy the inversion definition, the whole temperature profile is considered to take into account the less common CBL heights. In the event there is no single point in the whole profile that fits the definition, the CBL height is undefined for that profile.

Examining the spread of data daily, the distribution of all soundings for each hour of every month from 2001 to 2013 for LAX (and surrounding airports) in figure 5 are consistent with the daily cycle of air traffic for the area. There is more air traffic during the day (e.g., 1300 UTC to 0300 UTC) and therefore, more soundings are available. A minimum number of soundings occur from 0700 to 1200 UTC due to less traffic over night. It is important to note that this ACARS dataset has a large amount of soundings available over this 13 year period for most hours. At peak times there are upwards of 30,000 total soundings and at minimum there are 10,000 for the southern California bight region for 2001 to 2013.

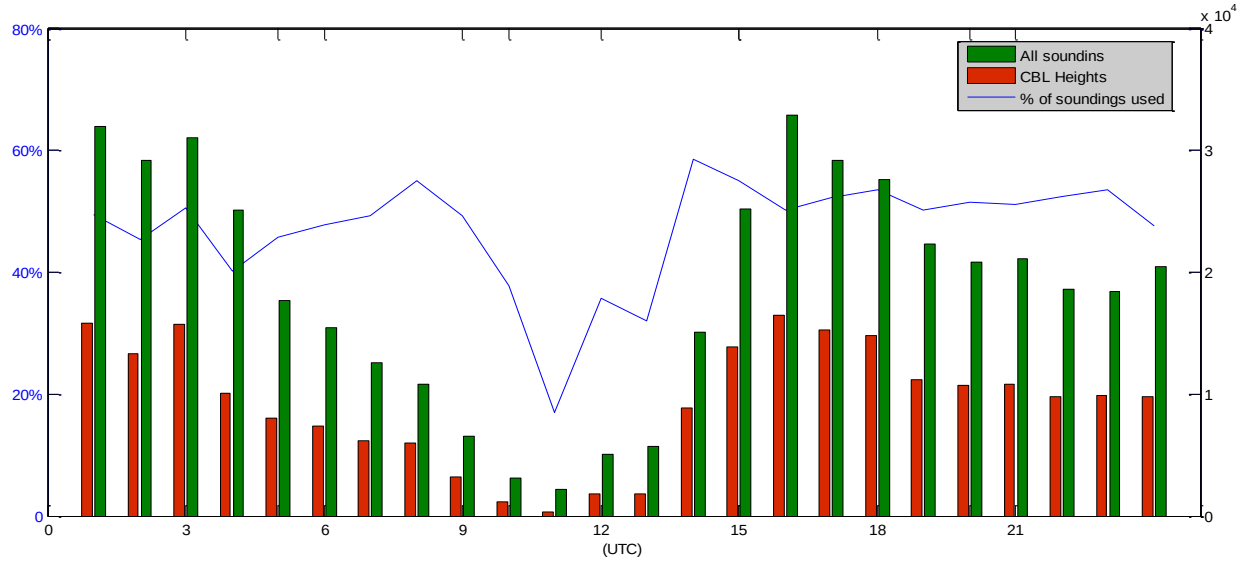

Figure 5. The ACARS dataset from 2001 to 2013 with the number of soundings available for LAX in green bars and the number of base inversion heights found in red bars. Both correspond to the right y-axis. The blue line is the ratio and corresponds to the left y-axis.

Comparing the amount of soundings extracted from ACARS to the identified CBL heights gives an indication of how often a CBL is detected. Figure 5 is a comparison of the CBL heights identified to the total number of soundings extracted for LAX each hour and includes the percentage of soundings that have identified a temperature inversion. The amount of soundings used for identifying CBL heights averages 50.5% for all hours with the exception of a window between 0800 UTC to 1400 UTC where the amount of CBL heights found drops to 17% at 1100 UTC (0400 LST). This is likely due in part to the sharp drop off in the total amount of soundings available coupled with issues dealing with the nocturnal radiation inversion layer, which often has the minimum temperature at the surface. This leads to a sounding that the algorithm passes over because if the minimum temperature is at the surface then there cannot be a point below to evaluate. Other than a small window of limited soundings available, there seems to be an adequate number of soundings for all other hours.

Summarized difficulties processing ACARS

The following is a summary of the difficulties associated with processing the ACARS dataset and how these difficulties were dealt with for this specific study.

1) The dataset is rather large (on the order of TBs for this study region) and requires access to server-based processing power to manipulate the entire dataset at once. Subsetting is likely required to perform analysis on a desktop. For this study, tabled subsets reduced this large dataset to a few hundred Mbs each, which was adequate for analysis.
2) Random data was found to be erroneously multiplied by 10. To combat this, a check was developed and placed within the data pre-processing. However; there are difficulties associated with objectively checking the data. On rare occasions, data that was multiplied by 10 was also comparable in magnitude with correct data which made it difficult which data to correct and which to leave alone.
3) Majority of data at lower levels is confined to within close proximity to airports, which drops off sharply in coverage with distance and therefore; favors higher traffic airports (e.g. LAX as opposed to SAN). This restricts more complete climatologies of the lower atmosphere to larger high traffic airports.

5. Diurnal climatology

The climatologies presented in this section show variations of the lower boundary layer during cloudy and clear conditions with the aim of examining the characteristics of the CBL under specific circumstances. Surface data (METARS) from the National Weather Service stations at LAX and SAN are used to obtain cloud fraction and cloud base height. To insure cloudy conditions apply to the clouds in the boundary layer and not aloft, cloud heights of 3,000 meters and less are used. Thus, cloudy refers to the presence of low-level (presumable boundary layer) clouds only. A cloud fraction of four or greater is used as cloudy and less than 4 is defined as clear. While examining other thresholds, it was found that for the ACARS dataset, increasing the threshold for cloudiness (e.g. a cloud fraction of 6 or 7 and higher) resulted in too few observations left to build a useful

climatology; likewise using less than 3 or 2 for clear conditions. Also, as will be shown, relaxing the cloudy and clear conditions still yields realistic climatologies.

Climatology of base inversion height using all data

The first climatology in this study is the diurnal cycle of the CBL depth using the base height of the inversion layer as the indicator. This is done using all available data, cloudy or clear, provided by the ACARS dataset from August 2001 through December 2014. Although the dataset covers Los Angeles year-around, this climatology focuses on California's dry season which is late spring and summer. This is in an effort to reduce the influences of synoptic scale phenomena such as mid-latitude cyclones and their associated frontal passages that regularly disturb the CBL in the fall and winter. This approach helps to insure that more of the climatology reflects a daily cycle and also gives a sense of the dataset's capabilities. Diurnal cycles for other bi-monthly periods can be found in the appendix.

Figure 6 shows a definitive diurnal cycle for the base inversion height of the CBL which deepens considerably just after sunset. The mean height of the boundary layer deepens 217 meters from a minimum of 440 meters an hour after sunset and deepens at a linear rate of 20 meters per hour overnight to a maximum height of 657 meters around sunrise (between 0400 UTC to 1200 UTC). The 52 m hr^{-1} drop in median height from 1700 UTC to 2000 UTC is likely an artifact from pre-processing. Heights were determined with a preference for the lower inversion height in the event there were two inversions found. This situation is most probable around sunrise to shortly after as a new CBL grows from the surface. This appears to be the case for 1900 UTC where 62.4% of all heights were below 600 meters of which 35% were between 200 and 400 meters. This is at a time when solar heating of the surface aids in the development of a new convective layer starting at the surface thus a rapid lowering of the median.

The diurnal signal in this climatology is similar to a cloud topped boundary layer in which the depth is driven by radiatively cooled, convectively unstable cloud topped air parcels turbulently mixing into the boundary layer below. The signal is evident in the data even though this climatology includes some frontal passages, cloudy and clear days, and soundings over the land and sea surfaces. The following climatologies in this section explore how much of an impact the above mentioned conditions have on the diurnal cycle of the CBL height. The climatologies are

examined by comparing the diurnal signal for a cloudy CBL verses a clear CBL to show that the dominate mechanism driving the boundary layer is indeed consistent with radiatively cooled cloud tops (at least for May and June).

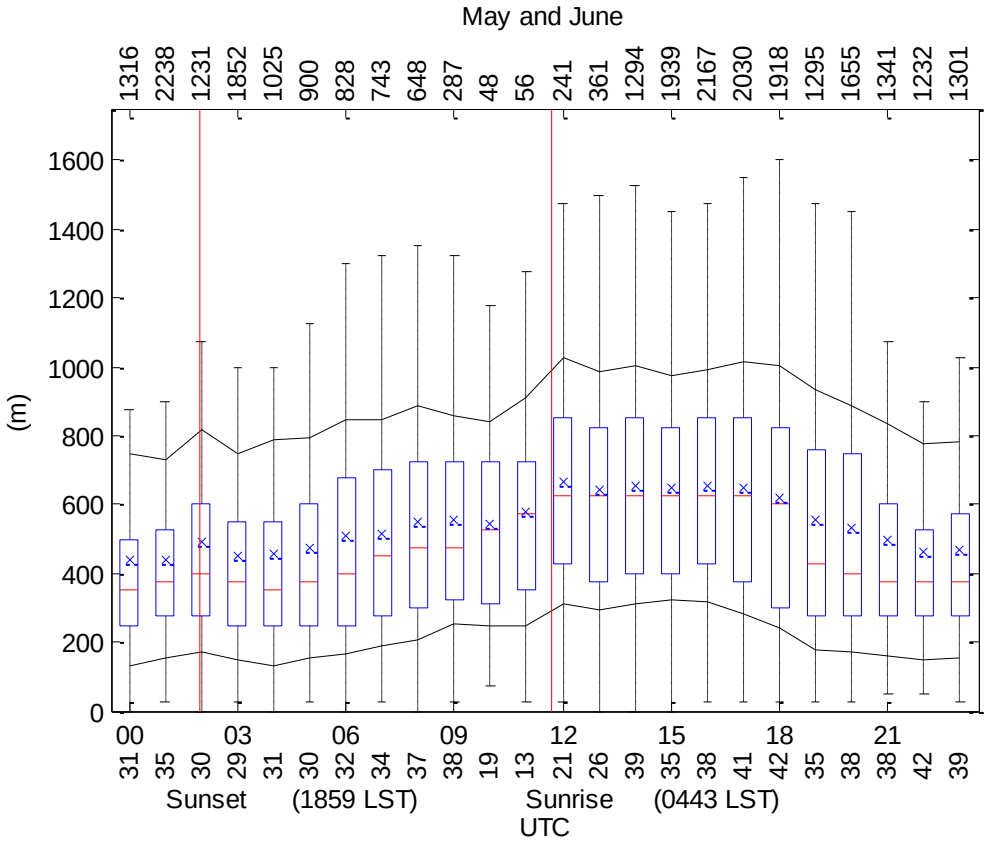

Figure 6. Mean and Median diurnal cycle of CBL heights for May and June where the blue box is the middle 50% of data (25% to 75%), red lines mark the median, blue Xs mark the mean, the black lines on above and below are the standard deviation and the whiskers show the spread of data not considered outliers. The top row of numbers is the total number of base heights used for that hour. The Bottom row of numbers is the ratio of heights to total soundings for that hour.

East verses west

The coastal city of Los Angeles is at the forefront of two distinct boundary layers. To the east is a continental boundary layer whose dynamics are dominated by daily solar insolation striking the land surface and to the west, the boundary layer is modulated by the higher heat capacity and relatively cooler temperature of the Pacific Ocean. The following climatology separates these two

distinct diurnal cycles, which may help to explain the driving force behind the overall diurnal cycle.

The climatology on the east side of LAX in figure 7b is not strictly representative of a continental boundary layer. Daily onshore flow from the sea breeze advects marine air onshore, which intrudes several kilometers inland before meeting resistance from the higher terrain of the San Gabriel's further to the east. This is especially true east and near LAX due to the airport's close proximity to the Pacific Ocean. As mentioned above, the data becomes sparser for the lower boundary layer with distance from an airport. LAX is no exception, most of the data from ACARS defined here as "east" of the airport are actually within 20 to 30 km from LAX, the majority of which are within 10 km while a few dozen have made it as far east as perhaps El Monte or Glendale. Therefore, the climatology for base inversion heights to the east of LAX are the result of a boundary layer with both marine and continental influences competing with each other. For these reasons as well as the inevitable difficulties associated with extracting strictly marine boundary layer as opposed to continental measurements from ACARS data to the east of the airport, all eastern data will be excluded from subsequent climatologies.

The climatology to the west on the other hand, largely retains the same shape as the previous climatology, comparable in shape and may perhaps have increased the smoothness. In fact, only a minor amount of data is lost when comparing the total number of soundings used per hour for figure 6 and figure 7a. This indicates that data to the east has little influence on the overall daily behavior of the boundary layer and gives greater confidence in the data to the west's ability to produce a realistic climatology. This works well for the purposes of this study because 63.7% of all boundary layer heights found in ACARS are to the west of LAX in the primary area of interest and yet a robust diurnal signal is still present.

The climatology to the west itself is indeed similar to figure 6. The boundary layer is at a minimum of 389 m to 409 m during the late afternoon (2100 UTC) to shortly after sunset (0400 UTC) then deepens at a rate of 24 meters per hour to a maximum of 662 m to 704 m overnight (1200 to 1400 UTC). A minor difference of note with figure 6 and 7a is the slightly sharper maximum in figure 7a as opposed to figure 6 where the maximum is flattened. It is not clear if this is an artifact of the data or a product of using location specific data as opposed to all data. This climatology; however, does not take into account the effects of clouds which can have a major

impact on the depth of the boundary layer. As a result, the sensitivity of the CBL from clouds is the main focus for the next section.

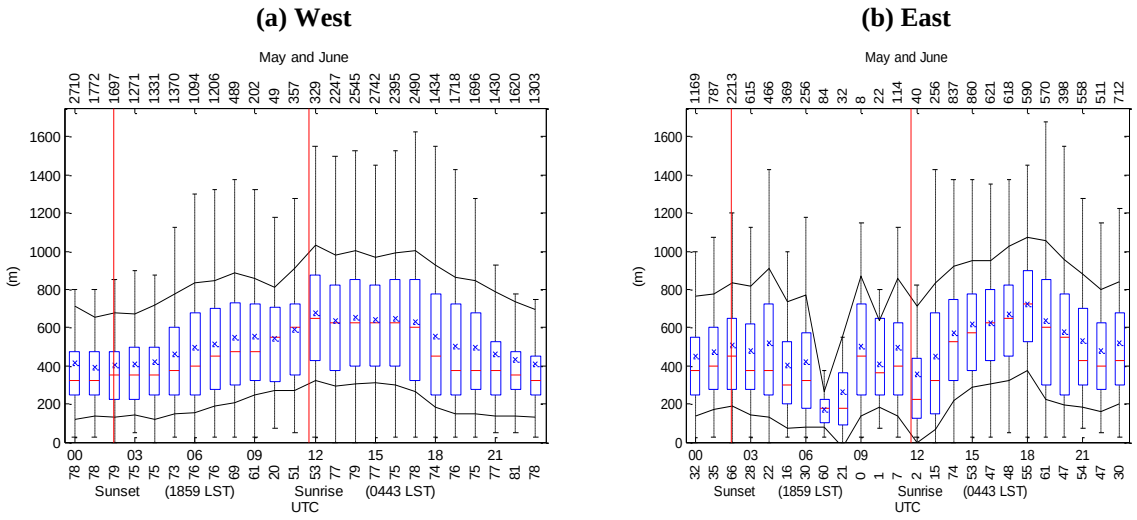

Figure 7. Diurnal cycle of CBL heights to the west of LAX (a) and to the east (b), which is presented in the same manner as figure 6.

Cloudy verses clear CBL

By reflecting and scattering incident solar radiation during the day coupled with radiational cooling of the cloud tops from the emission of longwave radiation at night, clouds play a prominent and complex role in regulating the radiation budget of the lower atmosphere. This is especially true for LAX, in which METARS report a cloud fraction of greater than 82% of every hour of the year and 52% of which are less than 2,500 m (presumably boundary layer clouds). Depending on the amount and height of cloud coverage, the diurnal cycle of the CBL depth can evolve differently in rates of deepening in times of peak boundary layer depth. The next climatology will use ACARS and METAR reports to illustrate the difference between cloudy and clear diurnal cycles and highlight the importance clouds have on the depth of the CBL.

Despite having less total data available for cloudy conditions, the diurnal signal in figure 8 is clear and robust. The difference in diurnal evolutions for the height of the CBL under cloudy and clear conditions illustrated in figure 8, significantly highlights the influence of clouds on the depth of the CBL Beginning at 0300 UTC, the boundary layer begins to gradually deepen at a rate of

12.5 meters per hour, which is consistent with the end of daytime solar insolation marking the onset of negatively buoyant parcels at the top of the stratus layer thereby promoting entrainment and deepening the CBL. The height of the CBL deepens to a peak around 1900 UTC. Interestingly enough, the transition from deepening the boundary layer to becoming shallower is faster than the averaged diurnal cycle involving all data. This brings the question as to whether this peak is real or (in part) a product of the algorithm because around 1900 UTC the CBL has had enough time to be diurnal heated and lifted perhaps out of the algorithm's priority level which would be manifested as a sharp discontinuity. Also, the response in the CBL depth is well defined at sunset as the CBL begins deepening. This is contrasted by the lag in response at sunrise where the CBL continues to deepen well into the early afternoon. The reason for this is unclear, perhaps a response to the time required for the insolation to evaporate the extensive stratus layer, in which the CBL would continue to deepen until the stratus layer is lifted and evaporated.

Due to the high heat capacity, the ocean lacks a large diurnal surface heating such as that found inland. Strong surface heating over the land during a clear day promotes turbulence that efficiently mixes and deepens the boundary layer that peaks in the late afternoon (~2300 UTC). Without the presence of clouds and little diurnal temperature change, there is a lack of a diurnal signal with the exception of two minor peaks at 1200 UTC (where there is a large range of values) and 1600-1700 UTC (figure 8). These peaks seem to be data processing related. Examining the diurnal signal for cloudy verses clear conditions, it is evident that over the ocean, the depth of the CBL is governed primarily by low level stratus and is virtually static when clear.

(a) Cloudy

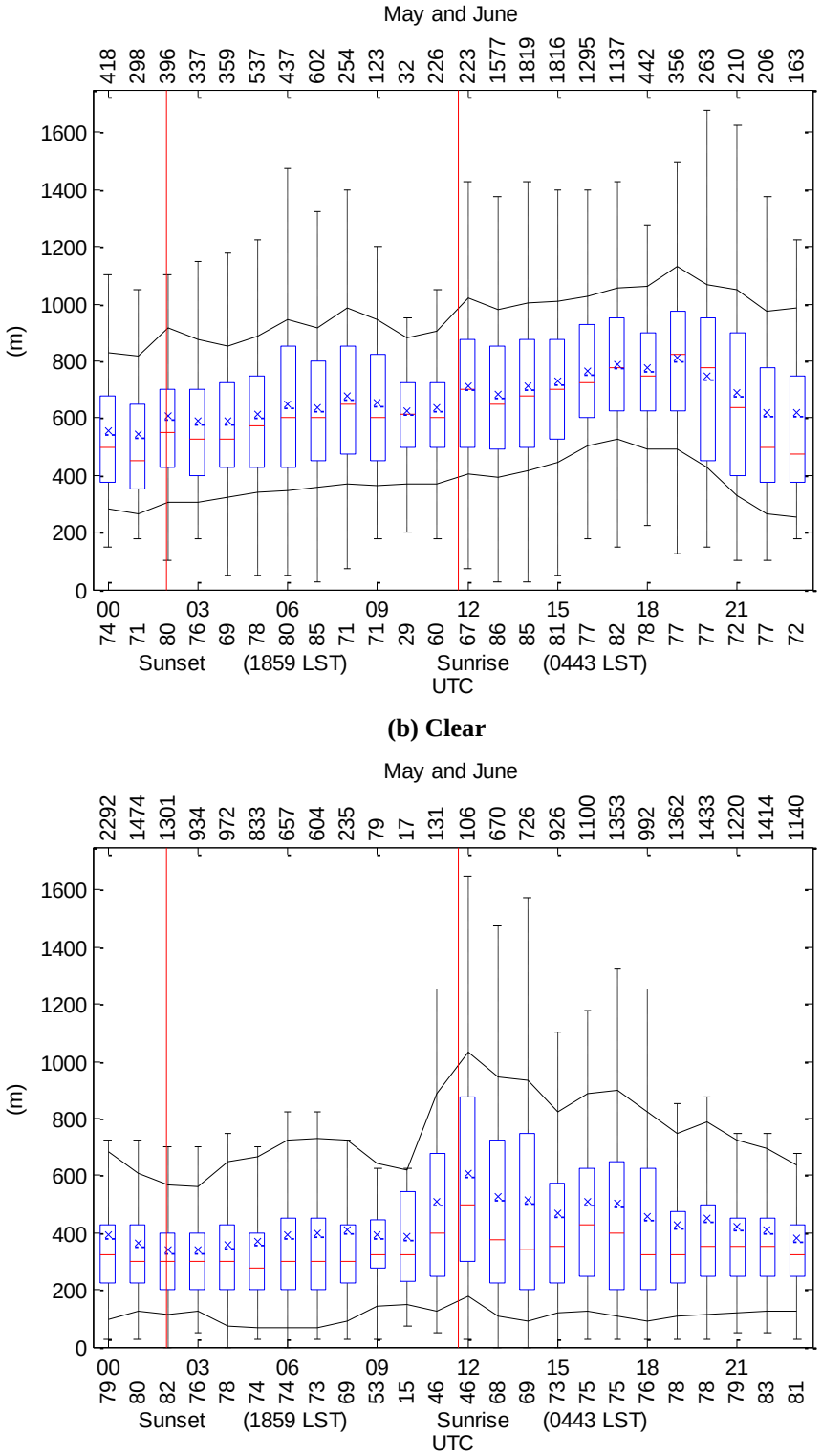

Figure 8. Diurnal cycle of CBL heights under cloudy (a) and clear conditions (b), which is presented the same as figure 6.

Climatology of the along-shore and cross-shore winds

Examining the prevailing winds in combination with the base height of the inversion layer can be an important indicator for several areas such as temperature forecasts, visibility forecasts for airports and motorists and advection of pollution. An onshore breeze can advect coastal fog and low clouds inland creating costly delays for LAX. A low CBL height (e.g. the minimum near sunset) concentrates pollution from nearby transportation hubs and industrial complexes and is transported by the prevailing wind. In this section, the winds measured from flights taking off and landing at LAX are combined with the base inversion height developed earlier to obtain a detailed picture of the climatology of the lower atmosphere. Similarly, May and June will be the focus of the discussion; however, a complete bi-monthly evolution of the along and cross-shore flow can be found in the appendix.

To get a sense of the capabilities of ACARS from LAX flights, ACARS winds are compared to the NWS surface station winds shown in figure 9. The 0 to 10 meter winds gathered from ACARS, corresponded well with wind data from the nearby NWS surface station. The results show that the two datasets are virtually identical in direction with minor differences in how often a particular wind speed and direction occurred. Both wind roses show that the prevailing winds are out of the west (285^{o}) for the majority of time, which is likely due to the sea breeze. This result shows that ACARS can indeed accurately record winds at different levels useful for climatologies.

(a)

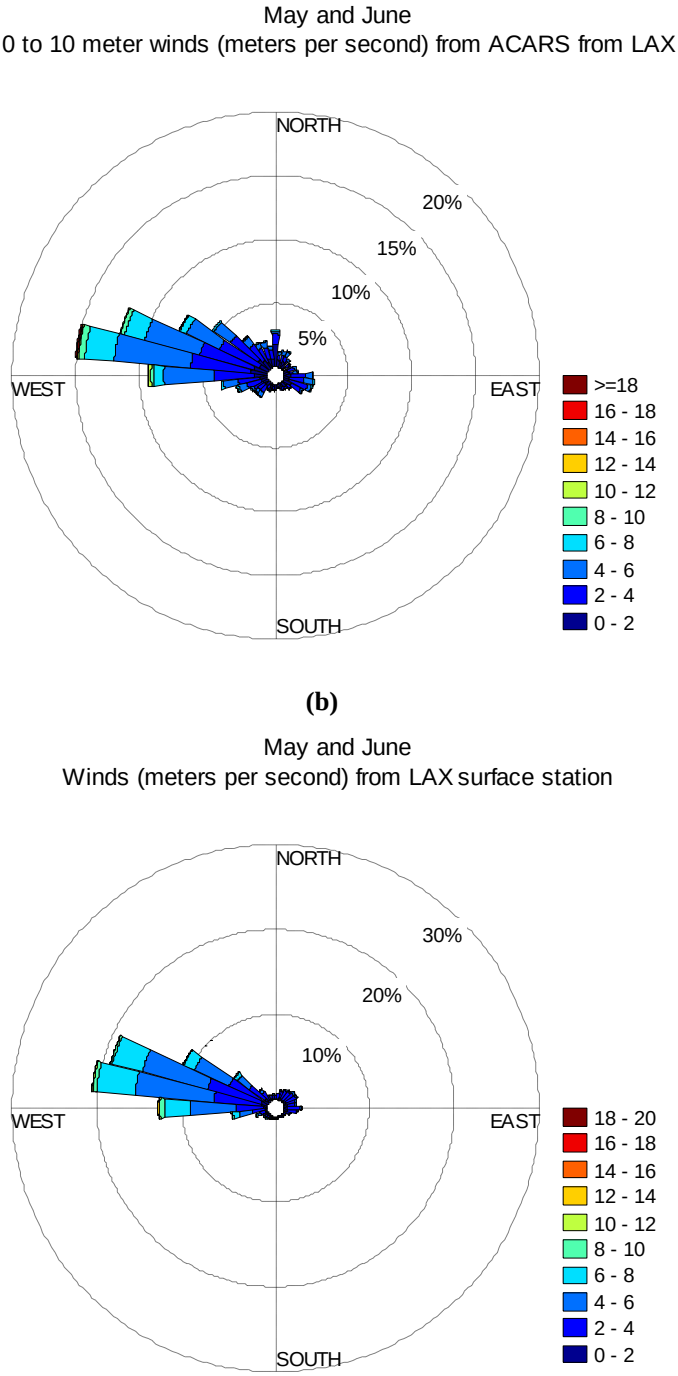

Figure 9**.** 0 to 10 meter winds (m s^{-1}) from ACARS (a) and surface winds from the NWS surface station at LAX (b).

Perhaps the greatest success using ACARS for this study is the evolution of the vertical wind profile. Overall, along-shore and cross-shore minimums and maximums are clearly evident for all bi-monthly plots presented. This is true even examining a bi-monthly period for a single

year. ACARS wind data comes in speed and direction thus all winds were converted to zonal (u) and meridional (v) components and rotated -65^{o} to align with the orientation of the coast and give the alongshore and cross-shore wind components. The observations are binned every hour and the components were linearly interpolated to regular vertical intervals to construct the average diurnal cycle.

A sea breeze is clearly evident when examining the top of figure 10, which shows the cross-shore winds for an average 36 hour period (the first 12 hours repeated) during May and June. The cross-shore wind profile suggests the sea breeze initiates roughly 3 hours after sunrise indicated by a shift from offshore to onshore flow at the surface. This is consistent with the onset of differential heating between inland and offshore. Onshore flow is initially evident at the surface with weak off-shore flow aloft. As diurnal heating continues, onshore flow at the surface increases at a rate of 0.5 m s^{-1} hr^{-1} before reaching a maximum of 2.9 m s^{-1} at 2200 UTC (1500 LST). As time progresses, the cross-shore wind component gradually shifts onshore vertically from the surface at a rate of 133 m hr^{-1} until reaching the top of the CBL when all flow within the average CBL shifts onshore at 2200 UTC. This shift to onshore flow with height also extends beyond the depth of the average CBL from 2200 UTC when the CBL nears its minimum until 0500 UTC when the CBL deepens overnight. The maximum onshore flow aloft of 2.6 m s^{-1} at 350 m lags an hour behind the surface maximum. Onshore flow at all heights within the CBL uniformly decrease at a rate of 0.33 m s^{-1} before shifting to offshore flow 5 hours after sunset at 0800 UTC (0100 LST). Offshore flow over night is much weaker than onshore flow during the day with values < 1 m s^{-1}. This is consistent with the climate for LAX this time of year, which has average afternoon high temperatures of 23^{o}C inland and a near-shore sea surface temperature 16^{o}C. This is in contrast to overnight inland temperatures that approach 16^{o}C.

A clear diurnal cycle is also present in the along-shore component of the winds within in the CBL. At sunrise, along-shore flow is from the southeast at all heights within the CBL. Flow is light to calm at the surface and increases with height to the top of the CBL. A shift from southeasterly to northwesterly flow occurs gradually with height starting from the surface shifting at a rate of 75 m hr^{-1} until the top of the CBL beginning at 1600 UTC and lasting throughout the day. Along-shore flow at the surface shifts from a light breeze of 0.67 m s^{-1} out of the southeast shortly after sunrise, to a stronger northwesterly flow of -4.80 m s^{-1} just before sunset. Southeasterly along-shore flow near the top of the CBL increases to 3.0 m s^{-1} at 1700 UTC shortly

after sunrise. The maximum occurs before gradually decreasing in magnitude at a rate of 0.5 m s^{-1} hr^{-1} over 6 hours at which time the along-shore component briefly shifts to a northwesterly flow from 0000 UTC to 0200 UTC. At sunset the flow aloft shifts back to a southerly flow over 2 to 4 hours depending on the height. The exception being at the surface where the along-shore component remains northwesterly for all hours, apart from a small window between 1200 UTC and 1600 UTC where the flow briefly shifts southeasterly. The magnitude of this southeasterly flow at the surface is light remaining under 1 m s^{-1}.

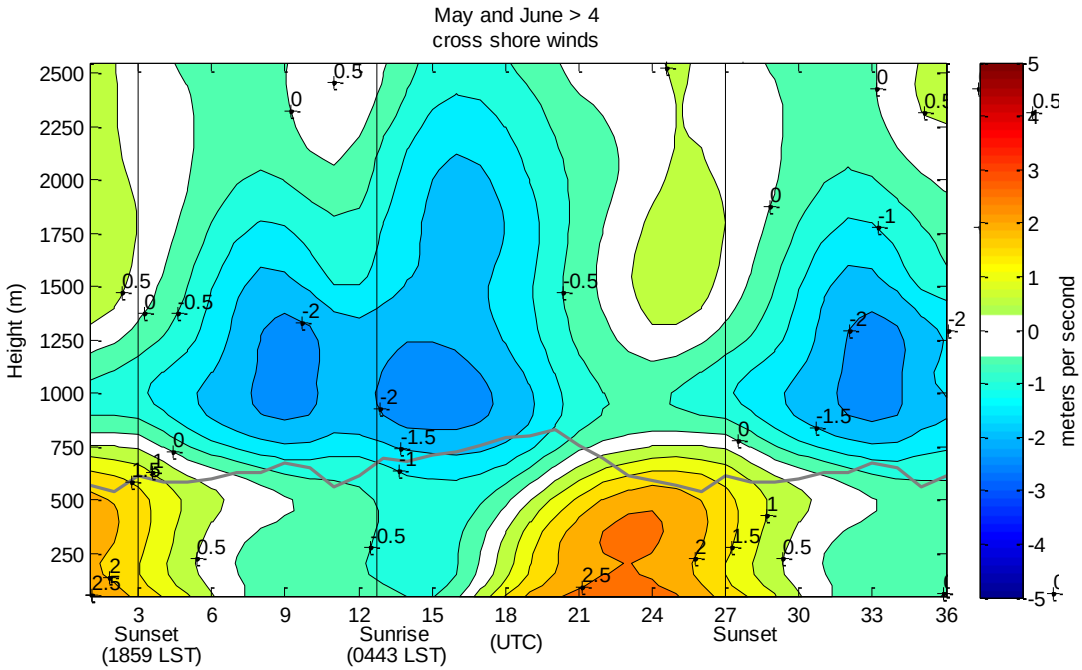

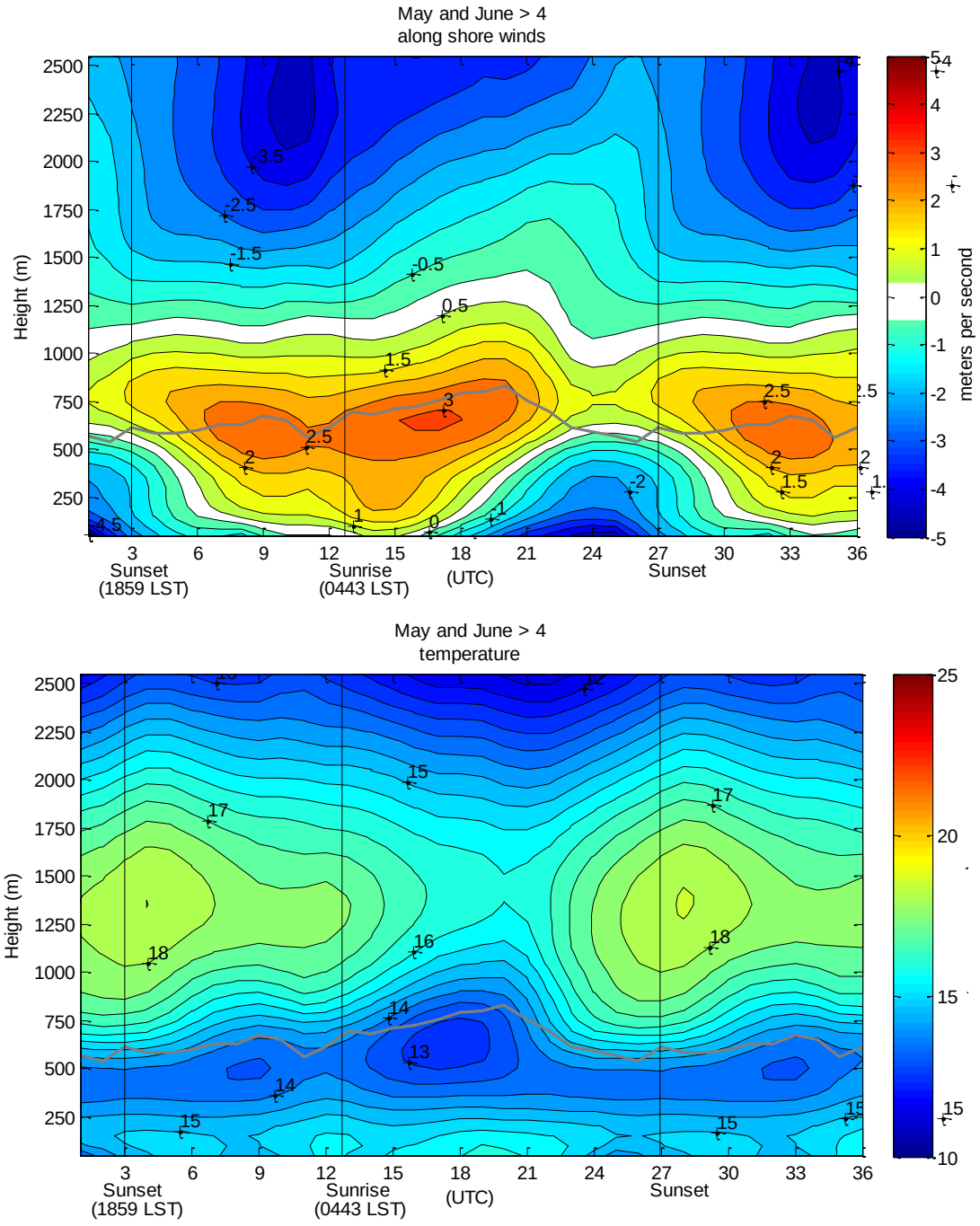

Figure 10. 36 hour climatology of the evolution of alongshore (295°), cross-shore (25°) winds (m s^{-1}) and temperature during cloudy days. Gray line is the average CBL height, the black vertical lines mark sunrise and sunset, which are annotated respectively.

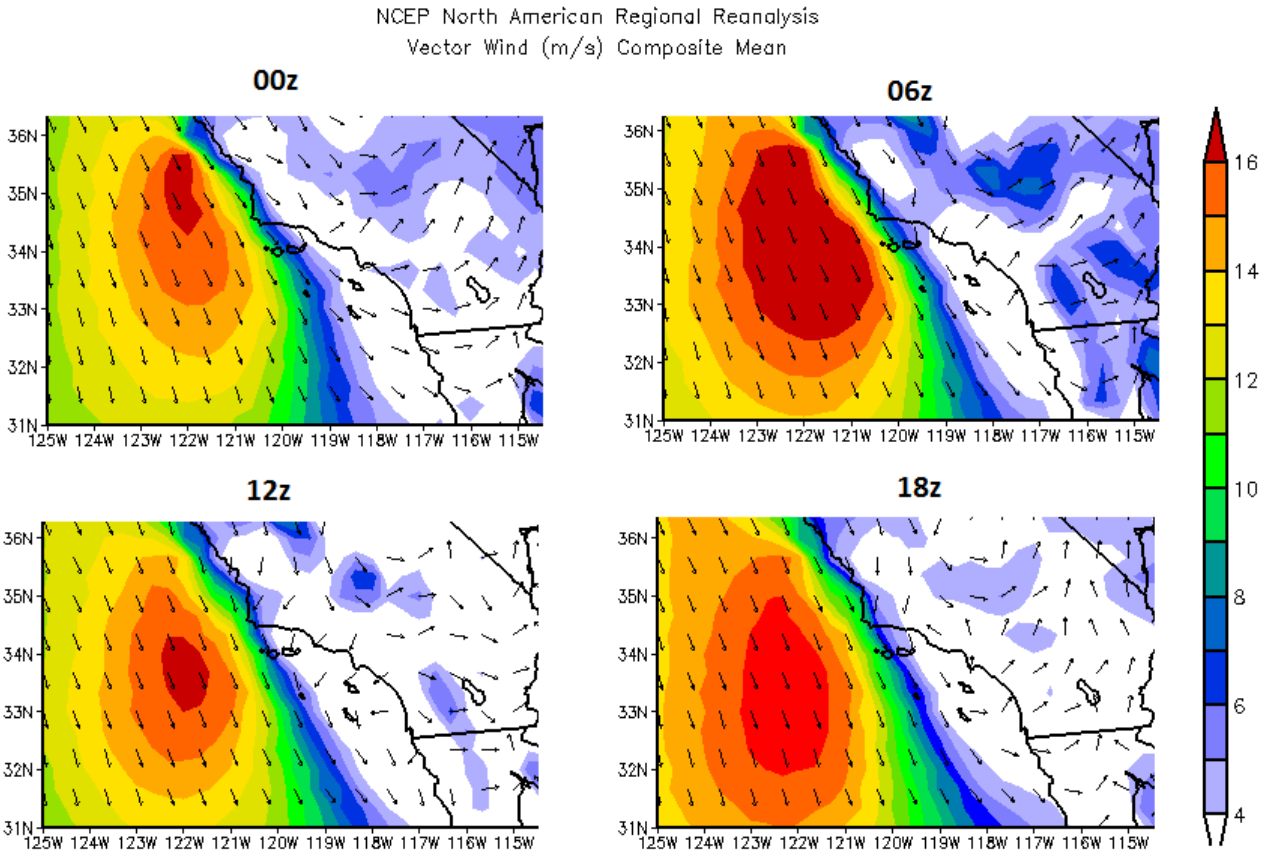

Figure 11. NARR reanalysis climatology of the 975 mb (~300 m) winds for June 2006.

Overall, winds at LAX show a clear diurnal cycle in both components. The sea breeze shows up clearly in the cross-shore flow with a maximum of onshore flow during the afternoon hours within the boundary layer. Aloft, the inversion layer is dominated by offshore flow and is assumed to be tied to synoptic flow although there is a weak diurnal signal as well. Within the persistent northerly flow aloft the speeds reach peak intensity overnight and become light in the afternoon hours. This type of cross-ridge flow looks similar to a local wind known as a "sundowner", which is a downslope, katabatic wind that occasionally occurs in conjunction with northerly synoptic scale winds that flow over the Santa Monica or San Gabriel mountain range. Although this specific wind can occur at any time of year and at any time of day, northerly flow aloft is most frequent during May and June due to the synoptic conditions discussed earlier in the introduction. The better known Santa Ana winds which are also downslope winds are more prevalent in the fall and winter and are associated with a stronger anticyclone to the northeast. The NCEP climatology of 975 mb winds for June in figure 11 also support the northerly winds crossing

the mountain ranges at all hours given to some degree. NCEP climatologies at 925 mb and 850 mb were also found to be similar to 975 mb in that there exists cross-ridge flow aloft. The cross-shore and alongshore winds aloft suggests that this flow is contained above the inversion layer. This is where the boundary layer height developed in this study marks the base of the inversion. The temperature plot in figure 10 shows the average height of the inversion top at roughly 1300 m, which is beneath both the offshore flow and alongshore aloft. For the alongshore winds, southerly flow is at a maximum in the morning at the top of the boundary layer, which is neatly tied with the slope of the maximum depth of the CBL. As the stratus deck thins or evaporates due to diurnal heating, the height of the boundary layer drops and the alongshore component aloft decreases to a minimum during the late afternoon, while southerly flow at the surface in the morning quickly transitions to a northerly flow late in the afternoon hours at the same time the sea breeze is occurs.

6. Summary and conclusions

In this summary, along and cross shore winds as well as height differences from San Diego and Los Angeles are analyzed to paint an overall picture of the bight region and also offer evidence as to why conditions in the California bight are favorable for the development of eddies in May and June. Circulation within the Catalina eddy contains a southerly component near and along the coast north of the San Diego area, which propagates northward towards Los Angeles as discussed in Mass and Albright (1989). These eddies are constrained to the east by the coastal range and to the west by the low level coastal jet past Point Conception, which implies the initiation of an eddy is in some part mechanically generated. Two proposed forcing mechanisms for a Catalina eddy that were mentioned in the introduction are an ageostrophic response to blocked onshore flow and an offshore flow aloft that creates localized mesoscale leeside trough that induces cyclonic motion within the bight region, are both investigated using figures derived from ACARS.

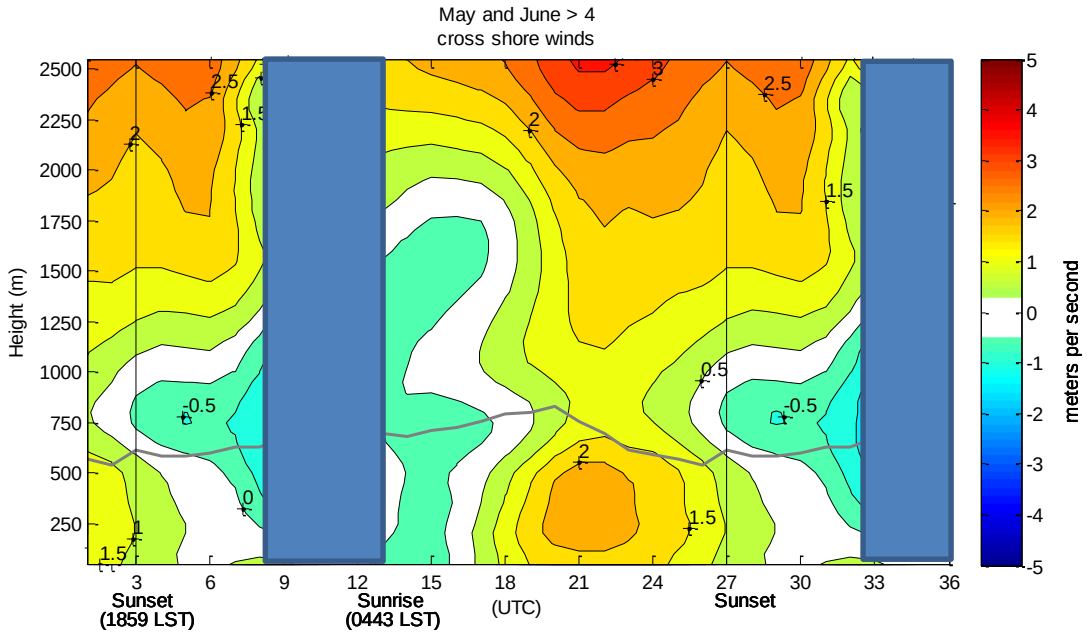
May and June > 4
cross shore winds
Height (m)
meters per second
Sunset
(1859 LST)
Sunrise
(0443 LST)
(UTC)
Sunset

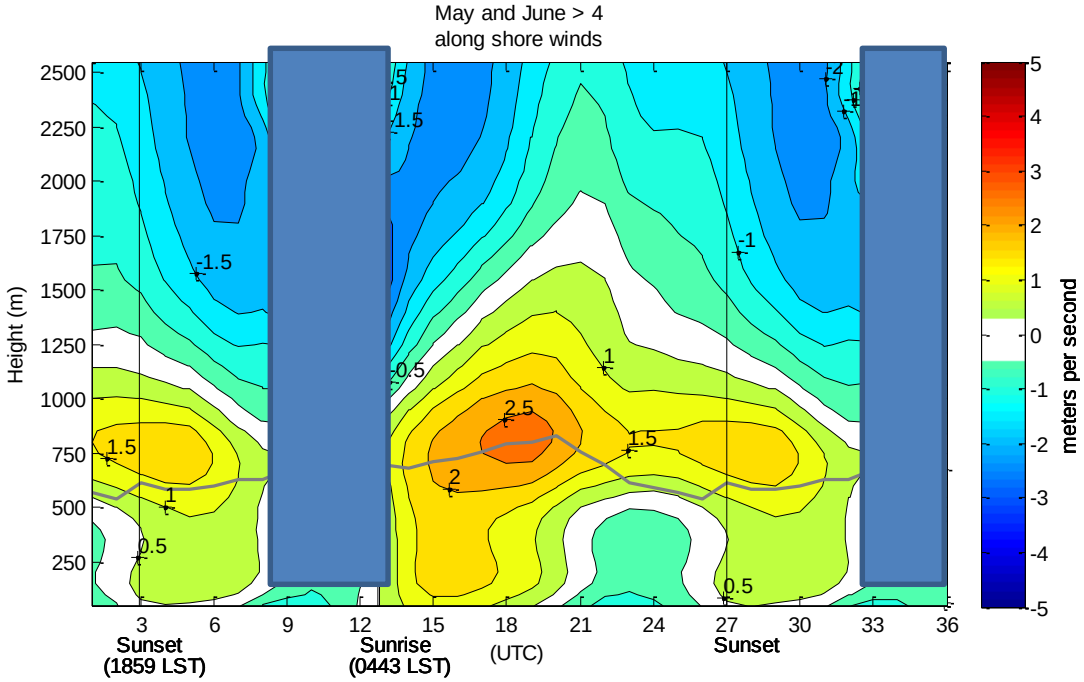
May and June > 4
along shore winds
Height (m)
meters per second
Sunset
(1859 LST)
Sunrise
(0443 LST)
(UTC)
Sunset

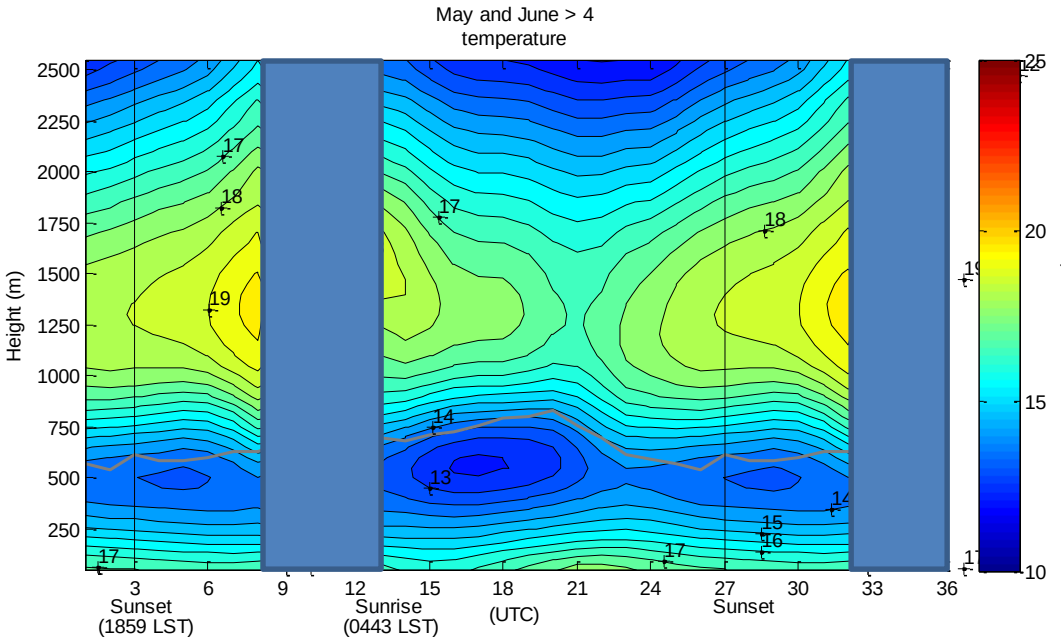

Figure 12. Climatology of alongshore and cross-shore winds at SAN (San Diego Int'l Airport) rotated 45º counter-clockwise and presented in the same manner as figure 10. The blue rectangles block hours with few observations.

As mentioned in the introduction, a persistent low level jet at the top of the marine boundary layer just off the coast turns toward the east to the south of Point Conception. This is evident in the 1800 to 0000 UTC reanalysis data (figure 11). A change to a more onshore direction is likely associated with some convergence with the coastal mountain range due to the height of the CBL being lower than the coastal mountains and would be consistent with typical visible satellite images, Mass and Albright (1989) and Eichelberger (1971). However, it is difficult to see any obvious signal for converging flow around San Diego in the cross-shore component directly from analysis. Northward acceleration associated with a concurrently deepening CBL (Figures 10 and 11) is evident in the along-shore component with a wind maximum around 1900 UTC at the top of the CBL. In fact, figure 11 suggests that southerly flow exists in various magnitudes throughout the CBL, which is initiated at sunrise and lasts until late afternoon. The southerly low level wind maximum near and parallel to the coast would propagate marine stratus northward, which is what is commonly observed during May and June and especially during a Catalina eddy event. This southerly flow could also converge on the San Gabriel and Santa Monica Mountain ranges, which would help to deepen the CBL overnight near LAX. An overnight increase in

southerly wind is evident in figure 10 where there is a large maximum in the along-shore component for LAX lasting all night and the mid-morning, which corresponds to the alongshore winds for SAN. However, this flow could also turn west toward the ocean north of LAX so comprehensive spatial measurements near and around the slopes of the San Gabriel and Santa Monica Mountains including pressure and winds for both May and June would be desired in order to be conclusive about convergence. The point measurements provided by ACARS, while sufficient in temporal resolution, lacks the horizontal resolution that is needed to make conclusions regarding the spatial characteristics and influence of convergence. That being said, assuming convergence occurs just north of LAX, buildup of mass within the boundary layer associated with a deeper CBL would occur overnight and is followed during the day by a thinning CBL and a reversal of the flow, which is suggested in figure 10. Of course this interpretation only considers the alongshore component and processes and neglects other factors like cross-shore convergence, radiational forcing, subsidence aloft, and so on.

Due to LAX's close proximity to the base of the Santa Monica and San Gabriel mountain ranges, the persistent northerly flow aloft (above the maximum height of the Santa Monica and San Gabriel Mountains (~2000 m) in figure 10) implies that this northerly flow originates from over the mountains. If this is the case, the shift from southerly to northerly flow could be the result of leeside troughing and suggests that the offshore flow above the CBL develops in the late afternoon and strengthens overnight. This northerly flow is likely downslope and associated with adiabatic warming from subsidence in the ~750-1500 m layer (figure 10). The warmer temperatures in the column would also be associated with lower pressure and promote a mesoscale pressure trough near LAX. The offshore flow at SAN is much less, which would suggest little to no leeside troughing. As a result, this would favor an alongshore pressure gradient with lower pressure near the San Madre and San Gabriel mountain ranges around Santa Barbara and LAX with higher pressure near SAN. This would result in northerly winds developing in the late afternoon and early evening, which is what is seen in LAX (figure 10) and to some extent, San Diego (figure 12).

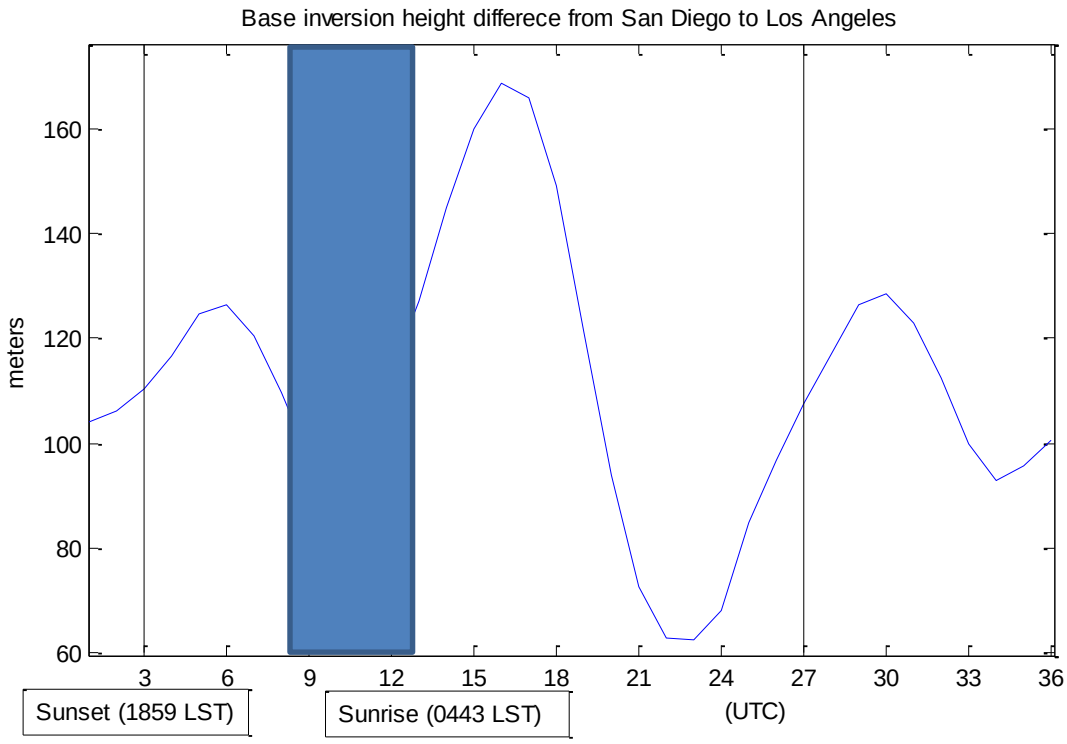

Figure 13. Base inversion height difference from SAN to LAX using all data available from ACARS for the months of May and June. The blue box blocks the hours where there is less data available particularly at SAN.

This southerly flow is allowed to continue to be maintained until the morning where the cycle starts over again, which satellite images support, commonly showing stratified low level clouds surging northward from the Baja Peninsula in the early morning hours during Catalina eddy events. One caveat to the importance of the offshore flow and strength of the subsidence and warming is that the maximum in northerly flow aloft for Los Angeles occurs during the overnight hours when the boundary layer is shown to be deepening. If there is strong downslope flow above the CBL overnight, this would promote a decrease in the depth of the CBL, suggesting that even if downslope leeside troughing does occur aloft, other forcing mechanisms (e.g., deepening overnight associated with cloud top cooling or convergence with the CBL) are more influential for controlling the overall depth of the CBL.

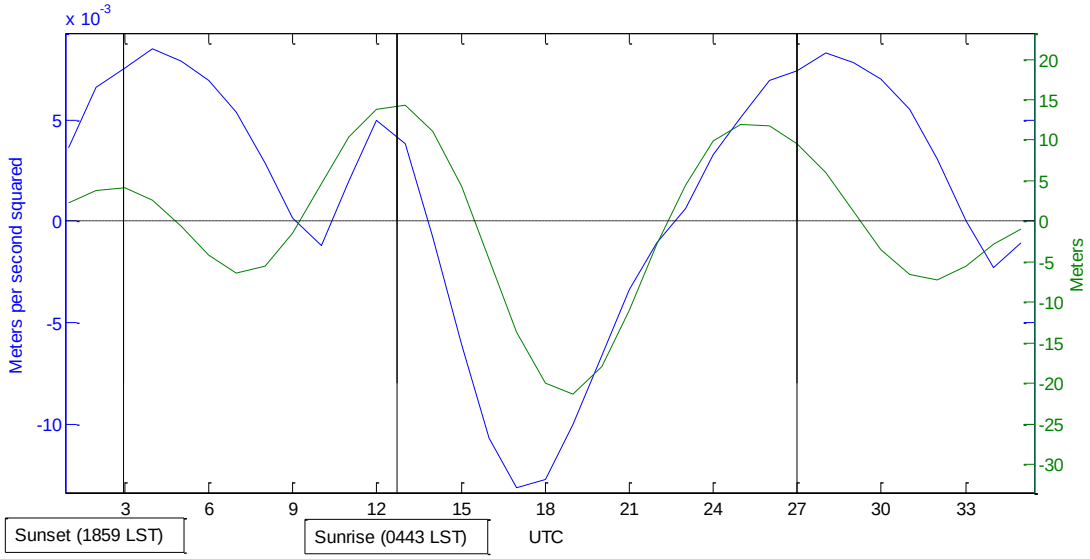

Figure 14. The acceleration of the along shore flow at 250 meters from LAX (blue line) and the inversion base height difference from San Diego to Los Angeles (green line) for the months of May and June.

Figure 13 shows the average diurnal CBL height difference from San Diego to Los Angeles. Due to less data available overnight for the smaller SAN airport, 0800 UTC to 1300 UTC is blocked out. Assuming a relatively deeper boundary layer results in a higher pressure, a CBL at SAN that is deepening more than at LAX would correspond to a northward acceleration. This is what figure 13 shows, which is a maximum difference in CBL height at 1600 UTC with a difference of 169 meters, suggesting an acceleration of alongshore flow. This maximum in the difference in CBL height and subsequent average acceleration also coincides with the southerly alongshore wind maximum shown in figures 10 and 12. This result is more indicative of convergence at or to the south of San Diego at explaining the height difference and thus southerly flow at both locations. In either case, the change in the difference in base inversion height from San Diego to Los Angeles does well in explaining the diurnal acceleration in the alongshore component of the flow over Los Angeles as shown in figure 14. This result not only shows how well the ACARS dataset can be for examining the CBL, but also shows that perhaps with a bit of refinement, the acceleration of the southerly component over LAX can be predicted using CBL height (an r^2 value of 0.6078).

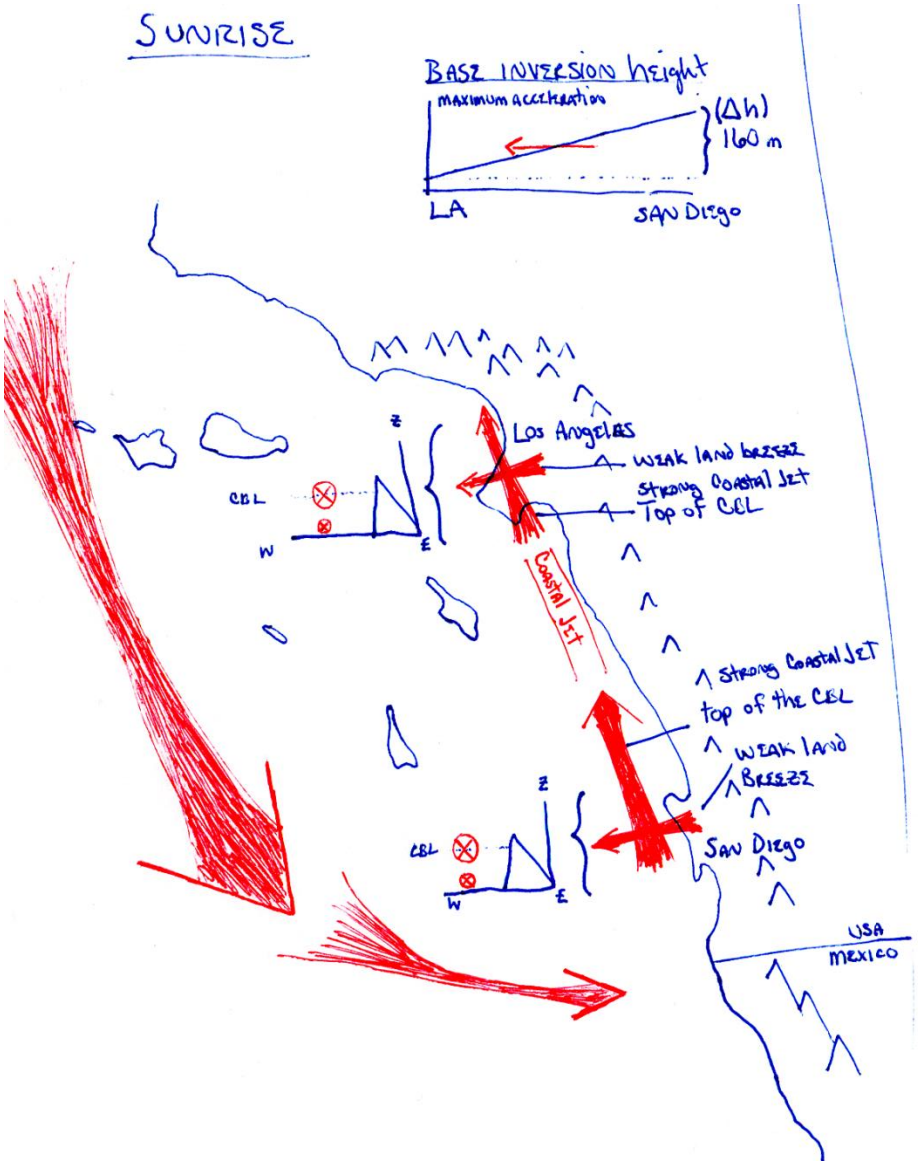
SUNRISE
BASE INVERSION height
maximum acceleration
(Δh)
160 m
LA
SAN Diego
Los Angeles
weak land breeze
strong coastal jet
Top of CBL
CBL
W
E
z
Coastal Jet
strong Coastal Jet
top of the CBL
weak land
Breeze
San Diego
USA
MEXICO

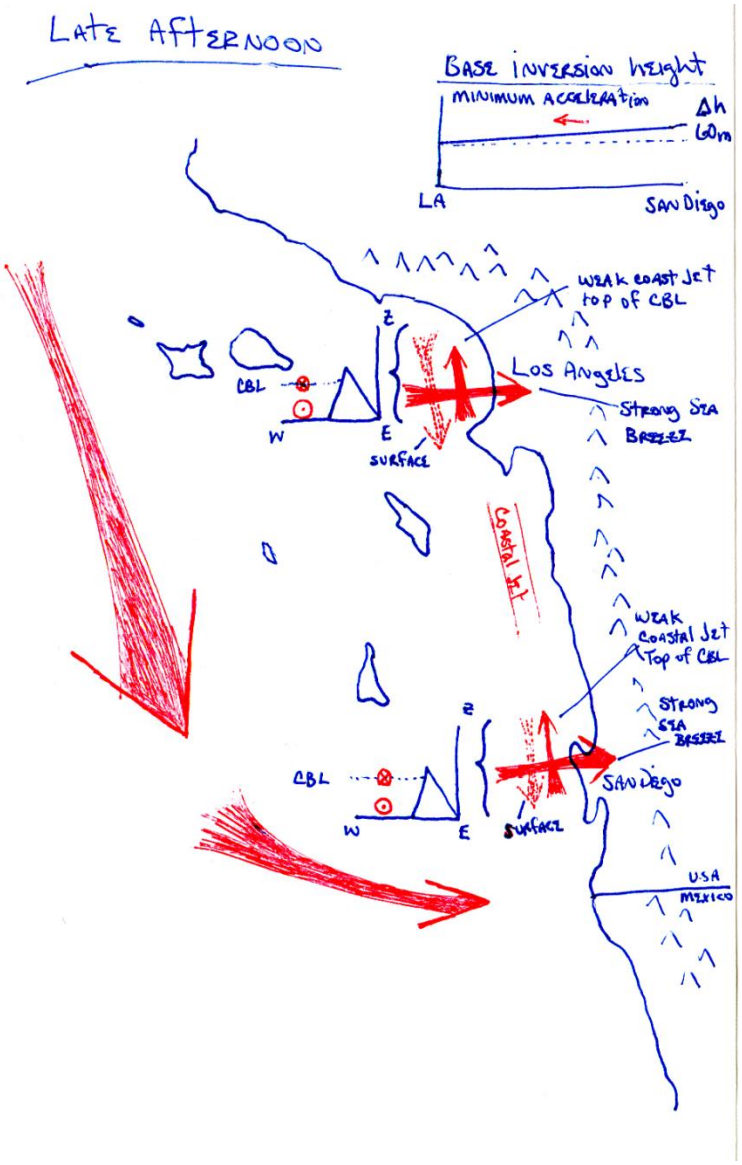
LATE AFTERNOON
BASE INVERSION height
minimum acceleration
Δh
60m
LA
SAN Diego
weak coast jet
top of CBL
Los Angeles
strong SEA
BREEZE
CBL
W
E
z
surface
Coastal Jet
weak
Coastal Jet
Top of CBL
strong
SEA
BREEZE
San Diego
USA
MEXICO

Figure 15. Conceptual diagram of known flow patterns and results from the ACARS climatologies with average conditions at sunrise on the left and average conditions for the late afternoon of the right. Conclusions at the bottom right.

Figure 15 summarizes the above results from ACARS to draw an average scenario for the bight region of southern California. At sunrise convergence near and to the south of San Diego is associated with a relatively deeper CBL as compared to Los Angeles where there is less onshore wind. The difference in CBL depth and the alongshore wind speed are both a maximum at sunrise. The alongshore CBL supports a strong northward alongshore pressure gradient with maximum acceleration pointing to the north. This results in strong southerly flow throughout the depth of the boundary layer and a coastal jet parallel to the mountain ranges at the top the CBL from San Diego to Los Angeles. At the same time, the land breeze is decelerating and transitioning to a sea breeze as differential heating continues. Due to relatively higher stability at the top of the CBL than in the afternoon, blocking to the north and deflection to the west seems likely which would also be aided by the land breeze. The overall wind field is conducive of a large scale counter-clockwise circulation within the CBL.

During the afternoon hours, a maximum diurnal heating is in effect resulting in strong onshore flow and less stability. The difference in CBL depth resulting in strong southerly flow from San Diego to Los Angeles in the morning has decreased to a minimum although is still deeper at San Diego. This results in a weak acceleration to the north and a weak coastal jet at the top of the CBL. Southerly flow at the top of the CBL at near LAX would likely encounter the San Gabriel and Santa Monica Mountains to the north and either be blocked or flow over them. Weakening stability during the afternoon hours could result in some upslope flow to the north and east of LAX depending on the strength of the sea breeze and southerly flow at the top of the CBL. The height of the Channel Islands (~400-800 meters) to the west of LAX near Point Conception is often higher than the low level jet resulting in split flow with a portion of the northwesterly winds flowing around the north side of the islands. SSTs near Point Conception are cooler than SSTs in the southern bight and so these winds close to the surface would likely be denser than air within the bight. If that is the case, then that would explain the observations showing strong northerly flow in the afternoon with relatively weaker flow at the top of the CBL. The observations for the bight region in the afternoon are relatively less conducive of counter-clockwise circulation, which is

consistent with satellite observations that show eddy circulations losing strength in the afternoon hours.

Conclusions about the dataset

An inversion capped turbulently well mixed coastal boundary layer in combination with the coastal range acting as a lateral barrier sets the stage for several coastal phenomena including wind reversals, hydraulic jumps, expansion fans, and eddies. All of which present difficulties for forecasting, transportation and recreation. Field studies have been conducted in an effort to better understand these phenomena, but the lack of long term data due to the length of the campaign is usually the limiting factor. While operational soundings offer adequate vertical temperature and wind profiles at those specific times, as this study has shown, ACARS can provide the same quality of data at different times and at long timescales and at less of a cost than a field study accomplishing the same task.

Several difficulties associated with constructing these climatologies were noted in this study. Some quality control was needed for pre-processing including flagging formatting issues, double entries, and missing data. A plane's ascent rate is usually higher than the decent rate resulting in slightly less vertical resolution of the measurements during takeoff. If a particular application depends greatly on the vertical resolution, consideration should be given to whether the flight is landing or taking off. ACARS's ability to produce soundings is of course dependent on the air traffic and subject to highly variable sampling. Thus, at low traffic times such as from 0000 to 0500 LST, there is a drop in the amount of data available and much more during the morning and afternoon high traffic times. If this data is to be used to study the boundary layer, coverage for the lower atmosphere, it will be limited to within close proximity of airports. However, even with these difficulties and limitations, ACARS is able to produce high quality climatologies of winds and temperature at or near airports, especially at higher traffic airports e.g. LAX. Humidity sensors in the fleet are currently sparse, but advances in reliable equipment are likely to increase the number of sounding reporting the humidity.

Additional findings

- The CBL over LAX deepens overnight on average, which is consistent with cloud topped radiative cooling playing an important role in the mean diurnal cycle of the depth for this region.

- The diurnal signal for the base inversion height is much smoother to the west than to the east. This suggests that west of the airport is more consistently a marine layer while there are likely competing influences of marine and continental processes that add to the spread of CBL height to the east.

- The strongest northerly winds happen overnight when the boundary layer is deepening and the weakest northerly flow occurs in the afternoon when the boundary layer is thinning, suggesting leeside troughing is unlikely the main control for CBL depth over LAX.

- The northward flow from San Diego to Los Angeles is the strongest at the base of the inversion in the morning and is the weakest in the afternoon and evening.

- The largest difference in base inversion heights from San Diego to Los Angeles occurs at sunrise with a corresponding maximum in alongshore wind acceleration and wind speed. A minimum in difference occurs during the afternoon with a corresponding minimum in acceleration of the alongshore flow and wind speed. This relationship correlates well diurnally with a correlation coefficient of 0.6.

- Southerly flow aloft with northerly flow at the surface for both locations suggests a return flow in the afternoon hours.

Future possibilies

- Concerning leeside troughing near LAX, although analysis here has shown little evidence of this, wind and pressure measurements on the lee of the San Gabriels and Santa Monica Mountains would be desired to detect downslope winds and pressure drops before being conclusive.
- After finding how correlated the acceleration in the along shore wind component is to the change in the height difference, this relationship may be of use in predicting Catalina eddies and should be investigated further due to the disruption and delays these events cause.

Appendix

Climatology of CBL heights using all data

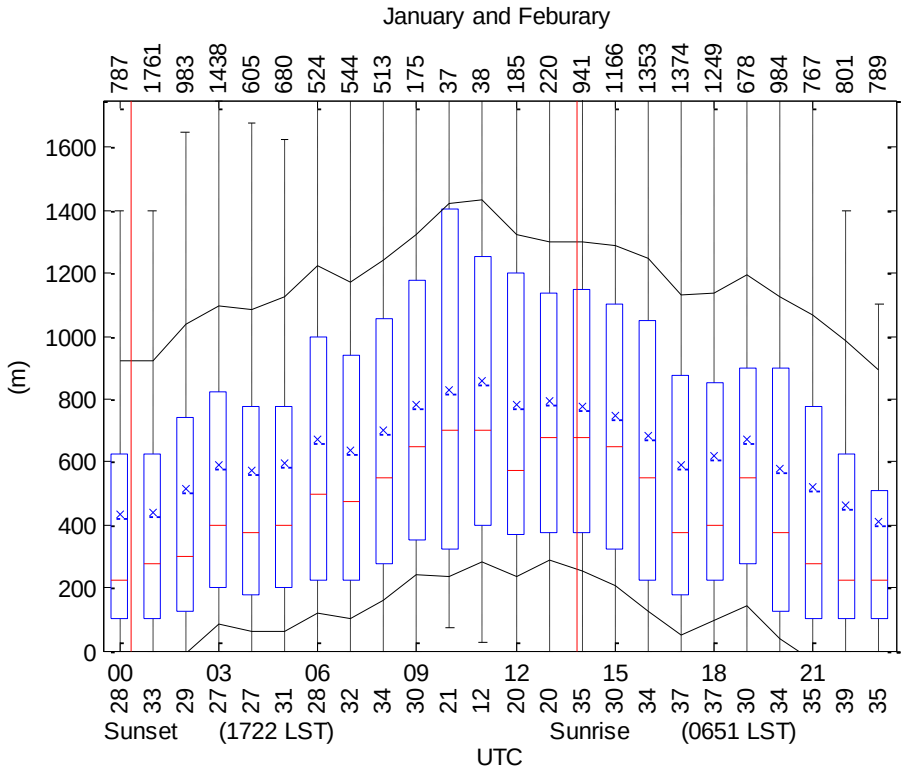

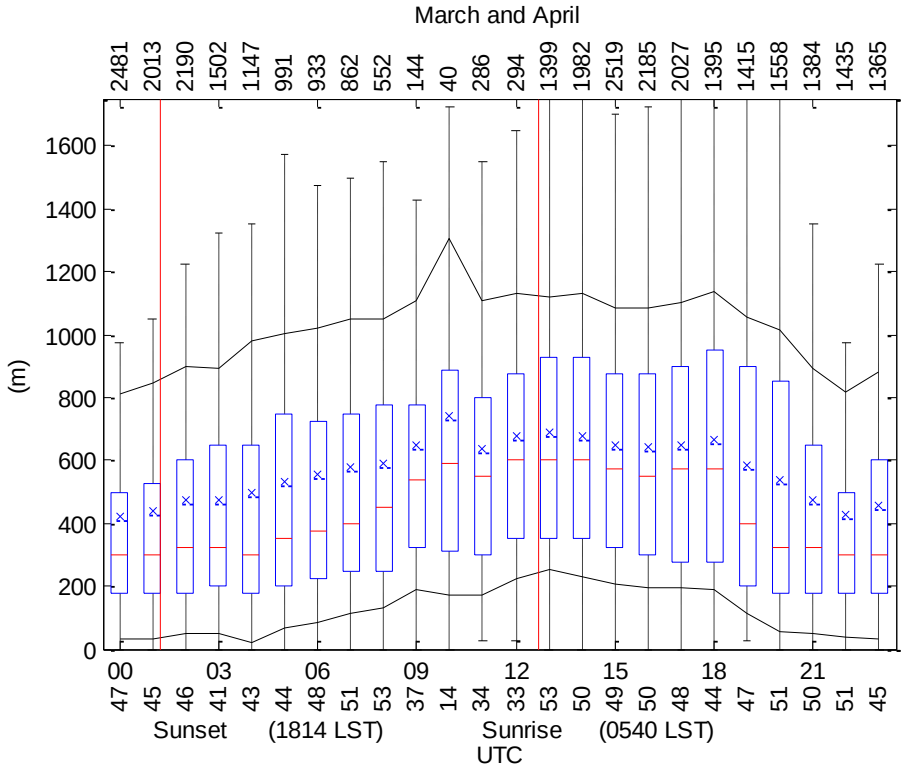
March and April
2481 2013 2190 1502 1147 991 933 862 552 144 40 286 294 1399 1982 2519 2185 2027 1395 1415 1558 1384 1435 1365
(m)
0 200 400 600 800 1000 1200 1400 1600
00 03 06 09 12 15 18 21
47 45 46 41 43 44 48 51 53 37 14 34 33 53 50 49 50 48 44 47 51 50 51 45
Sunset (1814 LST) Sunrise (0540 LST)
UTC

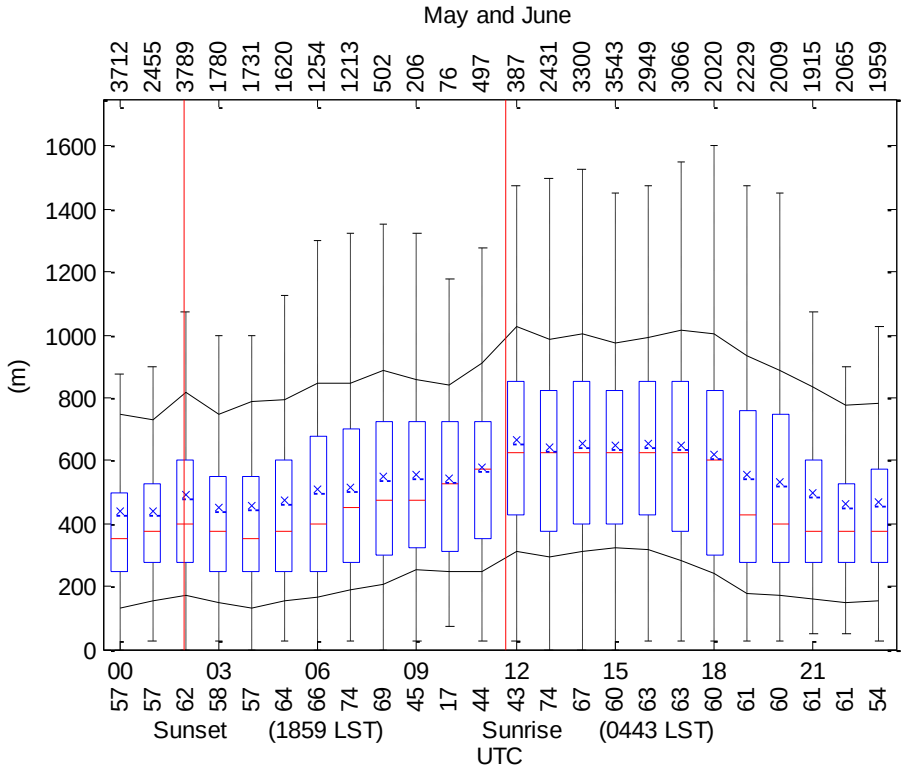
May and June
3712 2455 3789 1780 1731 1620 1254 1213 502 206 76 497 387 2431 3300 3543 2949 3066 2020 2229 2009 1915 2065 1959
(m)
0 200 400 600 800 1000 1200 1400 1600
00 03 06 09 12 15 18 21
57 57 62 58 57 64 66 74 69 45 17 44 43 74 67 60 63 63 60 61 60 61 61 54
Sunset (1859 LST) Sunrise (0443 LST)
UTC

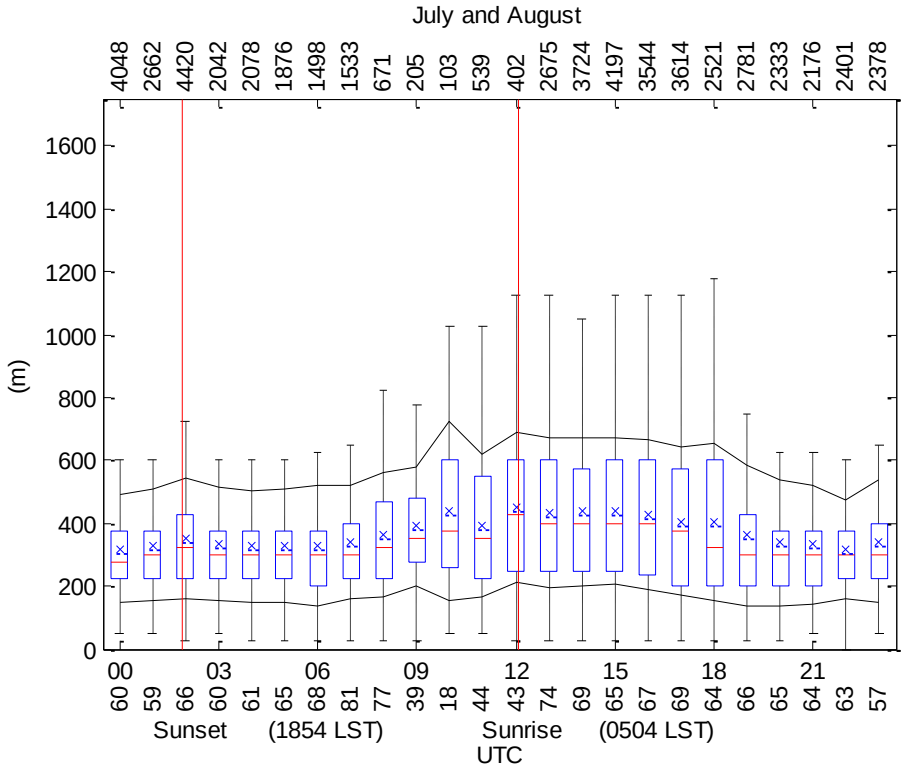
July and August
4048 2662 4420 2042 2078 1876 1498 1533 671 205 103 539 402 2675 3724 4197 3544 3614 2521 2781 2333 2176 2401 2378
1600
1400
1200
1000
800
600
400
200
0
(m)
00 03 06 09 12 15 18 21
60 59 66 60 61 65 68 81 77 39 18 44 43 74 69 65 67 69 64 66 65 64 63 57
Sunset (1854 LST) Sunrise (0504 LST)
UTC

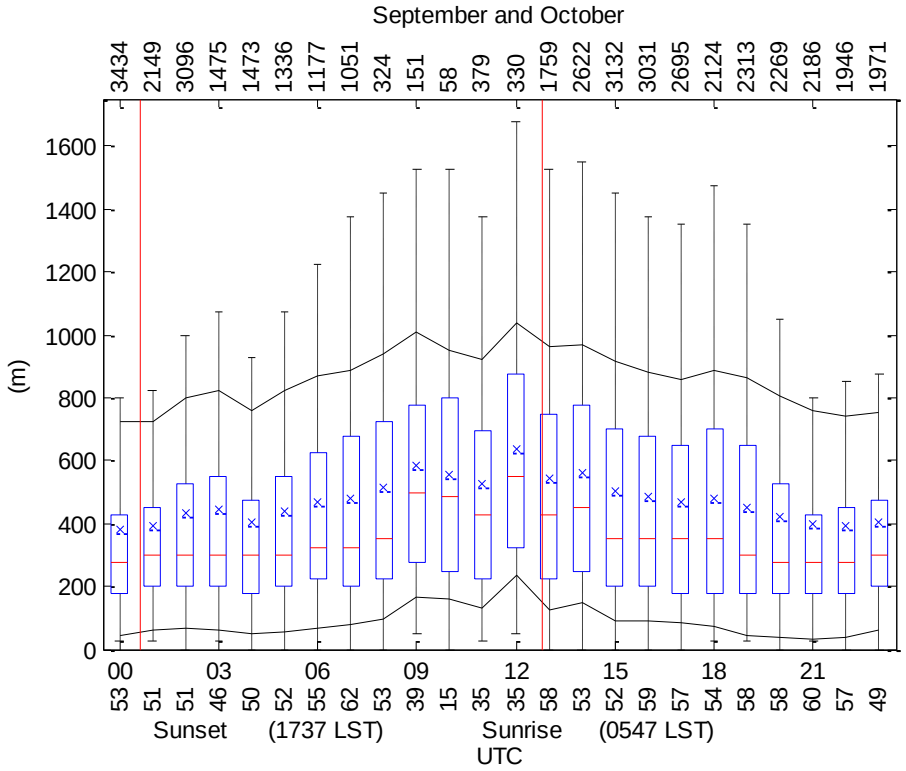
September and October
3434 2149 3096 1475 1473 1336 1177 1051 324 151 58 379 330 1759 2622 3132 3031 2695 2124 2313 2269 2186 1946 1971
1600
1400
1200
1000
800
600
400
200
0
(m)
00 03 06 09 12 15 18 21
53 51 51 46 50 52 55 62 53 39 15 35 35 58 53 52 59 57 54 58 58 60 57 49
Sunset (1737 LST) Sunrise (0547 LST)
UTC

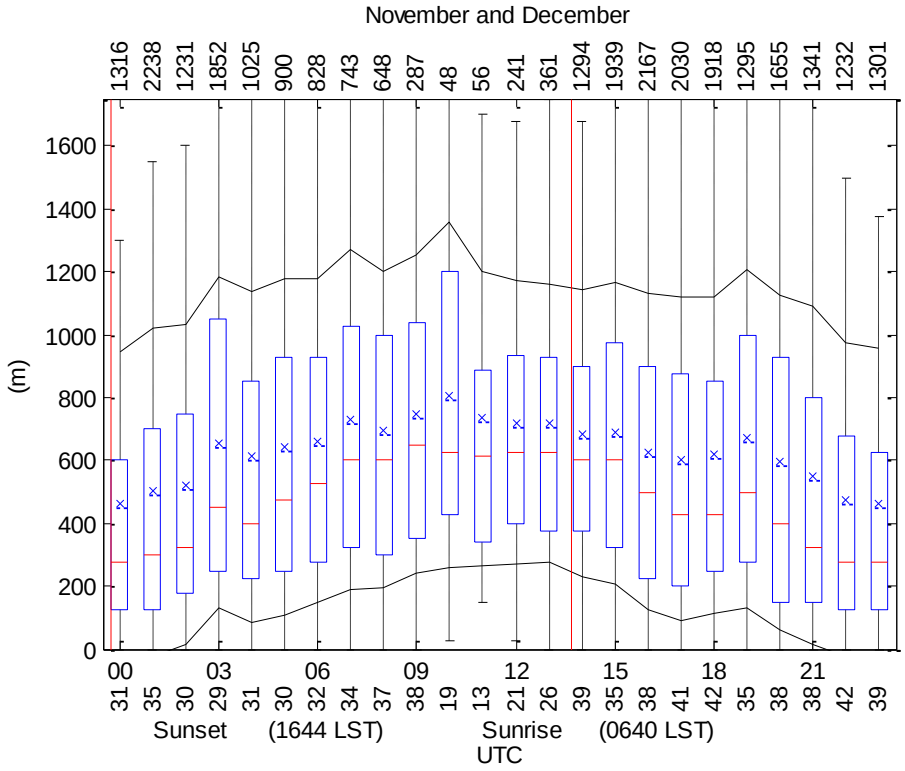

Figure 16. Mean and Median diurnal cycle of annual CBL heights presented bi-monthly where the blue box is the middle 50% of data (25% to 75%), red lines mark the median, the blue X marks the mean, the black lines on above and below are the standard deviation and the whiskers show the spread of data not considered outliers. The top row of numbers is the total number of base heights used for that hour. The Bottom row of numbers is the ratio of heights to total soundings for that hour.

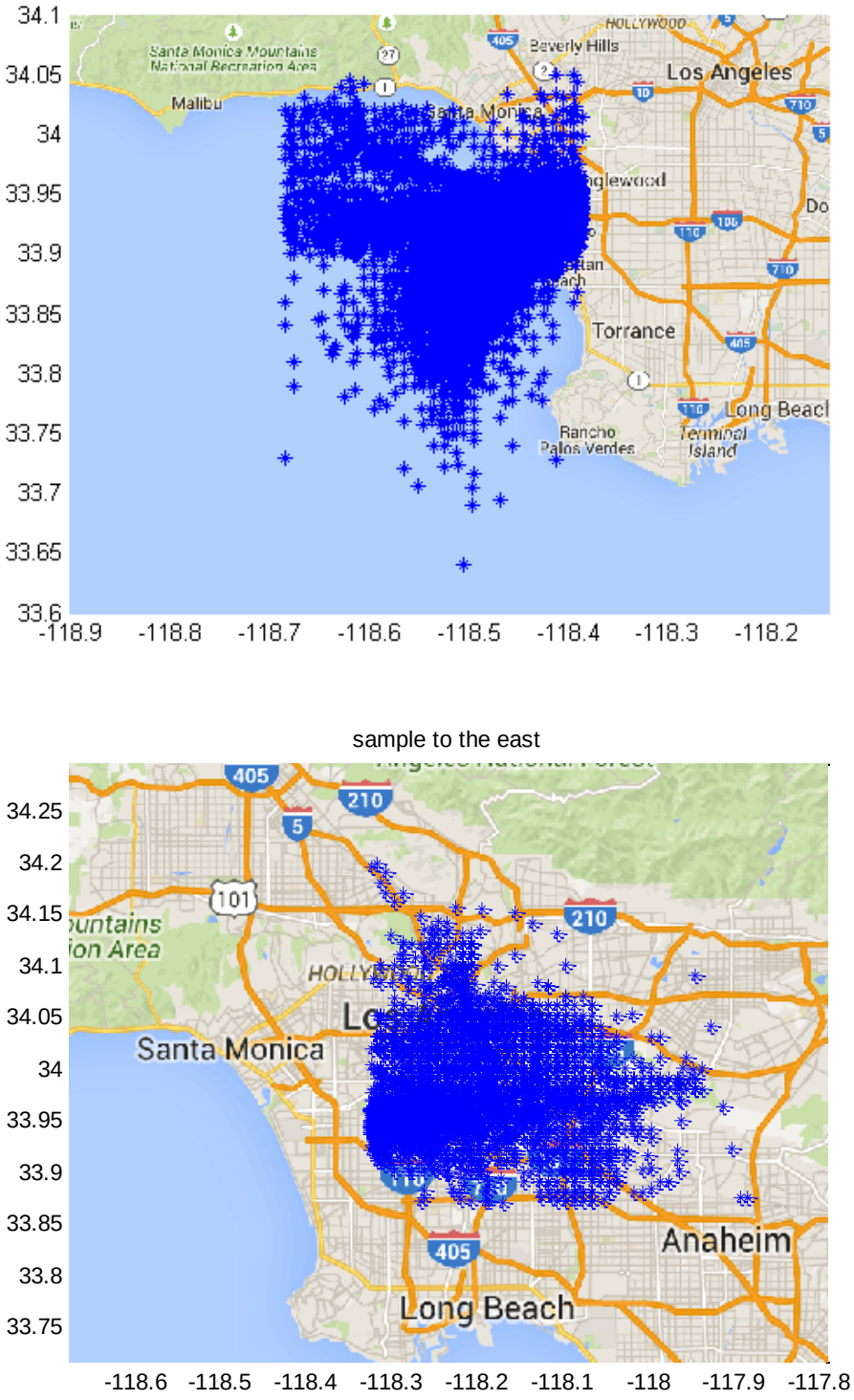

Figure 17. Location of data used to determine “west” CBL soundings (top) and “east” CBL soundings (bottom) overlaid on a google map.

Climatology of CBL heights to the west

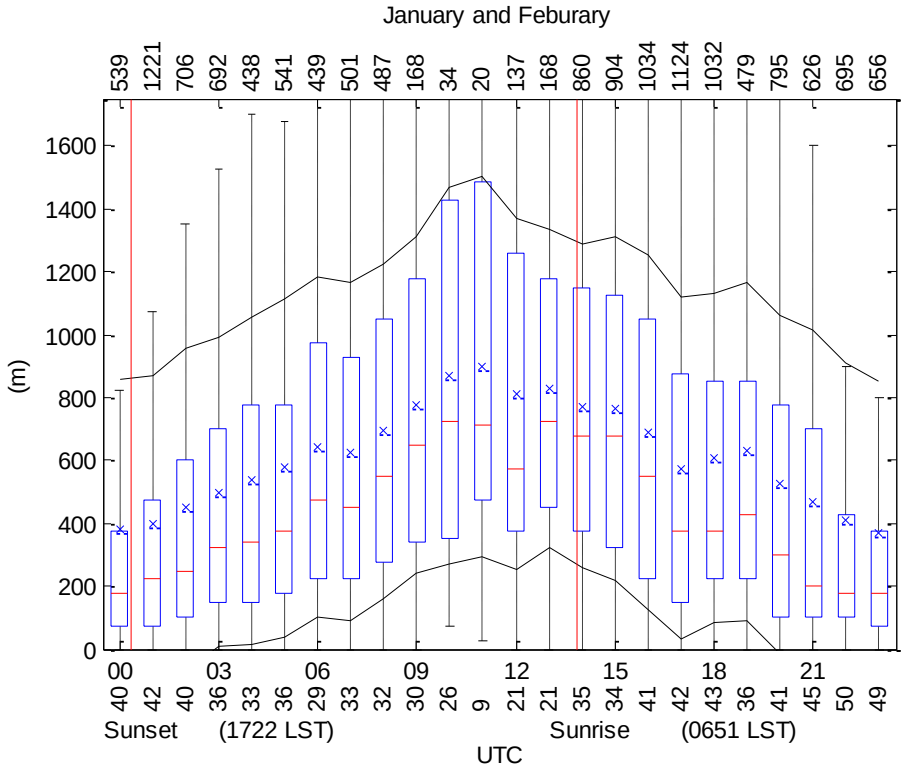

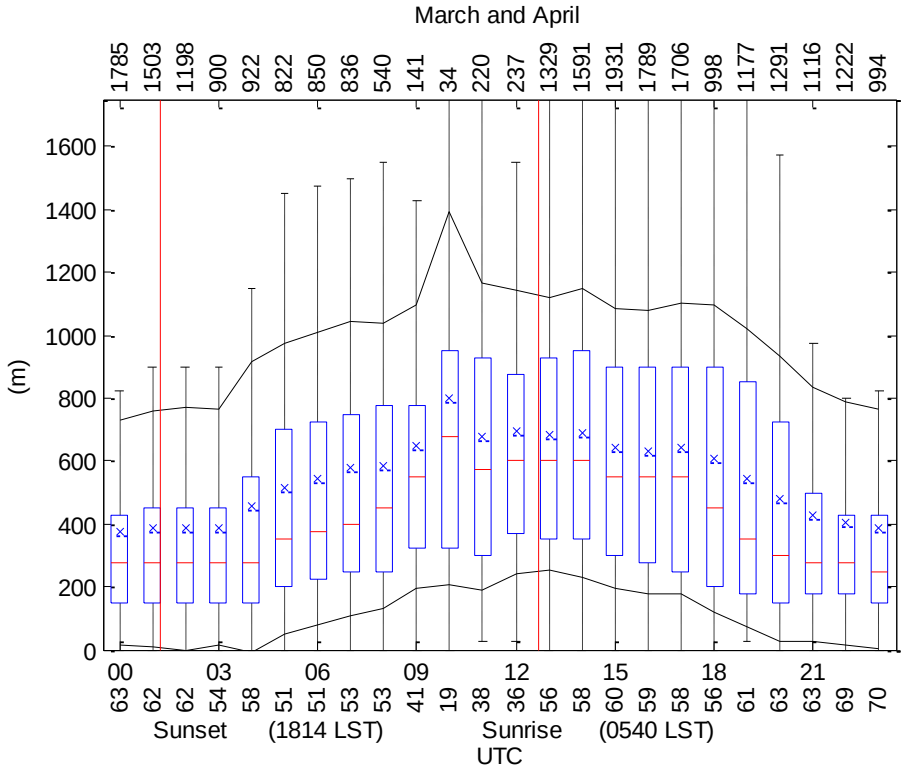

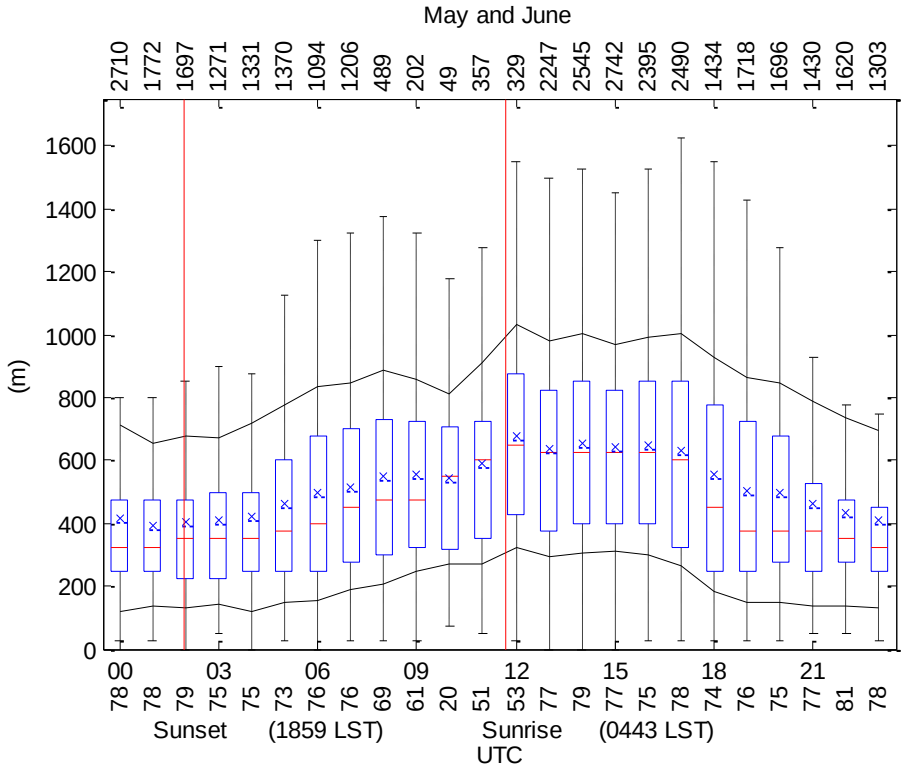
May and June
2710 1772 1697 1271 1331 1370 1094 1206 489 202 49 357 329 2247 2545 2742 2395 2490 1434 1718 1696 1430 1620 1303
(m)
0 200 400 600 800 1000 1200 1400 1600
00 03 06 09 12 15 18 21
78 78 79 75 75 73 76 76 69 61 20 51 53 77 79 77 75 78 74 76 75 77 81 78
Sunset (1859 LST) Sunrise (0443 LST)
UTC

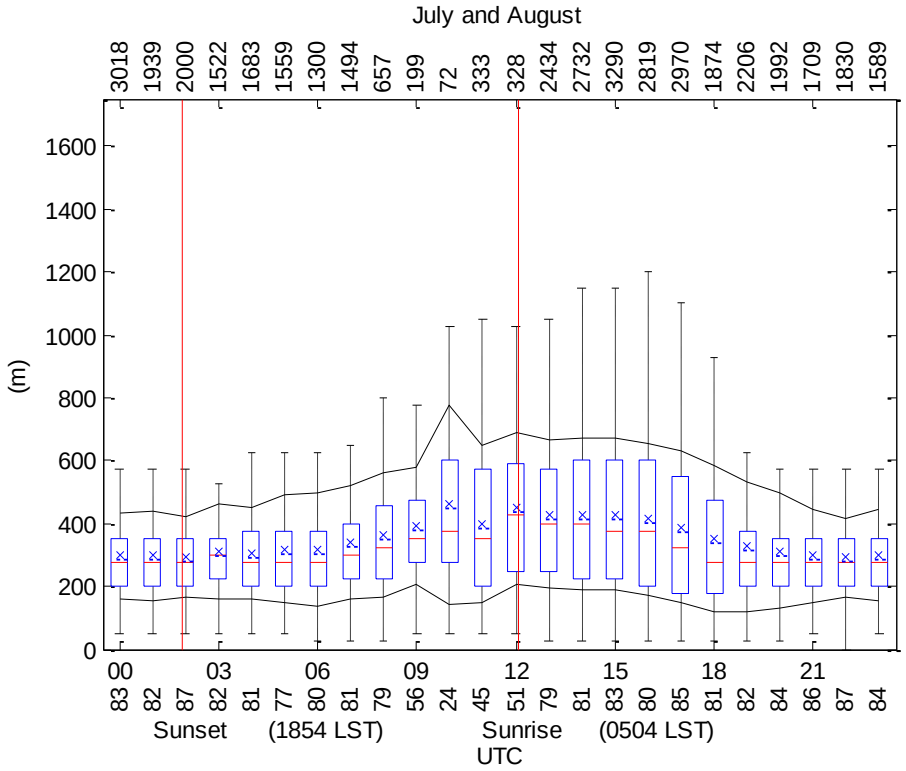
July and August
3018 1939 2000 1522 1683 1559 1300 1494 657 199 72 333 328 2434 2732 3290 2819 2970 1874 2206 1992 1709 1830 1589
(m)
0 200 400 600 800 1000 1200 1400 1600
00 03 06 09 12 15 18 21
83 82 87 82 81 77 80 81 79 56 24 45 51 79 81 83 80 85 81 82 84 86 87 84
Sunset (1854 LST) Sunrise (0504 LST)
UTC

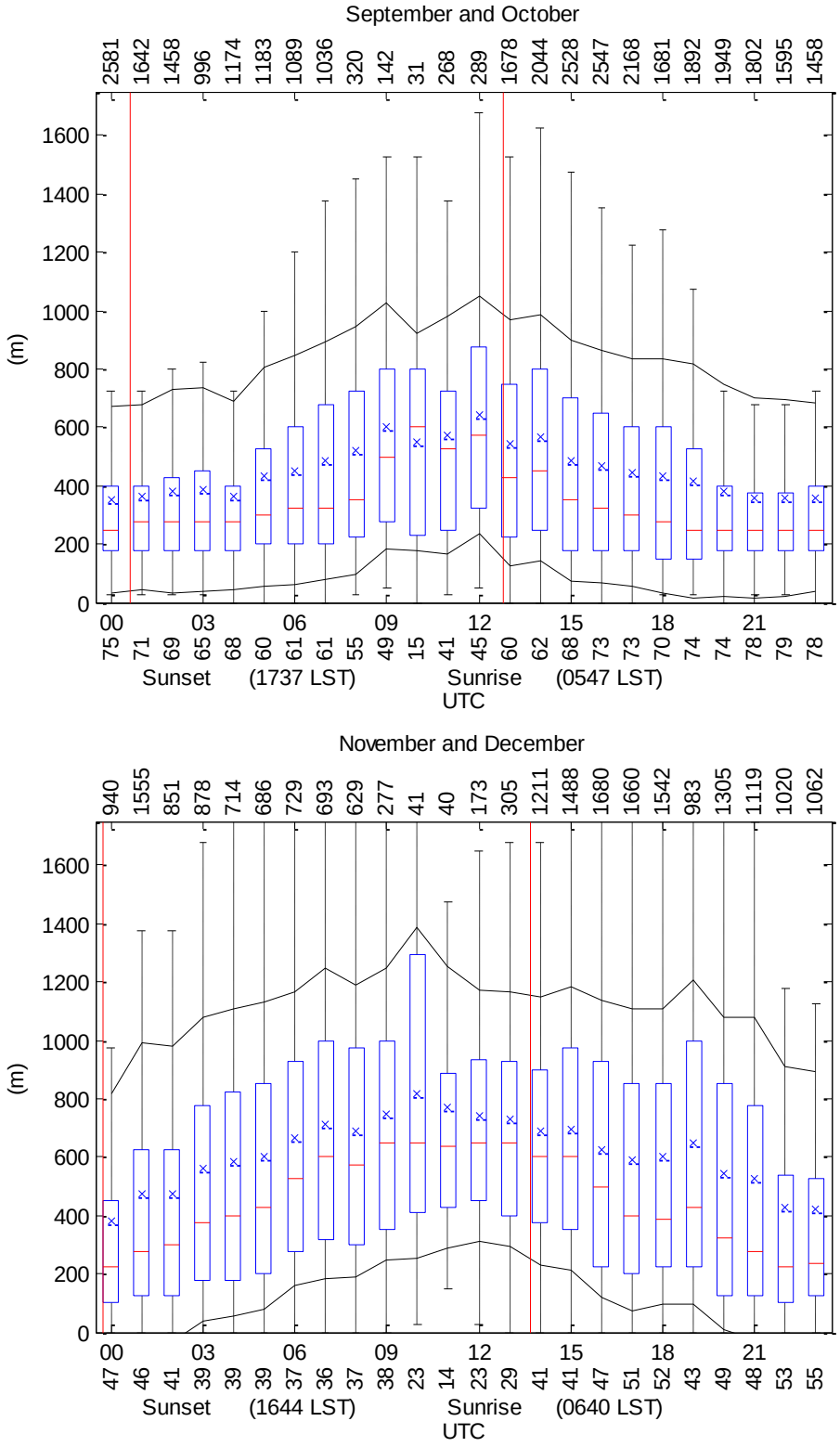

Figure 18. Mean and Median diurnal cycle of annual CBL heights presented bi-monthly where the blue box is the middle 50% of data (25% to 75%), red lines mark the median, the blue X marks the mean, the black lines on above and below are the standard deviation and

the whiskers show the spread of data not considered outliers. The top row of numbers is the total number of base heights used for that hour. The Bottom row of numbers is the ratio of heights to total soundings for that hour.

Climatology of CBL heights to the east

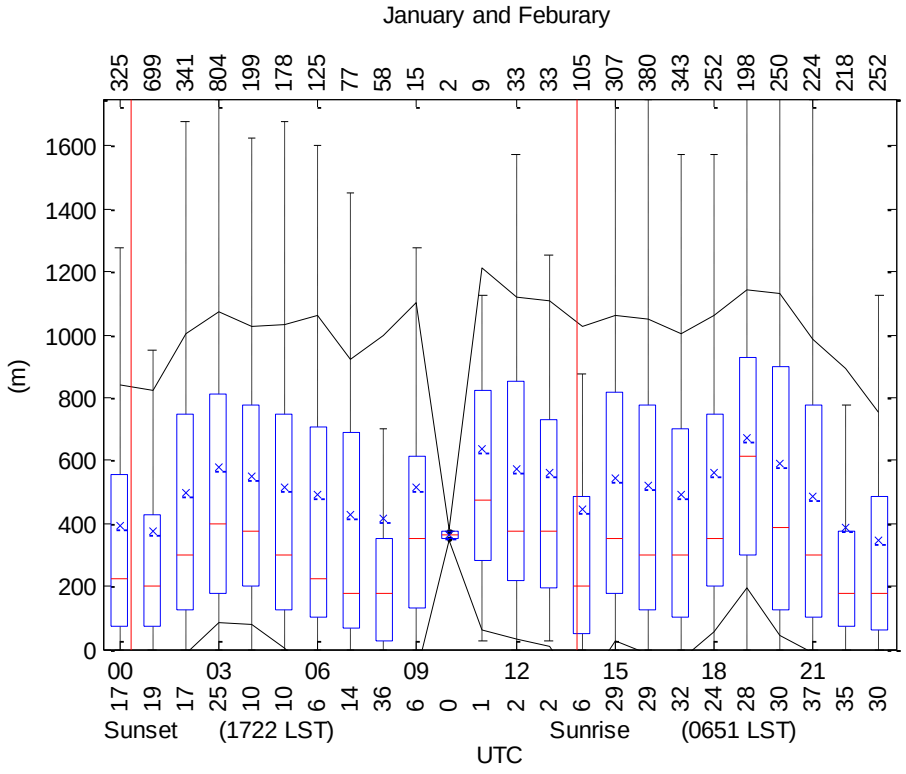

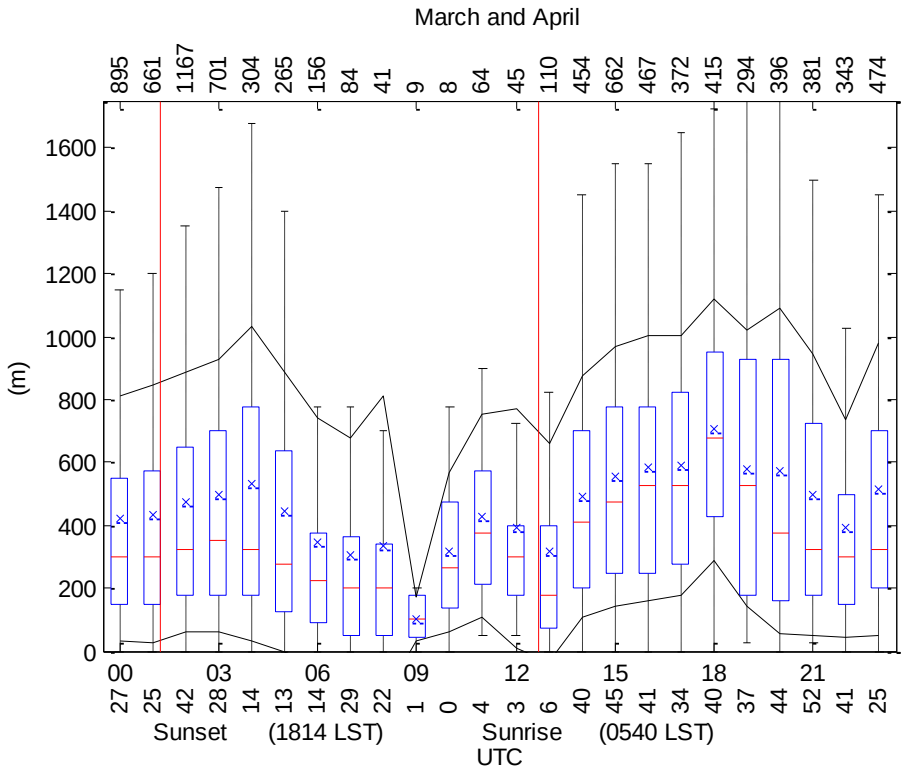
March and April
895 661 1167 701 304 265 156 84 41 9 8 64 45 110 454 662 467 372 415 294 396 381 343 474
(m)
0 200 400 600 800 1000 1200 1400 1600
00 03 06 09 12 15 18 21
27 25 42 28 14 13 14 29 22 1 0 4 3 6 40 45 41 34 40 37 44 52 41 25
Sunset (1814 LST) Sunrise (0540 LST)
UTC

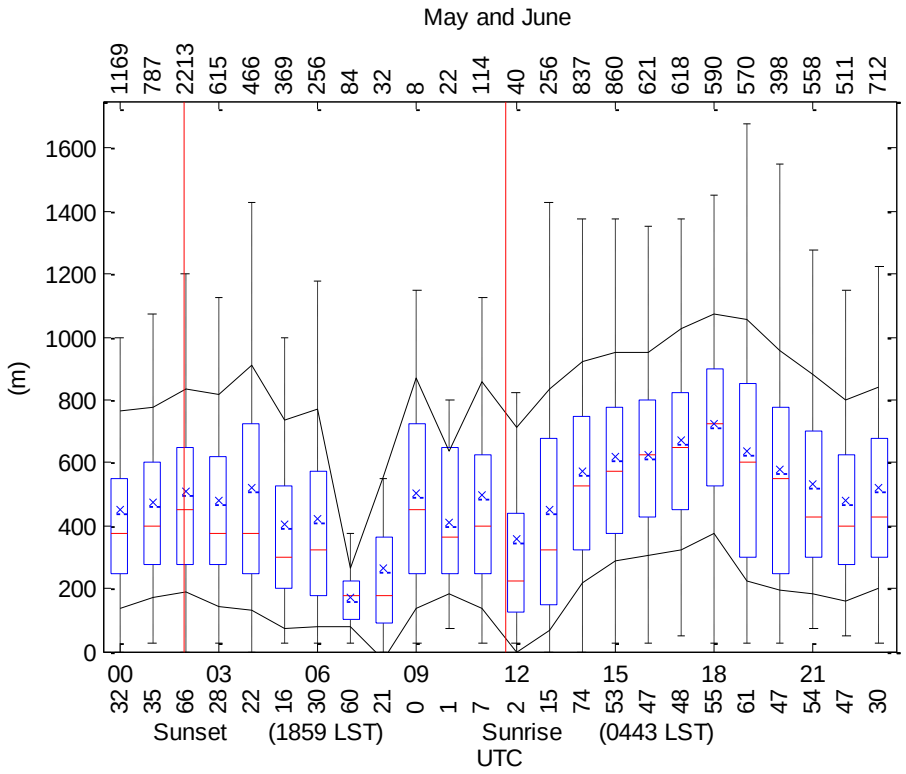
May and June
1169 787 2213 615 466 369 256 84 32 8 22 114 40 256 837 860 621 618 590 570 398 558 511 712
(m)
0 200 400 600 800 1000 1200 1400 1600
00 03 06 09 12 15 18 21
32 35 66 28 22 16 30 60 21 0 1 7 2 15 74 53 47 48 55 61 47 54 47 30
Sunset (1859 LST) Sunrise (0443 LST)
UTC

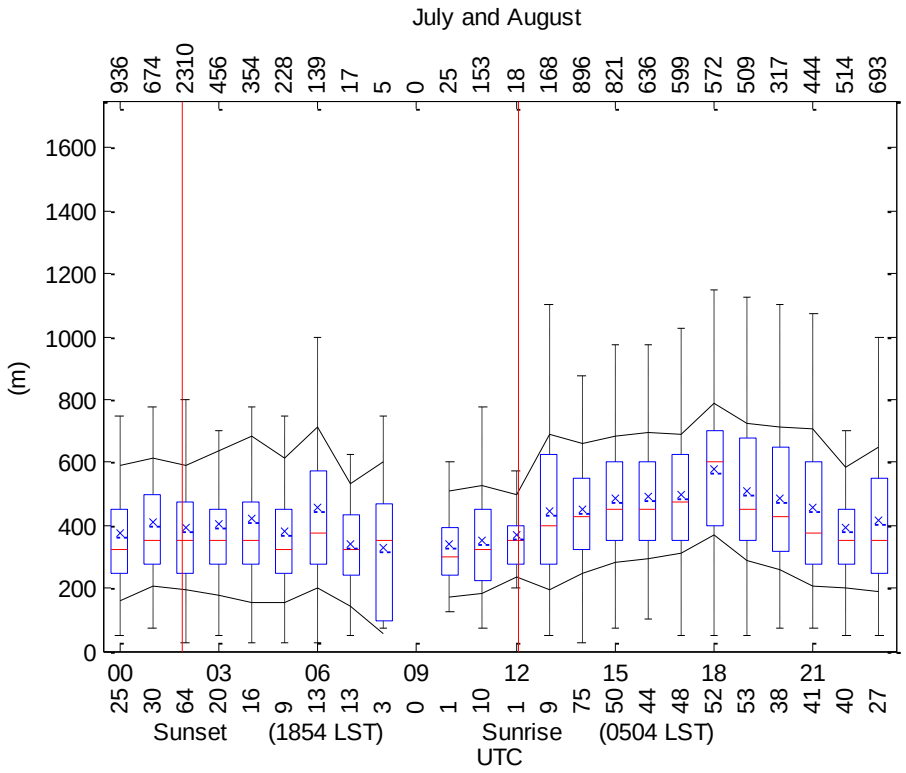
July and August
936 674 2310 456 354 228 139 17 5 0 25 153 18 168 896 821 636 599 572 509 317 444 514 693
(m)
0 200 400 600 800 1000 1200 1400 1600
00 03 06 09 12 15 18 21
25 30 64 20 16 9 13 13 3 0 1 10 1 9 75 50 44 48 52 53 38 41 40 27
Sunset (1854 LST) Sunrise (0504 LST)
UTC

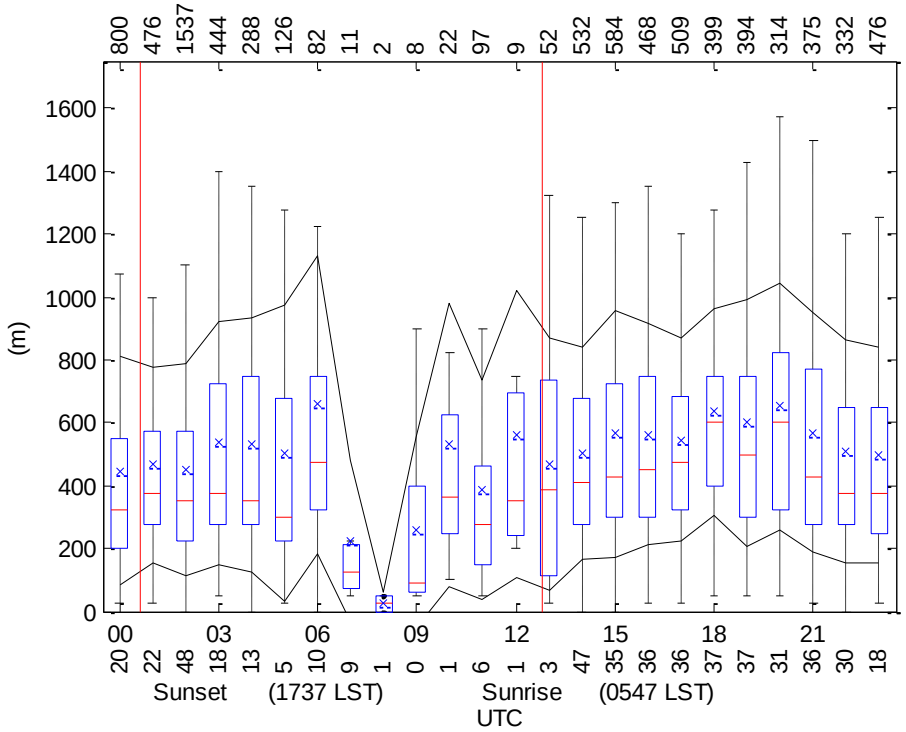
September and October
800 476 1537 444 288 126 82 11 2 8 22 97 9 52 532 584 468 509 399 394 314 375 332 476
(m)
0 200 400 600 800 1000 1200 1400 1600
00 03 06 09 12 15 18 21
20 22 48 18 13 5 10 9 1 0 1 6 1 3 47 35 36 36 37 37 31 36 30 18
Sunset (1737 LST) Sunrise (0547 LST)
UTC

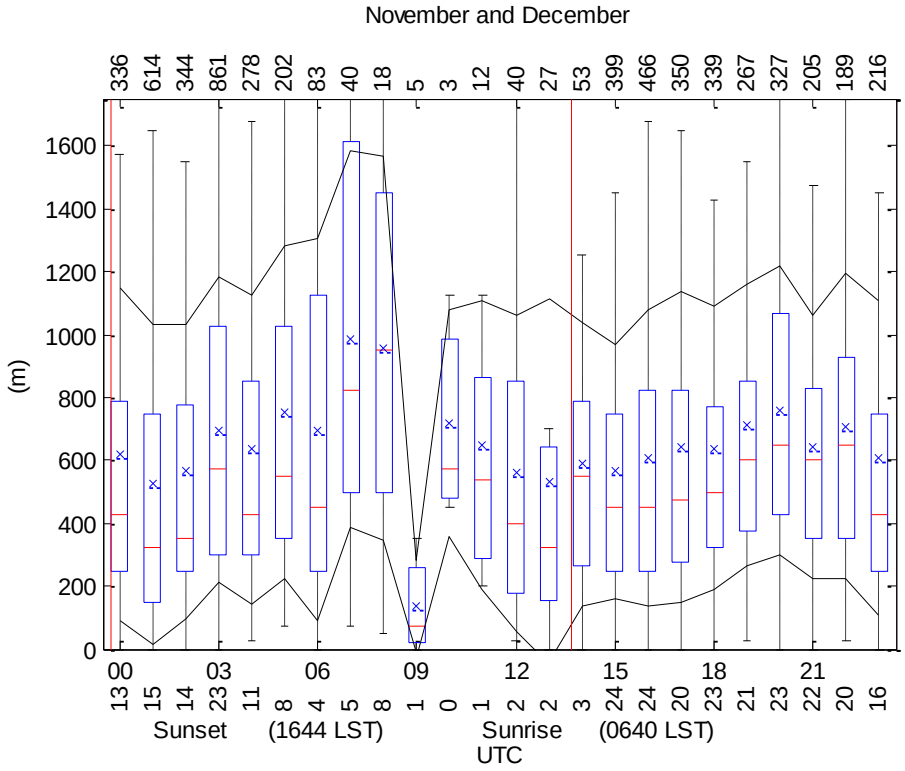

Figure 19. Mean and Median diurnal cycle of annual CBL heights presented bi-monthly where the blue box is the middle 50% of data (25% to 75%), red lines mark the median, the blue X marks the mean, the black lines on above and below are the standard deviation and the whiskers show the spread of data not considered outliers. The top row of numbers is the total number of base heights used for that hour. The Bottom row of numbers is the ratio of heights to total soundings for that hour.

Climatology of CBL heights to the west under cloudy conditions

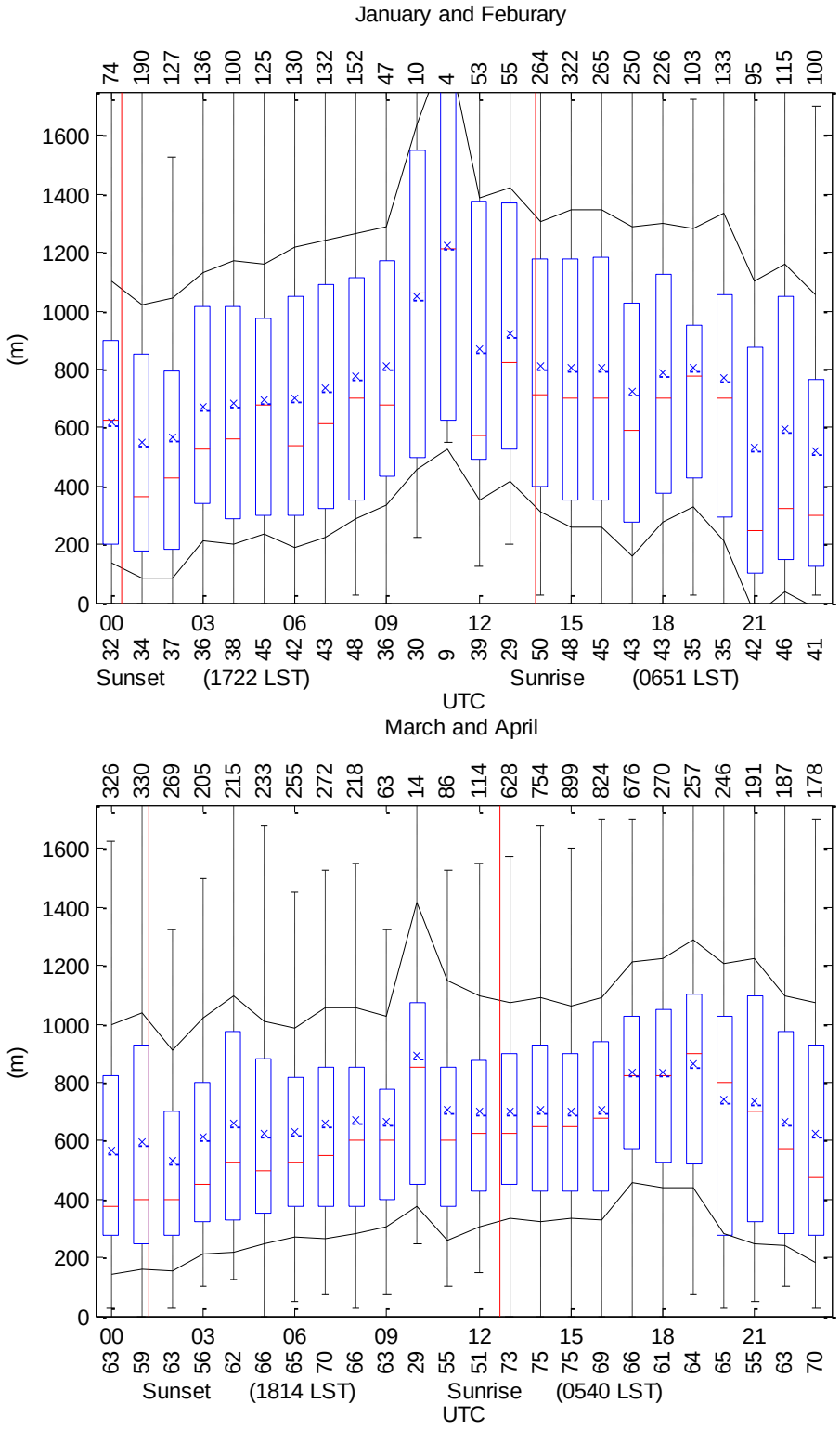

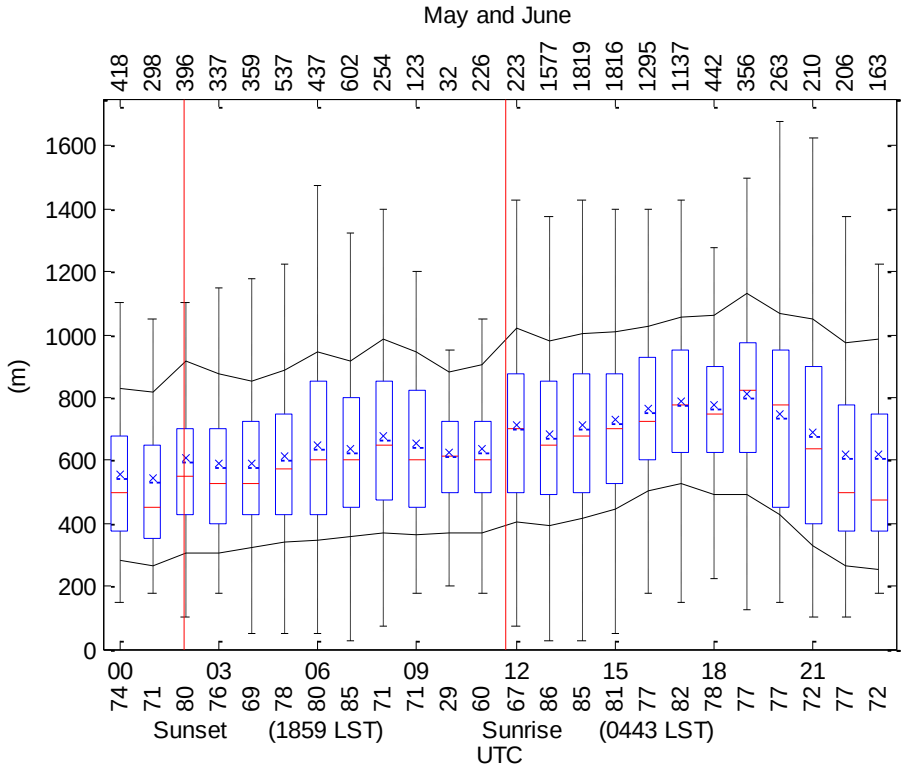
May and June
418 298 396 337 359 537 437 602 254 123 32 226 223 1577 1819 1816 1295 1137 442 356 263 210 206 163
1600
1400
1200
1000
800
600
400
200
0
(m)
00 03 06 09 12 15 18 21
74 71 80 76 69 78 80 85 71 71 29 60 67 86 85 81 77 82 78 77 77 72 77 72
Sunset (1859 LST)
Sunrise (0443 LST)
UTC

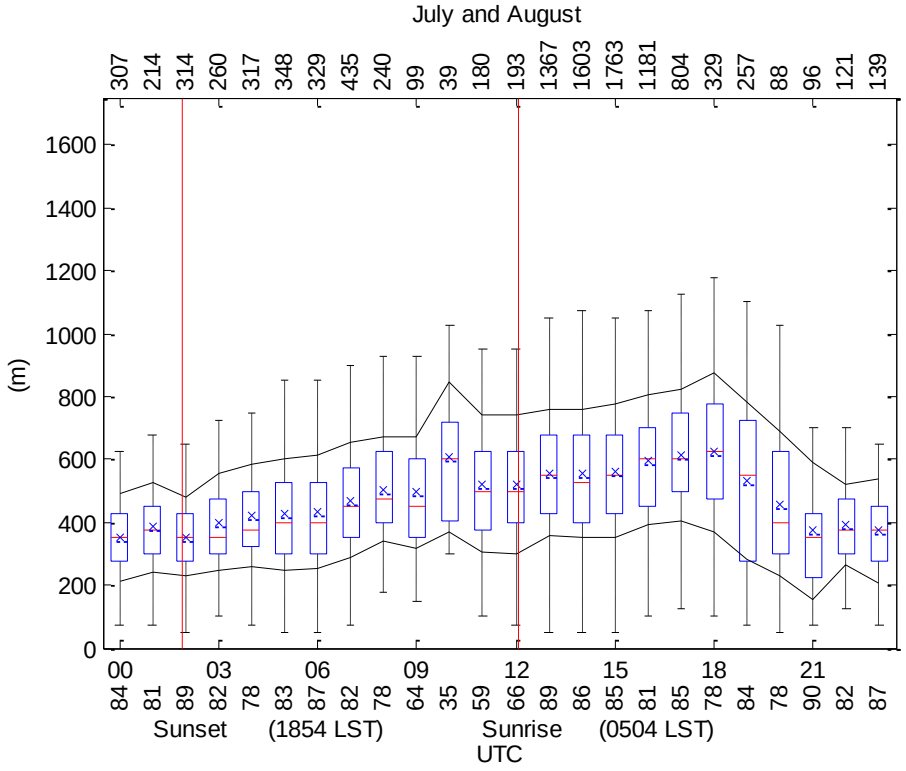
July and August
307 214 314 260 317 348 329 435 240 99 39 180 193 1367 1603 1763 1181 804 329 257 88 96 121 139
1600
1400
1200
1000
800
600
400
200
0
(m)
00 03 06 09 12 15 18 21
84 81 89 82 78 83 87 82 78 64 35 59 66 89 86 85 81 85 78 84 78 90 82 87
Sunset (1854 LST)
Sunrise (0504 LST)
UTC

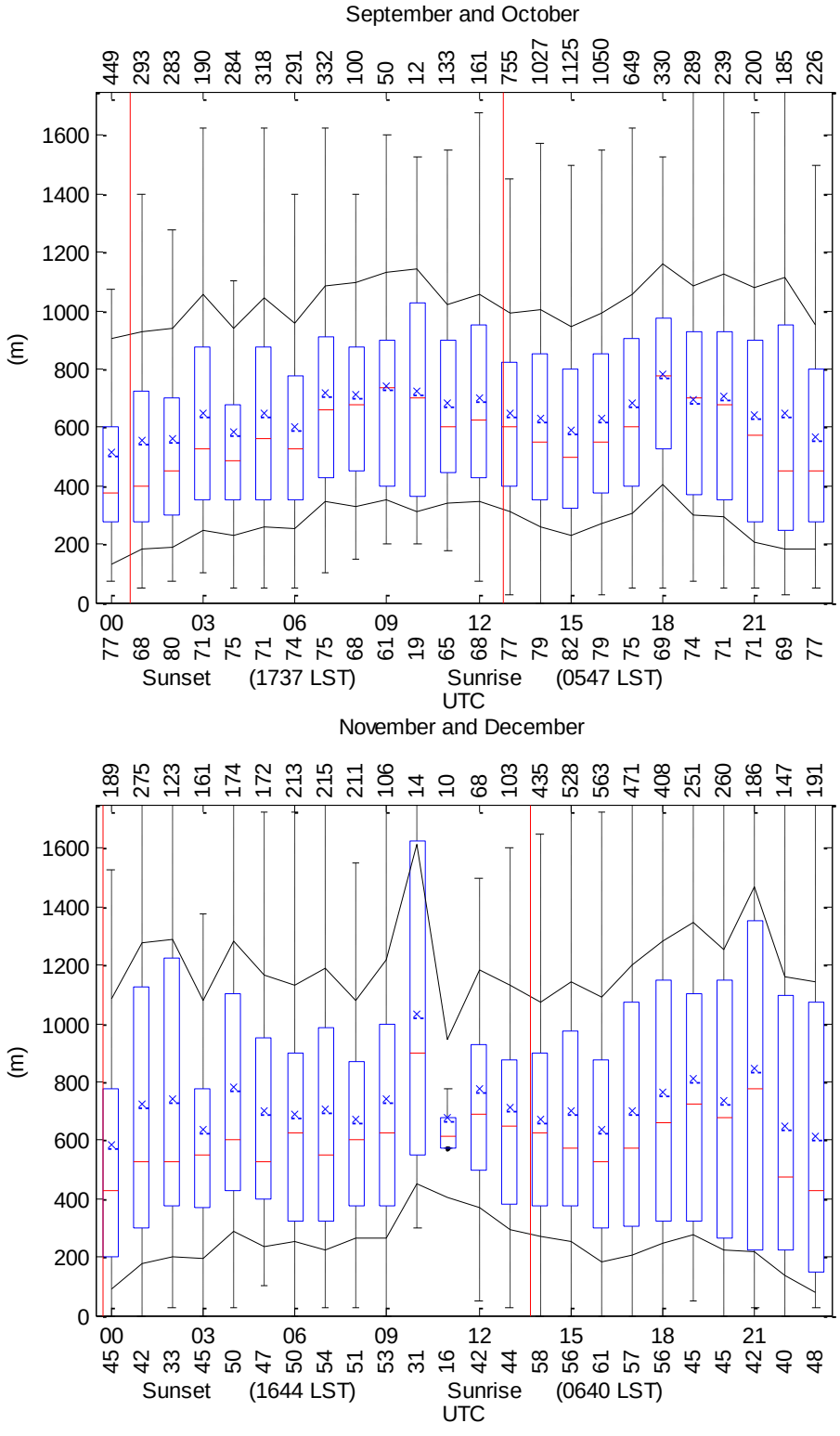

Figure 20. Mean and Median diurnal cycle of annual CBL heights presented bi-monthly where the blue box is the middle 50% of data (25% to 75%), red lines mark the median, the blue X marks the mean, the black lines on above and below

are the standard deviation and the whiskers show the spread of data not considered outliers. The top row of numbers is the total number of base heights used for that hour. The Bottom row of numbers is the ratio of heights to total soundings for that hour.

Climatology of CBL heights to the west under clear conditions

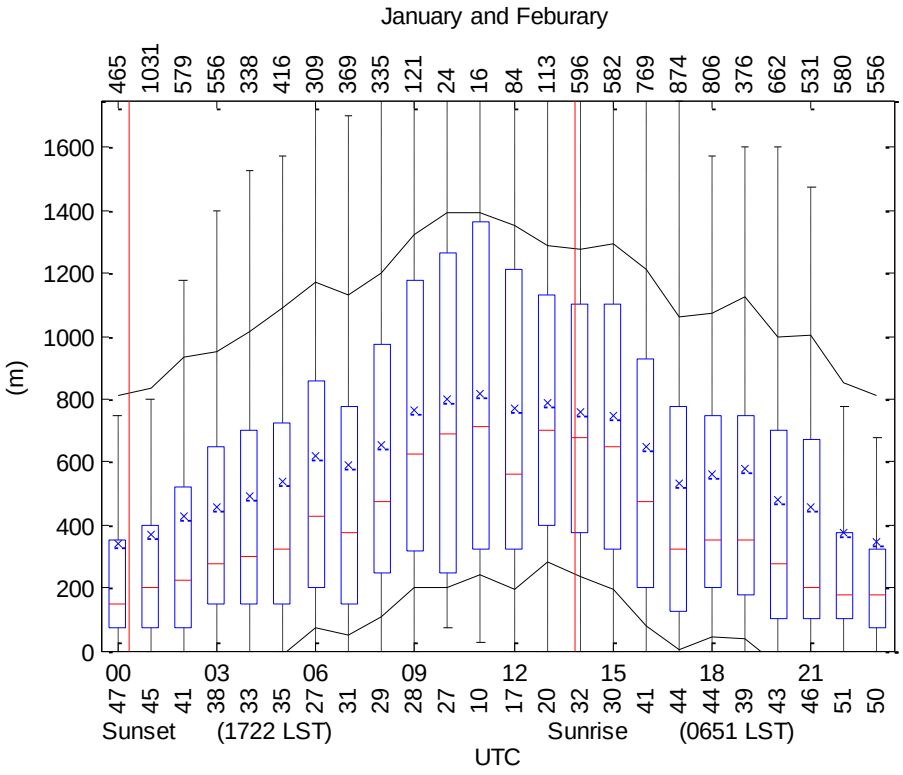

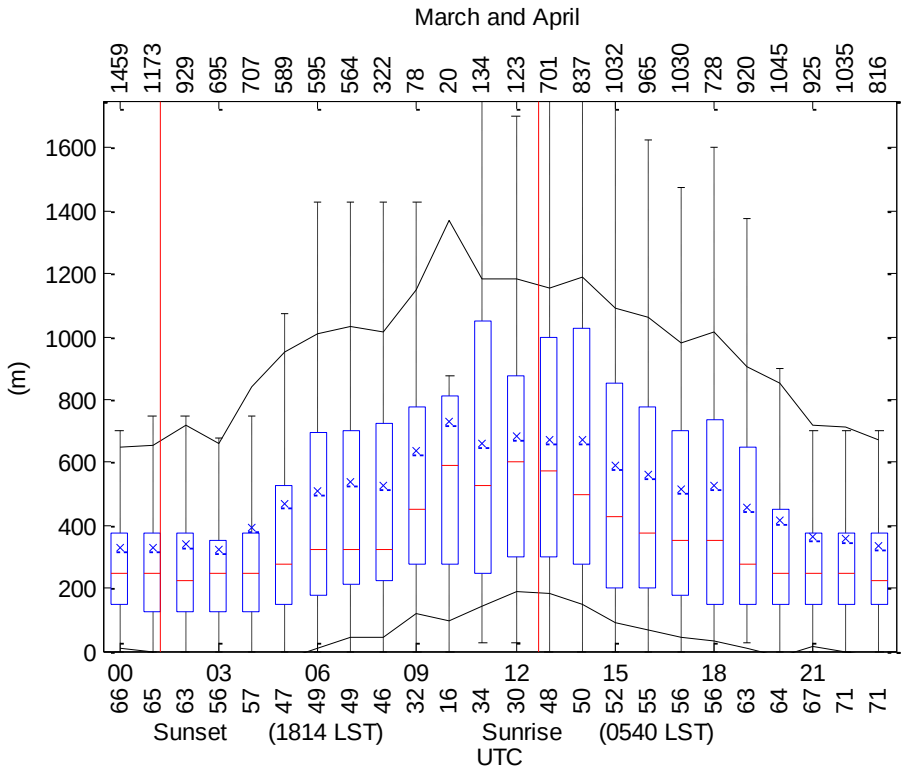
March and April
1459 1173 929 695 707 589 595 564 322 78 20 134 123 701 837 1032 965 1030 728 920 1045 925 1035 816
1600
1400
1200
1000
800
600
400
200
0
(m)
00 03 06 09 12 15 18 21
66 65 63 56 57 47 49 49 46 32 16 34 30 48 50 52 55 56 56 63 64 67 71 71
Sunset (1814 LST)
Sunrise (0540 LST)
UTC

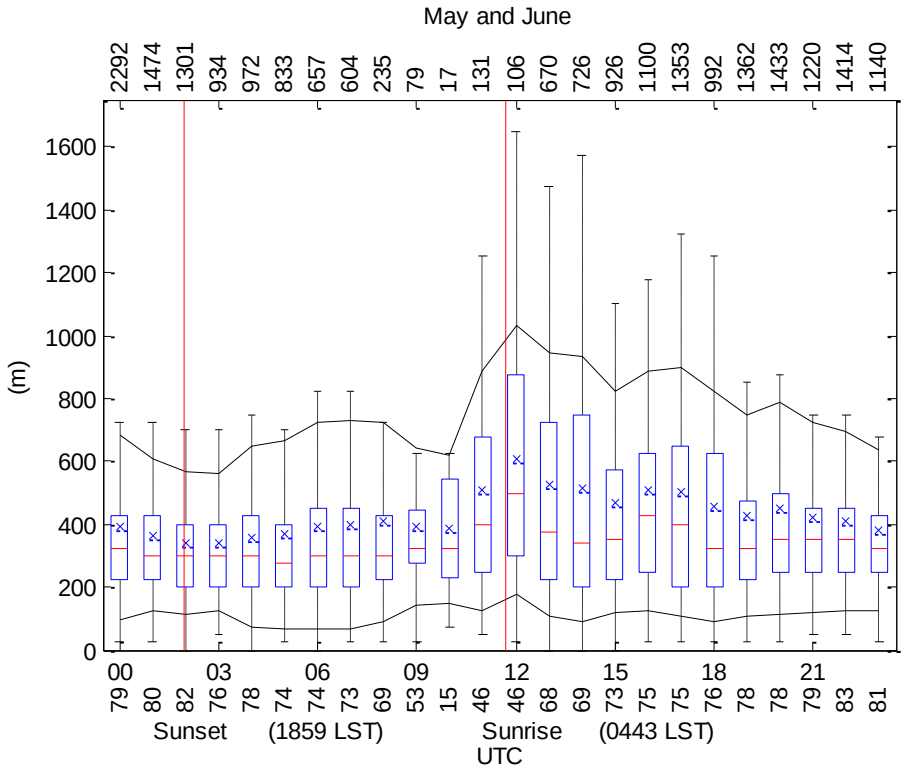
May and June
2292 1474 1301 934 972 833 657 604 235 79 17 131 106 670 726 926 1100 1353 992 1362 1433 1220 1414 1140
1600
1400
1200
1000
800
600
400
200
0
(m)
00 03 06 09 12 15 18 21
79 80 82 76 78 74 74 73 69 53 15 46 46 68 69 73 75 75 76 78 78 79 83 81
Sunset (1859 LST)
Sunrise (0443 LST)
UTC

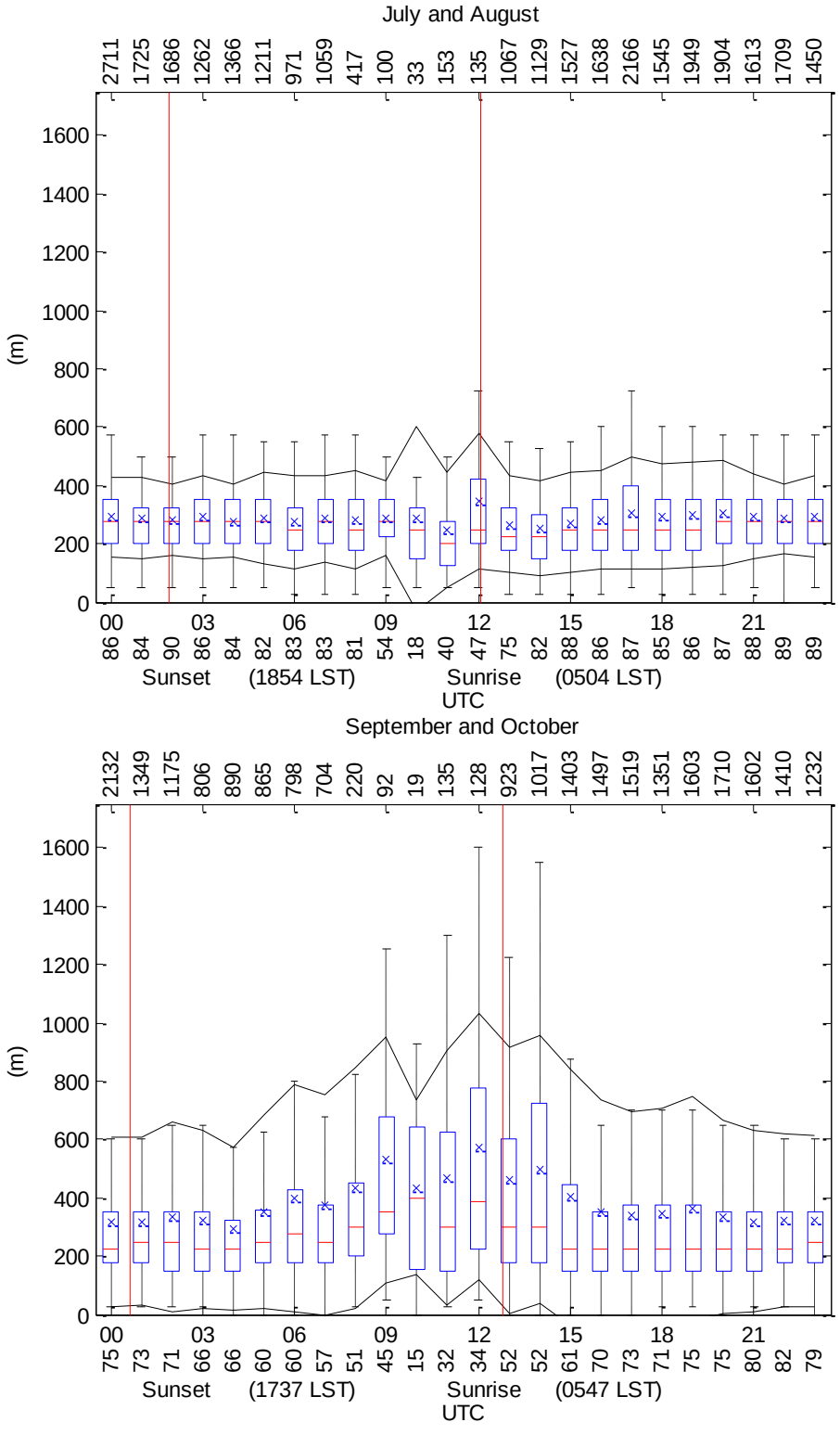
July and August
2711 1725 1686 1262 1366 1211 971 1059 417 100 33 153 135 1067 1129 1527 1638 2166 1545 1949 1904 1613 1709 1450
(m)
0 200 400 600 800 1000 1200 1400 1600
00 03 06 09 12 15 18 21
86 84 90 86 84 82 83 83 81 54 18 40 47 75 82 88 86 87 85 86 87 88 89 89
Sunset (1854 LST) Sunrise (0504 LST)
UTC
September and October
2132 1349 1175 806 890 865 798 704 220 92 19 135 128 923 1017 1403 1497 1519 1351 1603 1710 1602 1410 1232
(m)
0 200 400 600 800 1000 1200 1400 1600
00 03 06 09 12 15 18 21
75 73 71 66 66 60 60 57 51 45 15 32 34 52 52 61 70 73 71 75 75 80 82 79
Sunset (1737 LST) Sunrise (0547 LST)
UTC

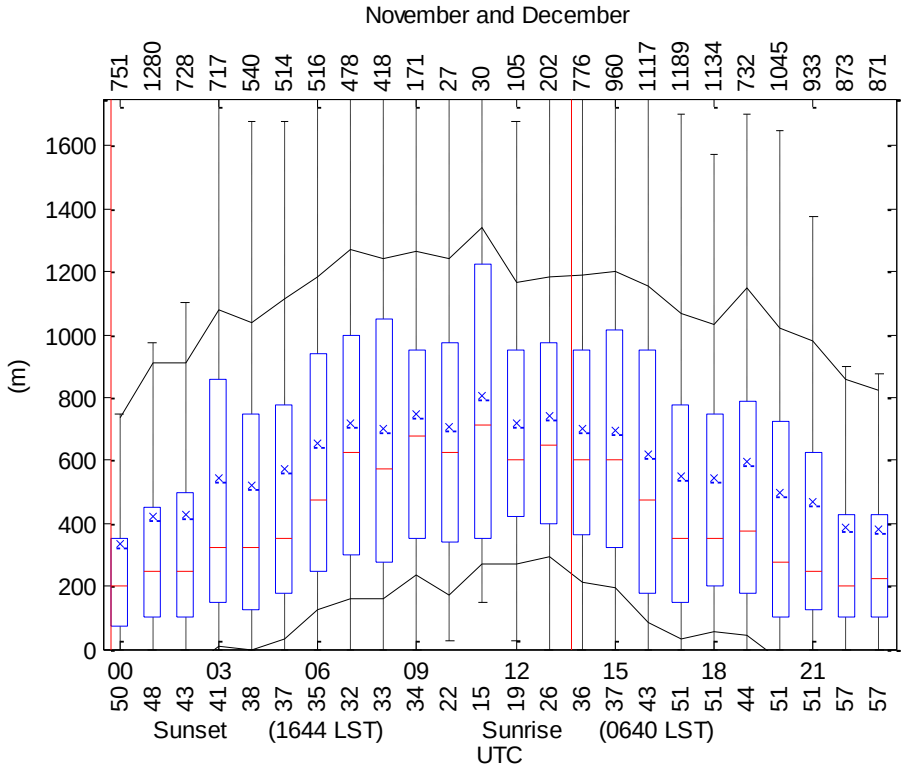

Figure 21. Mean and Median diurnal cycle of annual CBL heights presented bi-monthly where the blue box is the middle 50% of data (25% to 75%), red lines mark the median, the blue X marks the mean, the black lines on above and below are the standard deviation and the whiskers show the spread of data not considered outliers. The top row of numbers is the total number of base heights used for that hour. The Bottom row of numbers is the ratio of heights to total soundings for that hour.

36 hour climatological evolution of alongshore (295 deg.) and cross-shore (25 deg.) winds for a cloud topped CBL

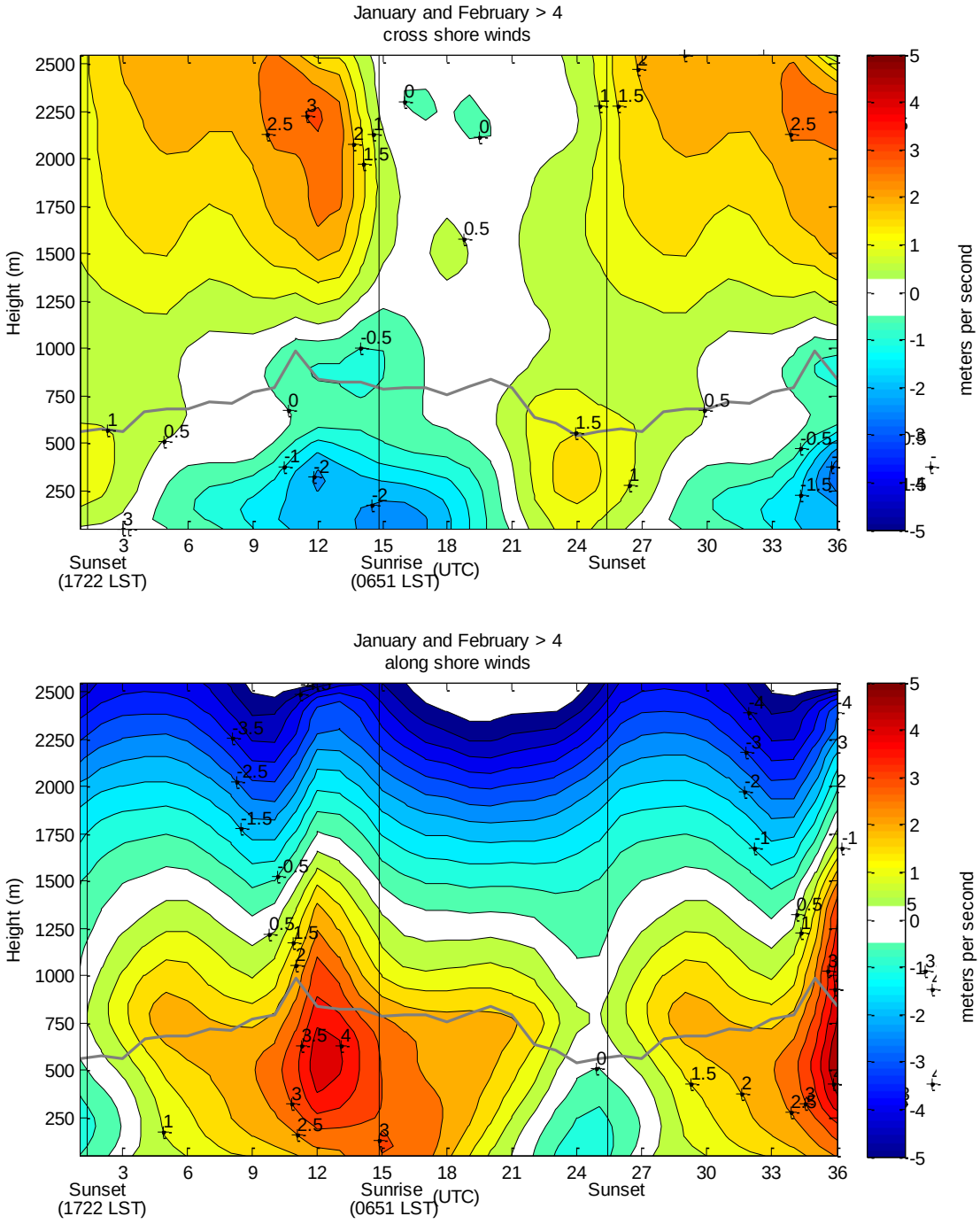

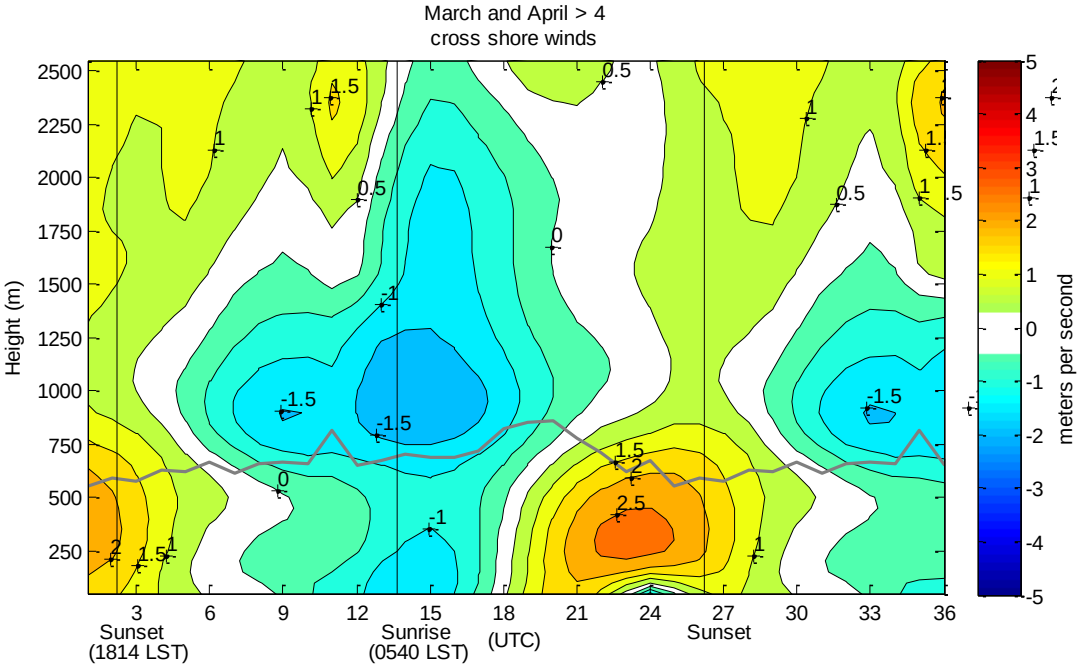
March and April > 4
cross shore winds
Height (m)
meters per second
Sunset
(1814 LST)
Sunrise
(0540 LST)
(UTC)
Sunset

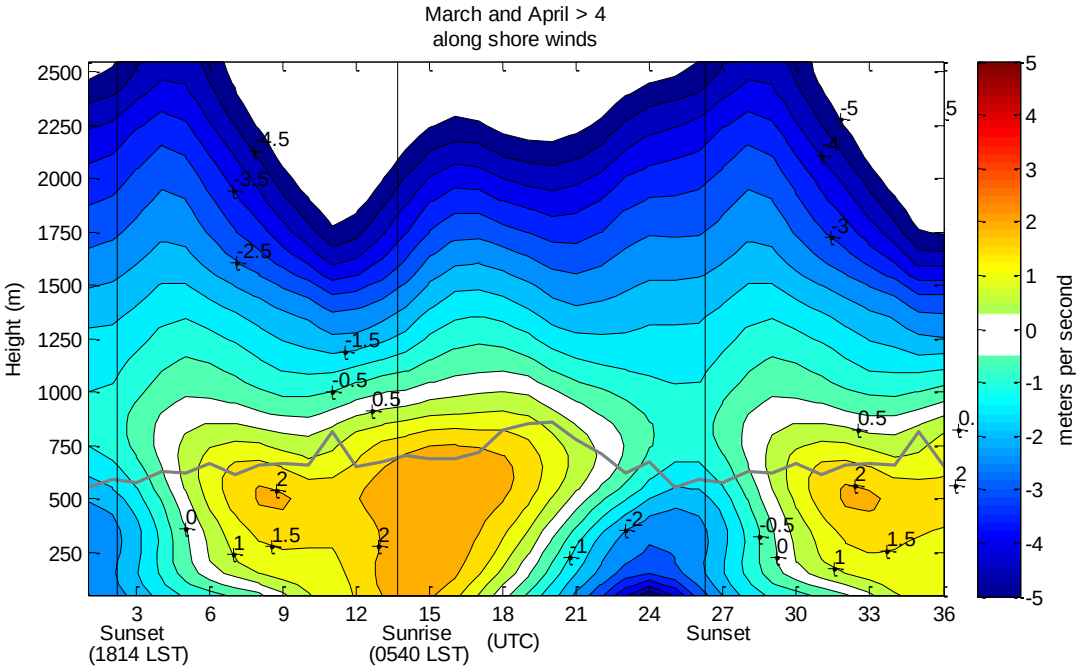
March and April > 4
along shore winds
Height (m)
meters per second
Sunset
(1814 LST)
Sunrise
(0540 LST)
(UTC)
Sunset

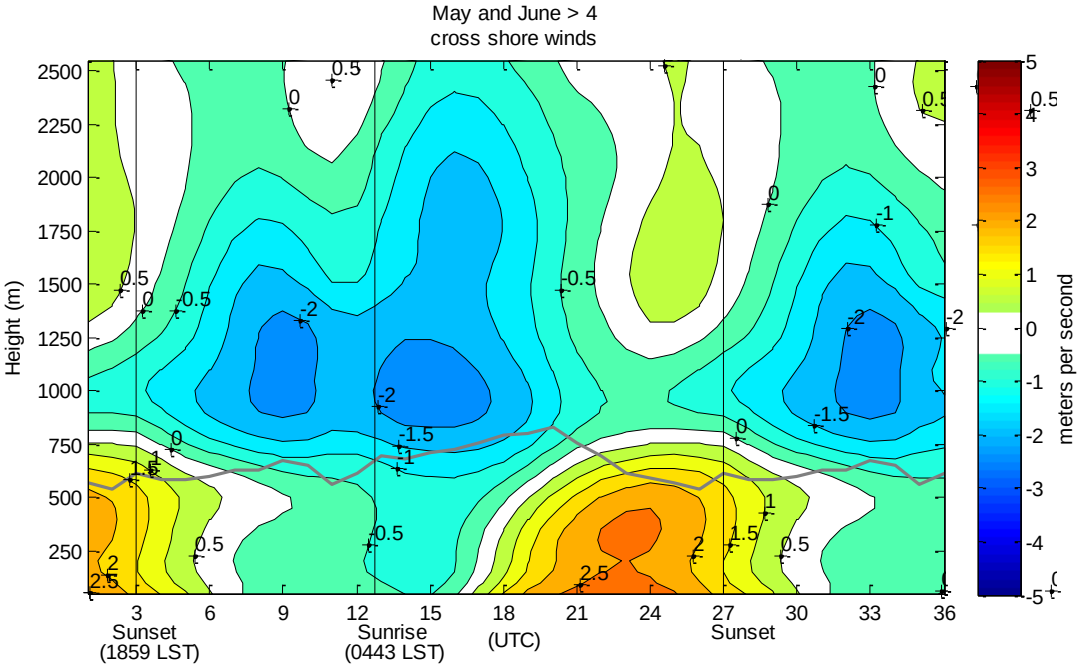
May and June > 4
cross shore winds
Height (m)
meters per second
Sunset
(1859 LST)
Sunrise
(0443 LST)
(UTC)
Sunset

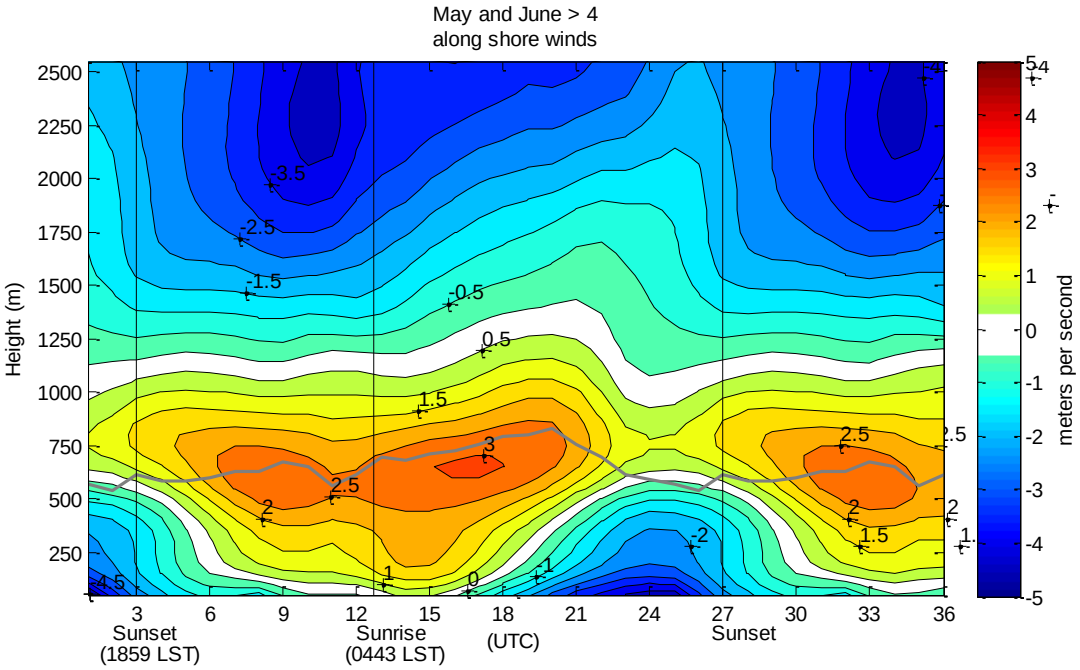
May and June > 4
along shore winds
Height (m)
meters per second
Sunset
(1859 LST)
Sunrise
(0443 LST)
(UTC)
Sunset

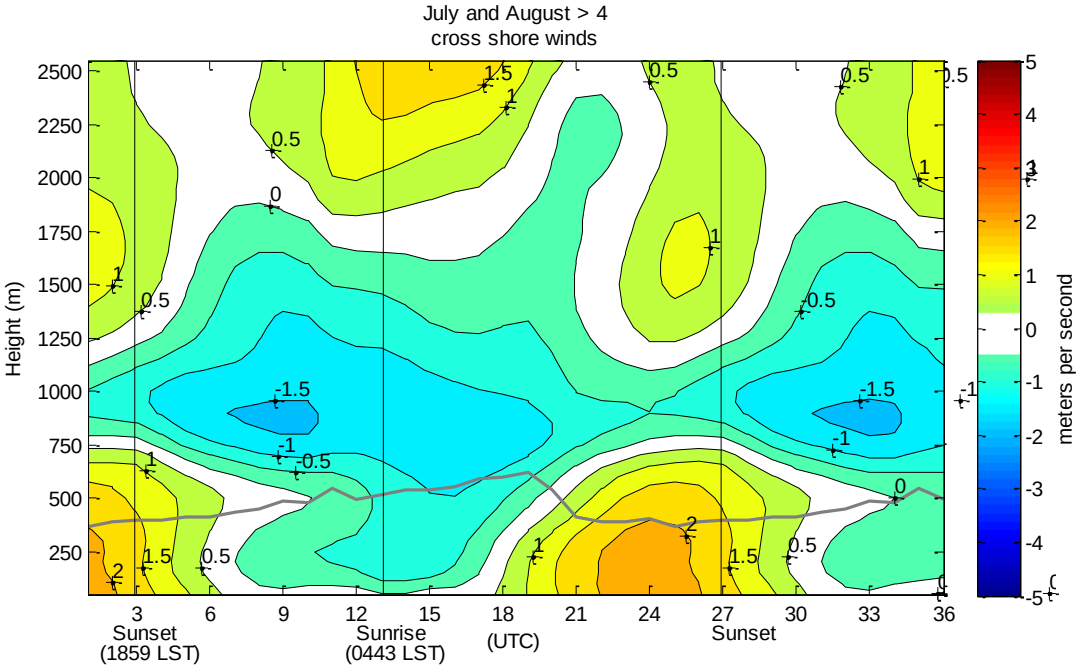
July and August > 4
cross shore winds
Height (m)
meters per second
Sunset
(1859 LST)
Sunrise
(0443 LST)
(UTC)
Sunset

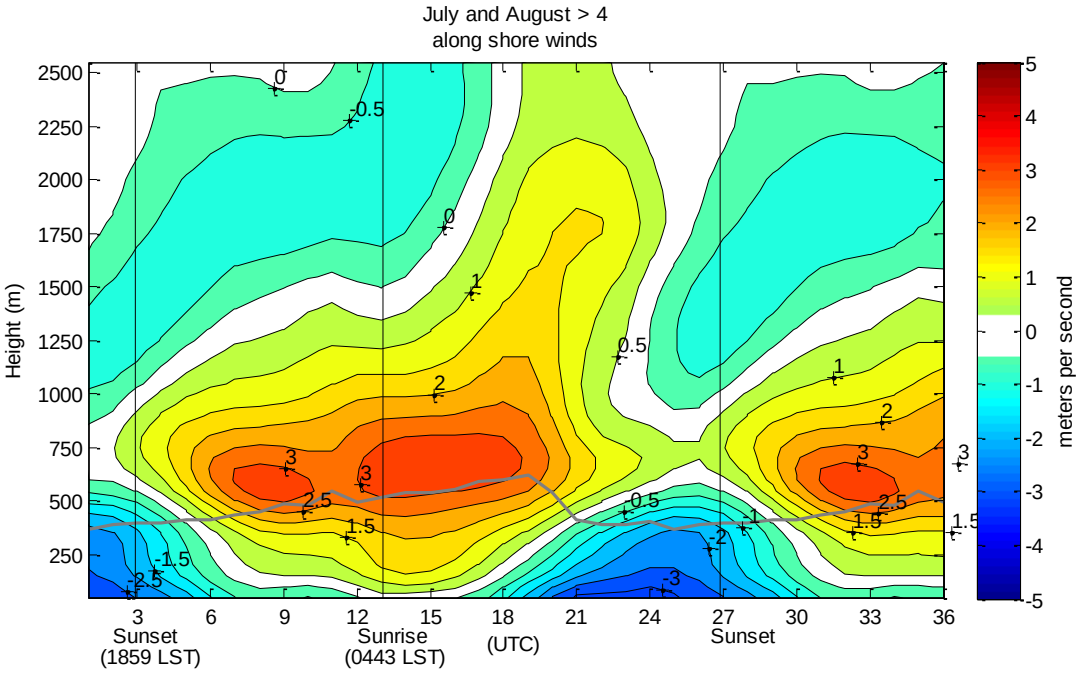
July and August > 4
along shore winds
Height (m)
meters per second
Sunset
(1859 LST)
Sunrise
(0443 LST)
(UTC)
Sunset

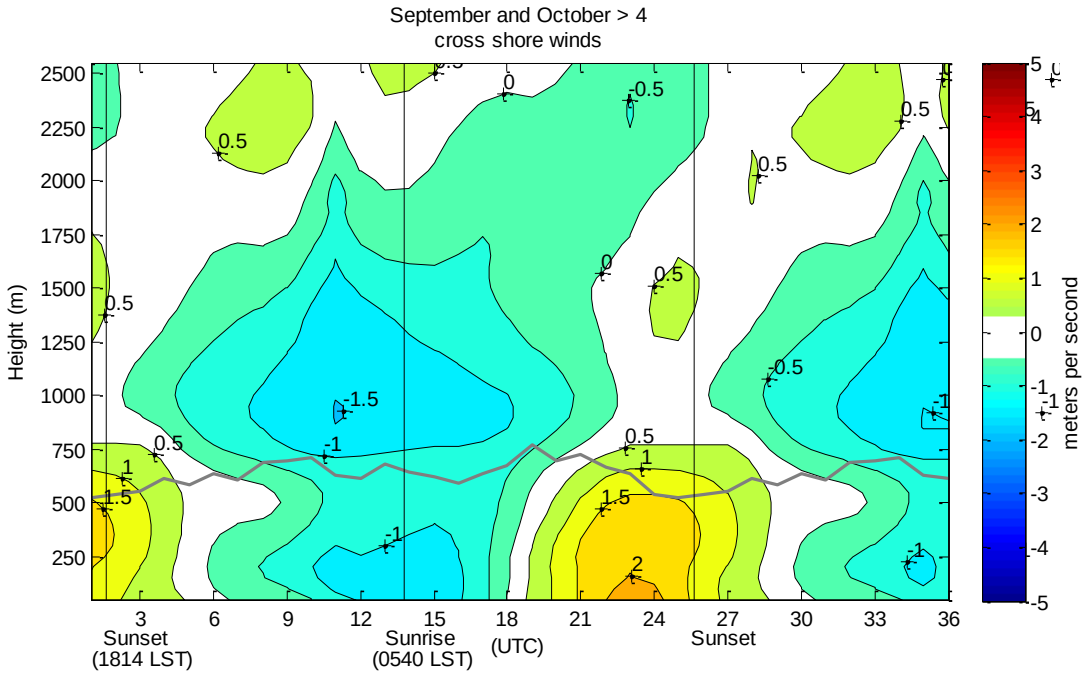
September and October > 4
cross shore winds
Height (m)
meters per second
Sunset
(1814 LST)
Sunrise
(0540 LST)
(UTC)
Sunset

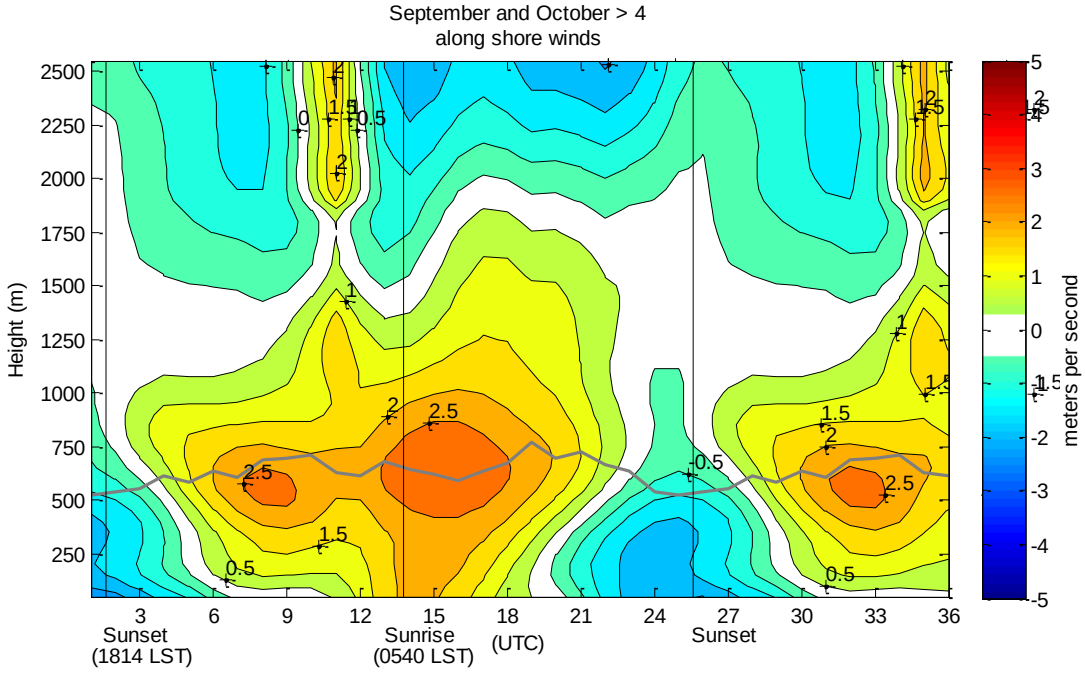
September and October > 4
along shore winds
Height (m)
meters per second
Sunset
(1814 LST)
Sunrise
(0540 LST)
(UTC)
Sunset

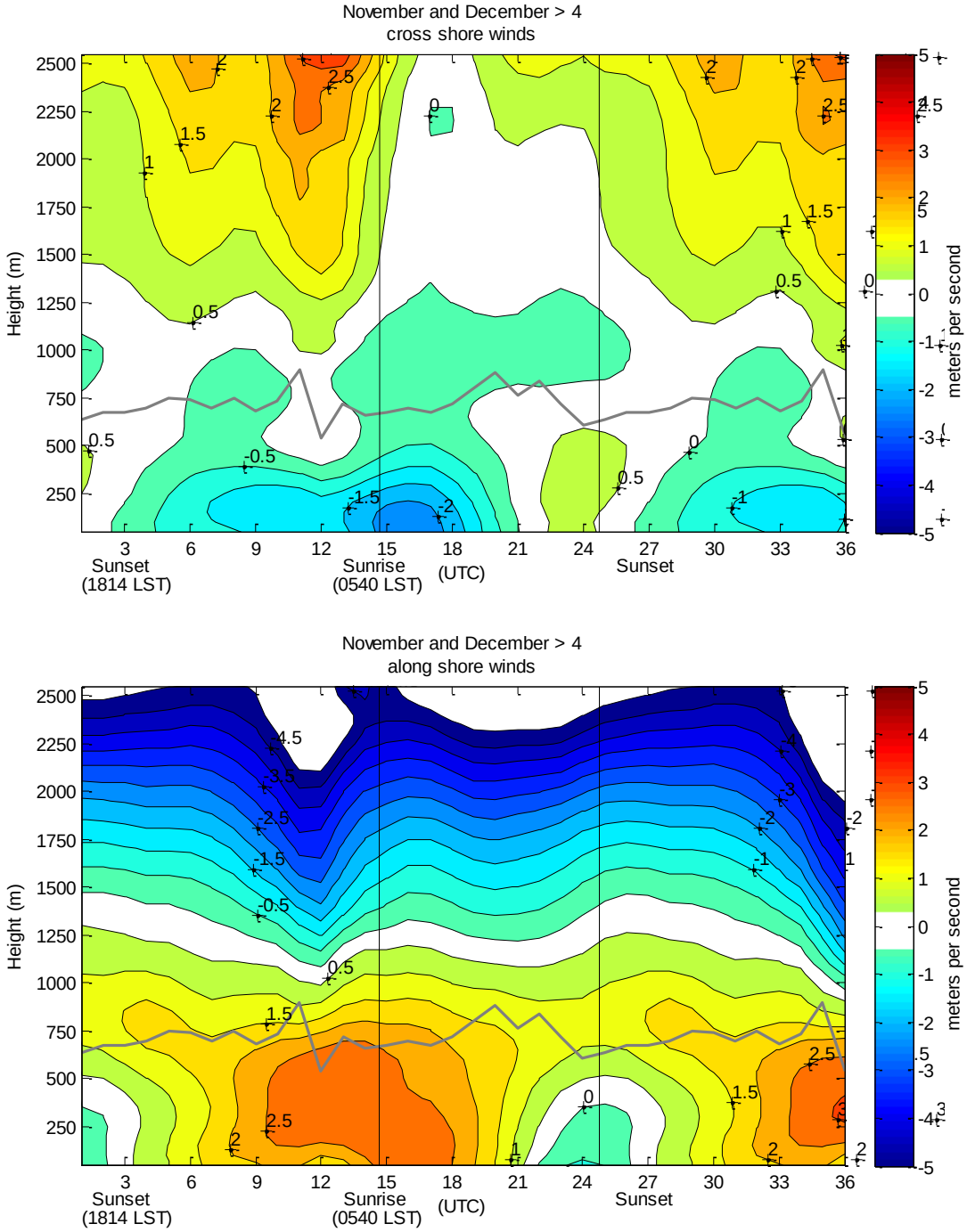

Figure 22. 36 hour climatology of the evolution of alongshore (295º), cross-shore (25º) winds (m s^{-1}) for cloudy days at LAX. Gray line is the average CBL height, the black vertical lines mark sunrise and sunset, which are annotated respectively.

36 hour climatological evolution of temperature

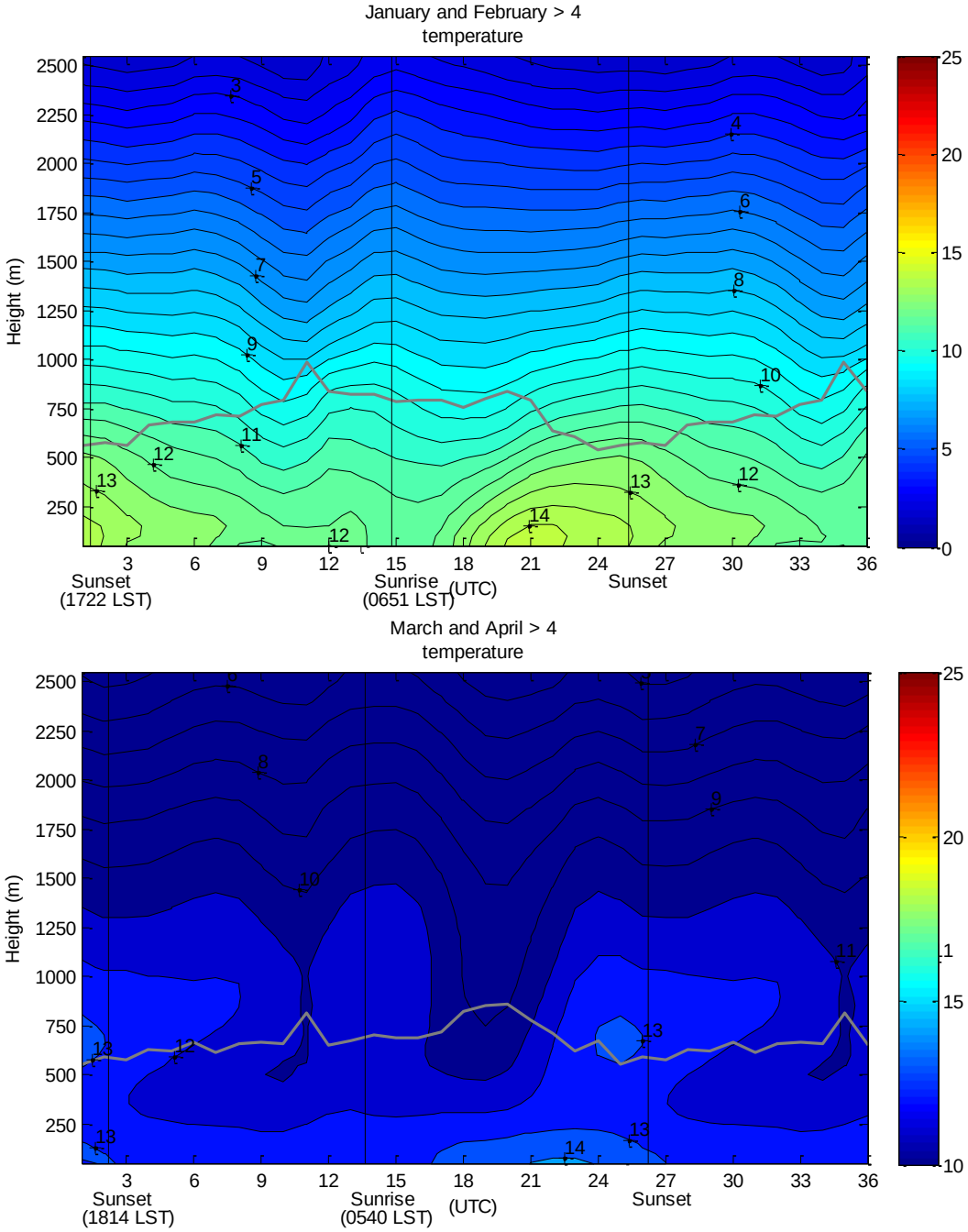

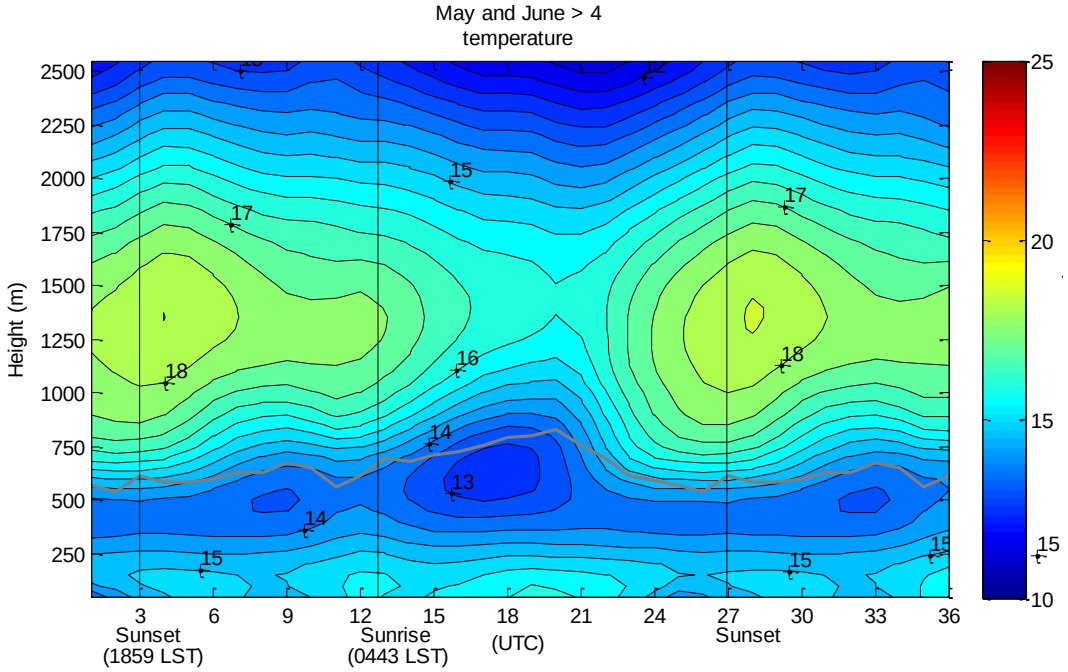
May and June > 4
temperature
Height (m)
2500
2250
2000
1750
1500
1250
1000
750
500
250
3 6 9 12 15 18 21 24 27 30 33 36
Sunset
(1859 LST)
Sunrise
(0443 LST)
(UTC)
Sunset
25
20
15
10

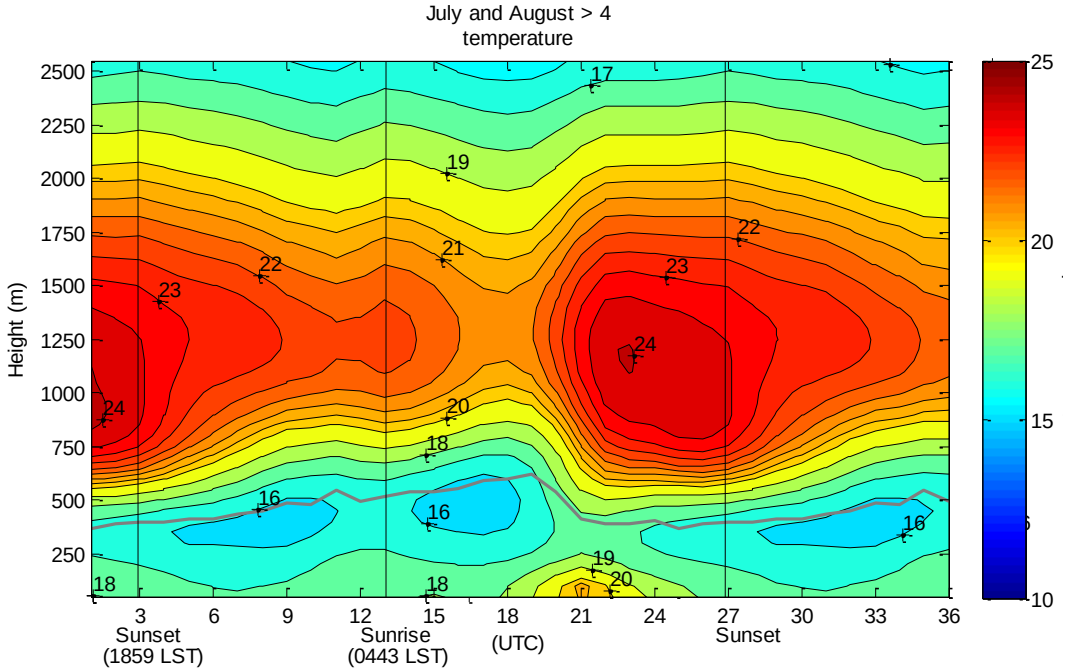
July and August > 4
temperature
Height (m)
2500
2250
2000
1750
1500
1250
1000
750
500
250
3 6 9 12 15 18 21 24 27 30 33 36
Sunset
(1859 LST)
Sunrise
(0443 LST)
(UTC)
Sunset
25
20
15
10

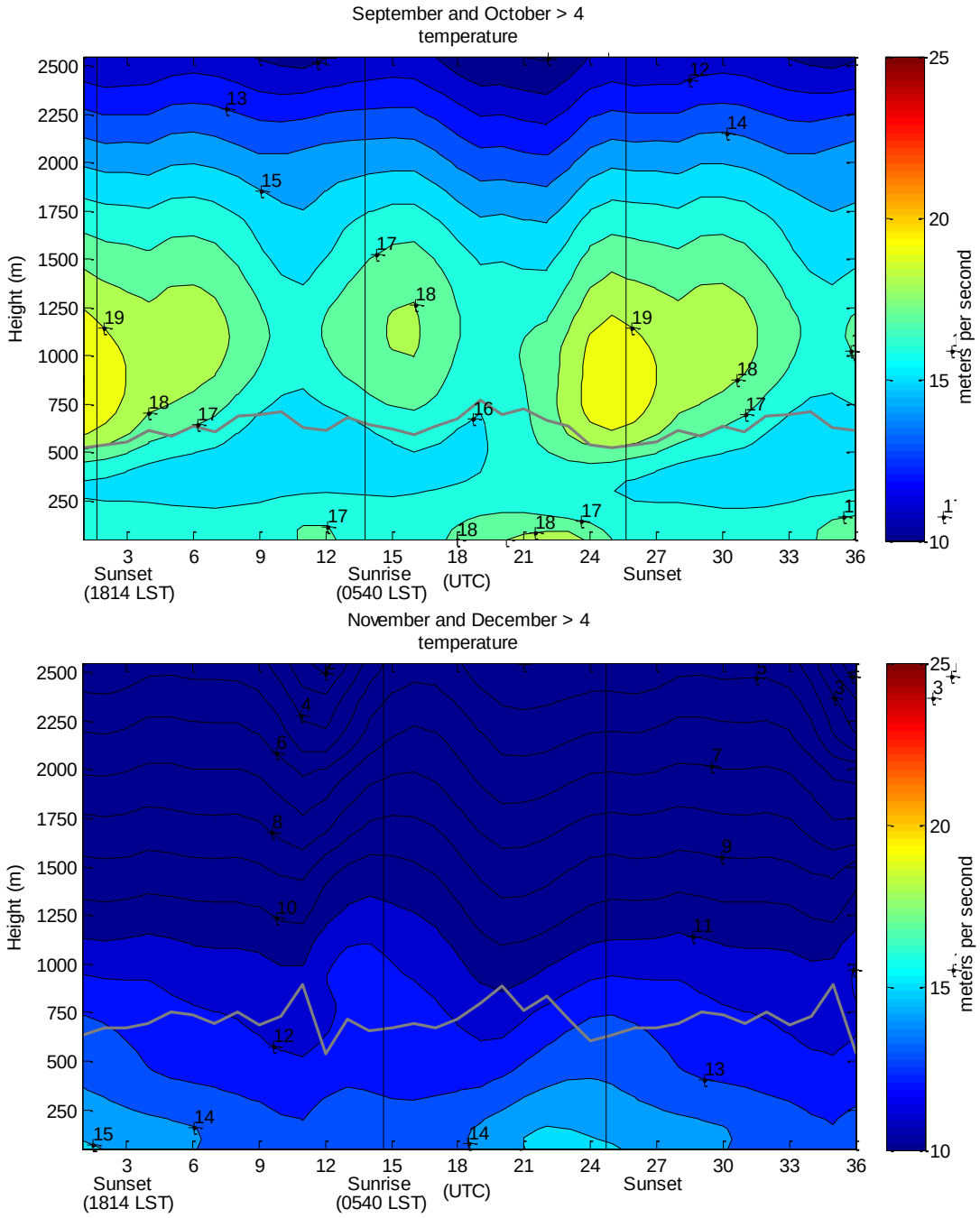

Figure 23. 36 hour climatology of the evolution of vertical temperature for cloudy days at LAX. Gray line is the average CBL height, the black vertical lines mark sunrise and sunset, which are annotated respectively.

REFERENCES

Blaskovic, M., R. Davies, and J. B. Snider, 1991: Diurnal variation of marine stratocumulus over San Nicolas Island during July 1987. *Monthly Weather Review*, **119**, 1469-1478, doi:http://dx.doi.org/10.1175/1520-0493(1991)119<1469:DVOMSO>2.0.CO;2.

Bond, N. A., C. F. Mass, and J. E. Overland, 1996: Coastally trapped wind reversals along the United States West Coast during the warm season. part I: climatology and temporal evolution. *Monthly Weather Review*, **124**, 430-445, doi:http://dx.doi.org/10.1175/1520-0493(1996)124<0430:CTWRAT>2.0.CO;2.

Brandli, H. W., J. W. Orndorff, and F. L. Guiberson, 1977: Eddy formation near San Simeon. *Bulletin of the American Meteorological Society*, **58**, 233-234.

Bridger, A. F., W. C. Brick, and P. F. Lester, 1993: The Structure of the marine inversion layer off the Central California Coast: Mesoscale Conditions. *Monthly Weather Review*, **121**, 335-351, doi:http://dx.doi.org/10.1175/1520-0493(1993)121<0335:TSOTMI>2.0.CO;2.

Burk, S. D., W. T. Thompson, 1996: The summertime low-level jet and marine boundary layer Structure along the California Coast. *Monthly Weather Review*, **124**, 668-686, doi:http://dx.doi.org/10.1175/1520-0493(1996)124<0668:TSLLJA>2.0.CO;2.

Cui, Z., M. Tjernström, and B. Grisogono, 1998: Idealized simulations of atmospheric coastal flow along the Central Coast of California. *Journal of Applied Meteorology*, **37**, 1332-1363, doi:http://dx.doi.org/10.1175/1520-0450(1998)037<1332:ISOACF>2.0.CO;2.

Davis, C., S. Low-Nam, and C. F. Mass, 2000:

Dynamics of a Catalina Eddy revealed by numerical simulation. *Monthly Weather Review*, **128**, 2885-2904, doi:http://dx.doi.org/10.1175/1520-0493(2000)128<2885:DOACER>2.0.CO;2.

Dorman, C. E., 1987: Possible role of gravity currents in northern California's coastal summer wind reversals. *Journal of Geophysical Research*, **92**, 1497-1506.

Dorman, C. E., 1988: Reply. *Monthly Weather Review*, **116**, 806-806, doi:http://dx.doi.org/10.1175/1520-0493(1988)116<0806:R>2.0.CO;2.

Dorman, C. E., T. Holt, D. P. Rogers, and K. Edwards, 2000: Large-scale structure of the June–July 1996 marine boundary layer along California and Oregon. *Monthly Weather Review*, **128**, 1632-1652, doi:http://dx.doi.org/10.1175/1520-0493(2000)128<1632:LSSOTJ>2.0.CO;2.

Dorman, C. E., D. Koračin, 2008: Response of the summer marine layer flow to an extreme California coastal bend. *Monthly Weather Review*, **136**, 2894-2992, doi:http://dx.doi.org/10.1175/2007MWR2336.1.

Dorman, C. E., D. P. Rogers, W. Nuss, and W. T. Thompson, 1999: Adjustment of the summer marine boundary layer around Point Sur, California. *Monthly Weather Review*, **127**, 2143-2159, doi:http://dx.doi.org/10.1175/1520-0493(1999)127<2143:AOTSMB>2.0.CO;2.

Dorman, C. E., C. D. Winant, 2000: The structure and variability of the marine atmosphere around the Santa Barbara Channel. *Monthly Weather Review*, **128**, 261-282.

Gerber, H., S. Chang, and T. Holt, 1989: Evolution of a marine boundary-layer jet. *Journal of the Atmospheric Sciences,* **46**, 1312-1326, doi:http://dx.doi.org/10.1175/1520-0469(1989)046<1312:EOAMBL>2.0.CO;2.

Halliwell, G. R., J. S. Allen, 1987: Wave-number frequency domain properties of coastal sea level response to alongshore wind stress along the west coast of North America. *Journal of Geophysical Research,* **92**, doi:10.1029/JC080i011p11761. issn: 0148-0227.

Hughes, P., D. Gedzelman, 1995: The new meteorology. *Weatherwise,* **48**, 26-36.

Koračin, D., C. E. Dorman, and E. P. Dever, 2004: Coastal perturbations of marine-layer winds, wind stress, and wind stress curl along California and Baja California in June 1999. *Journal of Physical Oceanography*, **34**, 1152-1173, doi:http://dx.doi.org/10.1175/1520-0485(2004)034<1152:CPOMWW>2.0.CO;2.

Lord, R. J., W. P. Menzel, and L. E. Pecht, 1984: ACARS wind measurements: an intercomparison with radiosonde, cloud motion and VAS thermally derived winds. *Journal of Atmospheric and Oceanic Technology,* **1**, 131-137, doi:http://dx.doi.org/10.1175/1520-0426(1984)001<0131:AWMAIW>2.0.CO;2.

Mass, C. F., M. Albright D., 1987: Coastal southerlies and alongshore surges of the west coast of North America: evidence of mesoscale topographically trapped response to synoptic forcing. *Monthly Weather Review,* **115**, 1707-1738, doi:http://dx.doi.org/10.1175/1520-0493(1987)115<1707:CSAASO>2.0.CO;2.

Mass, C. F., M. Albright D., 1988: Reply. *American Meteorological Society,* **116**, 2407-2410.

Mass, C. F., M. Albright D., 1989: Origin of the Catalina Eddy. *Monthly Weather Review*, **117**, 2406-2436, doi:http://dx.doi.org/10.1175/1520-0493(1989)117<2406:OOTCE>2.0.CO;2.

Mass, C. F., N. A. Bond, 1996: Coastally trapped wind reversals along the United States west coast during the warm season. Part II: Synoptic evolution. *Monthly Weather Review,* **124**, 446-461.

Mass, C. F., D. J. Brees, 1986: The onshore surge of marine air into the Pacific Northwest: A coastal region of complex terrain. *Monthly Weather Review,* **114**, 2602-2627.

Moninger, W. R., R. D. Mamrosh, and P. M. Pauley, 2003: Automated meteorological reports from commercial aircraft. *Bulletin of the American Meteorological Society*, **84**, 203-216, doi:http://dx.doi.org/10.1175/BAMS-84-2-203.

Neiburger, M., D. S. Johnson, and C. W. Chein, 1961: Studies of the structure of the atmosphere over the eastern Pacific Ocean in summer. *University of California Press*, **1**, 58.

Nuss, W. A., 2007: Synoptic-scale structure and the character of coastally trapped wind reversals. *Monthly Weather Review*, **135**, 60-81, doi:http://dx.doi.org/10.1175/MWR3267.1.

Parish, Thomas R., David A. Rahn, Dave Leon, 2013: Airborne observations of a Catalina eddy. *Mon. Wea. Rev.*, **141**, 3300–3313. doi: http://dx.doi.org/10.1175/MWR-D-13-00029.1

Pérez-Brunius, P., M. López, A. Parés-Sierra, and J. Pineda, 2007: Comparison of upwelling indices off Baja California derived from three different wind data sources. *CalCOFl Rep,* **48**, 204-214.

Pomeroy, K. R., T. R. Parish, 2001: A case study of the interaction of the summertime coastal jet with the California topography. *Monthly Weather Review*, **129**, 530-539, doi:http://dx.doi.org/10.1175/1520-0493(2001)129<0530:ACSOTI>2.0.CO;2.

Rahn, D. A., T. R. Parish, and D. Leon, 2013: Airborne measurements of coastal jet transition around Point Conception, California. *Monthly Weather Review*, **141**, 3827-3839, doi:http://dx.doi.org/10.1175/MWR-D-13-00030.1.

Ralph, F. M., L. Armi, J. M. Bane, C. E. Dorman, W. D. Neff, P. J. Neiman, W. A. Nuss, and P. O. G. Persson, 1998: Observations and analysis of the 10–11 June 1994 coastally trapped disturbance. *Monthly Weather Review*, **126**, 2435-2465.

Reason, C. J., R. Dunkley, 1993: Coastally trapped stratus events in British Columbia. *Atmosphere-Ocean*, **31**, 235-258.

Rogers, D. P., and coauthors, 1998: Highlights of Coastal Waves 1996. *Bulletin of the American Meteorological Society*, **79**, 1307-1326, doi:http://dx.doi.org/10.1175/1520-0477(1998)079<1307:HOCW>2.0.CO;2.

Rogerson, A. M., 1999: Transcritical flows in the coastal marine atmospheric boundary layer. *Journal of the Atmospheric Sciences*, **56**, 2761-2779, doi:http://dx.doi.org/10.1175/1520-0469(1999)056<2761:TFITCM>2.0.CO;2.

Rosenthal, J., 1968: PICTURE OF THE MONTH: A Catalina Eddy. *Monthly Weather Review*, **96**, 742-743, doi:http://dx.doi.org/10.1175/1520-0493(1968)096<0742:ACE>2.0.CO;2.

Samelson, R. M., 1992: Supercritical marine-layer flow along a smoothly varying coastline. *Journal of the Atmospheric Sciences*, **49**, 1571-1584, doi:http://dx.doi.org/10.1175/1520-0469(1992)049<1571:SMLFAA>2.0.CO;2.

Seo, H., K. Brink H., C. E. Dorman, and D. Koračin, 2012: What determines the spatial pattern in summer upwelling trends on the U.S. West Coast? *Journal of Geophysical Research*, **117**, doi:10.1029/2012JC008016.

Skamarock, W. C., R. Rotunno , and J. B. Klemp, 1999: Models of coastally trapped disturbances. *Journal of the Atmospheric Sciences*, **56**, 3349-3365, doi:http://dx.doi.org/10.1175/1520-0469(1999)056<3349:MOCTD>2.0.CO;2.

Skyllingstad, E. D., P. Barbour, and C. E. Dorman, 2001: The dynamics of northwest summer winds over the Santa Barbara Channel. *Monthly Weather Review*, **129**, 1042-1061, doi:http://dx.doi.org/10.1175/1520-0493(2001)129<1042:TDONSW>2.0.CO;2.

Sparkman, J. K., J. Giraytys, and G. J. Smidt, 1981: ASDAR: A FGGE real-time data collection system. *Bulletin of the American Meteorological Society*, **62**, 394-400.

Ulrickson, B. L., S. J. Hoffmaster, J. Robinson, and D. Vimont, 1995: A numerical modeling study of the Catalina Eddy. *Monthly Weather Review*, **123**, 1364-1373, doi:http://dx.doi.org/10.1175/1520-0493(1995)123<1364:ANMSOT>2.0.CO;2.

Winant, C. D., C. E. Dorman, C. A. Friehe, and R. C. Bearsley, 1988: The marine layer off Northern California: An example of supercritical channel flow. *Journal of*

the Atmospheric Sciences, **45**, 3588-3605, doi:http://dx.doi.org/10.1175/1520-0469(1988)045<3588:TMLONC>2.0.CO;2.

Wyant, M. C., R. Wood, C. S. Bretherton, C. R. Mechoso, J. Bacmeister, M. A. Balmaseda, B. Barrett, F. Codron, P. Earnshaw, J. Fast, C. Hannay, J. W. Kaiser, H. Kitagawa, S. A. Klein, M. K¨ohler, J. Manganello, H. -. Pan, F. Sun, S. Wang, and Y. Wang, 2010: The PreVOCA experiment: modeling the lower troposphere in the Southeast Pacific. *Atmospheric Chemistry and Physics*, **10**, 4757-4774, doi:10.5194/acp-10-4757-2010.

Zemba, J., C. A. Friehe, 1987: The marine atmospheric boundarylayer jet during the Coastal Ocean Dynamics Experiment. *Geophys. Res*, **92**, 1489-1496.